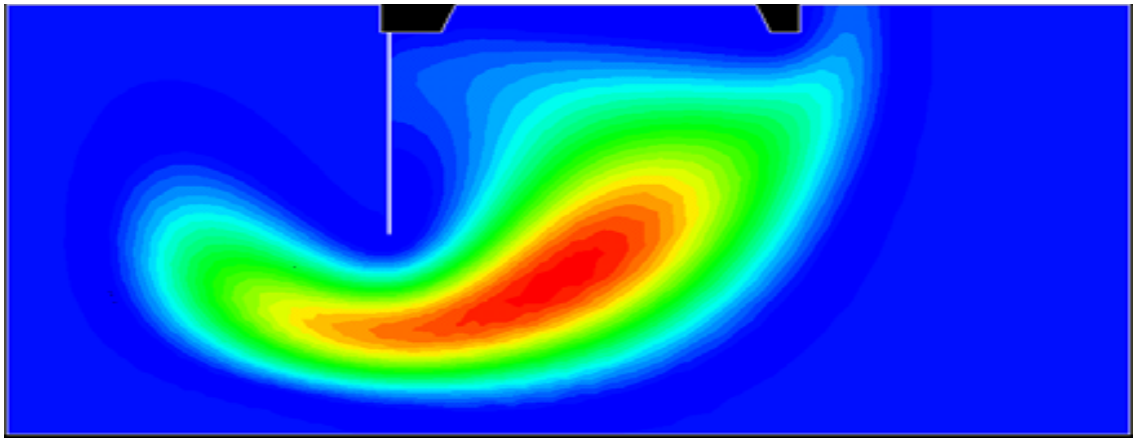

Proceedings of Workshop on HYDRUS Applications

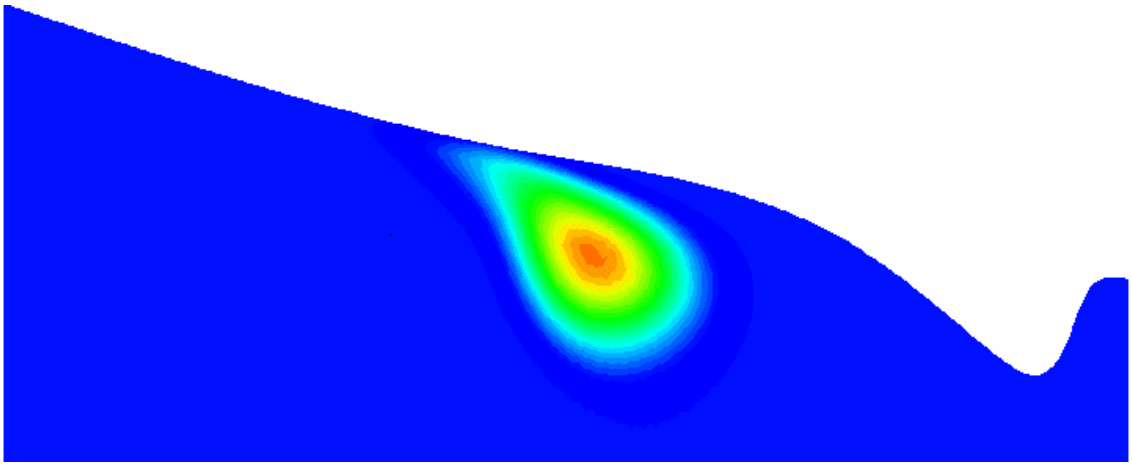

October 19, 2005
Department of Earth Sciences
Utrecht University, The Netherlands

Preface:

Soil and water resources are of great importance to the mankind. As the world population grows and increasing incidences of pollution of soil and groundwater are discovered, prudent management and protection of these resources becomes increasingly important. Most subsurface pollution problems stem from activities involving the unsaturated (vadose) zone between the soil surface and the groundwater table. As natural systems are extraordinarily complicated and the understanding and management of these resources cannot be accomplished effectively using heuristic means, mathematical modeling has played a critical role in the investigation and management of soil and water resources for the last three decades. The software packages HYDRUS-1D and 2D are a typical example of commonly used state-of-the-art codes involving variably saturated flow and transport.

This proceedings contains the collection of papers presented at the User's Workshop on Hydrus that was held in Utrecht, The Netherlands, following a short course on Hydrus. The purpose of the workshop was to bring together the users and developers of the HYDRUS software packages, to present the latest innovations in the model applications, and to discuss the capabilities and limitations of HYDRUS. This was a unique opportunity for all HYDRUS users to give a brief overview of their work and discuss future needs and directions for obtaining more reliable modelling results. This collective work includes contributions by many of the users of the HYDRUS software packages ranging from the very fundamental to the most compelling and important of applications.

The editors:

Saeed Torkzaban

S. Majid Hassanizadeh

Proceedings of Workshop on HYDRUS Applications

October 19, 2005
Department of Earth Sciences
Utrecht University, The Netherlands

Address for correspondence:
S. Majid Hassanizadeh
Department of Earth Sciences; Utrecht University
Budapestlaan 4
P.O. Box 80021; 3508 TA UTRECHT; The Netherlands
Tel: +31 30 253 7464; Fax: +31 30 2534900
E-mail: hassanizadeh@geo.uu.nl

Contents

Modeling of Colloid Transport and Deposition in Porous Media

Scott A. Bradford[1], Martinus Th. van Genuchten[1], and Jiří Šimůnek[2]

[1]George E. Brown Jr. Salinity Laboratory, USDA-ARS, Riverside, CA 92507

[2]University of California Riverside, Department of Environmental Sciences, Riverside, CA 92521

Abstract

A conceptual model for colloid transport is presented that accounts for colloid attachment, straining, and exclusion. Colloid attachment and detachment are modeled using conventional first-order rate expressions, whereas straining employs a first-order term that is depth-dependent. Time dependent colloid deposition as a result of blocking of favorable attachment sites or filling of straining sites is simulated using a Langmuirian type expression. The influence of colloid-colloid interactions on straining is also included using at term that is proportional to the concentration of colloids in suspension and strained on the solid phase. Finally, size exclusion is modeled by adjusting transport parameters for the colloid-accessible pore space. Numerical simulations are presented to highlight the various processes controlling colloid transport and deposition. The sensitivity of simulation results to selective model parameters is also demonstrated.

Introduction

Colloid transport models have typically been derived from a combination of convection-dispersion-retardation theory for solute transport and colloid attachment theory. Clean-bed attachment theory employs an irreversible first-order kinetic attachment term and predicts an exponential decrease in colloid concentration with transport distance. Over the past decade, a growing body of literature indicates that attachment theory frequently does not provide an accurate characterization of experimental deposit profiles [*Camesano and Logan*, 1998; *Bolster et al.*, 1999; *Redman et al.*, 2001; *Bradford et al.*, 2002; *Tufenkji et al.*, 2003; *Li et al.*, 2004; *Tufenkji and Elimelech*, 2005ab]. This is especially true for larger colloids and finer textured porous media, and when there are repulsive electrostatic interactions between colloids and grain surface.

Some of the discrepancies between colloid transport data and attachment theory may be due to the fact that colloid attachment theory does not account for straining. Straining, is the trapping of colloid particles in down-gradient pore throats that are too small to allow particle passage. Straining occurs when colloids are physically deposited in pores that are smaller than some critical size, although colloid transport may still occur in larger pores. Size exclusion is a second related factor that is generally neglected in colloid transport modeling. Size exclusion influences the transport behavior of colloids by physically limiting their mobility to the larger pore networks and the more conductive ranges of the pore water velocity distribution. Hence, colloids may be transported faster than a conservative solute tracer.

This extended abstract reports on modifications to the HYDRUS 1D code [*Simunek et al.*, 1998; *Simunek et al.*, 2005] to account for colloid attachment, straining, and size exclusion [*Bradford et al.*, 2003, 2004, 2005]. Selective model simulations are presented to

illustrate the roles of these processes. Special attention has been given to the roles of straining and size exclusion in these examples.

Numerical Modeling

The aqueous colloid mass balance equation is written as:

$$\frac{\partial(\theta_w C)}{\partial t} = -\frac{\partial J_T}{\partial z} - E_{sw} \tag{1}$$

where C [N L^{-3}; N denotes number and L length] is the aqueous phase colloid concentration, t [T] denotes time, J_T [N L^{-2} T^{-1}] is the total colloid flux (sum of advective and dispersive fluxes), and E_{sw}[N L^{-3} T^{-1}] is the colloid mass transfer terms between the aqueous and solid phases due to attachment and straining.

A generalized term for E_{sw}^{att} is given as:

$$E_{sw} = \frac{\partial\left(\rho_b\left(S_{att} + S_{str}\right)\right)}{\partial t} = \theta_w k_{att}\psi_{att} C - \rho_b k_{\det} S_{att} + \theta_w k_{str}\psi_{str} C \pm \rho_b k_{ci} S_{str} C \tag{2}$$

with S_{att} [N M^{-1}] as the solid phase concentration of attached colloids, k_{att} [T^{-1}] is the first order colloid attachment coefficient, k_{det} [T^{-1}] is the first order colloid detachment coefficient, ψ_{att} [-] is a dimensionless colloid attachment function, k_{str} [T^{-1}] is the straining coefficient, ψ_{str} [-] is a dimensionless straining function, S_{str} [N M^{-1}] is the solid phase concentrations of strained colloids, and k_{ci} [$^{-1}$ M T^{-1}] is the colloid interaction coefficient.

The first and second terms on the right hand side of (2) accounts for colloid attachment and detachment, respectively. When ψ_{att} equals 1 and k_{det} = 0, clean-bed attachment theory is incorporated into the k_{att} term. Time dependency in colloid attachment rates as a result of blocking can be accounted for using the ψ_{att} term in (2). During blocking the value of ψ_{att} decreases with increasing S_{att} as a result of filling of favorable attachment sites such as metal oxide surfaces or clay edges. According to the Langmuirian approach, ψ_{att} = 1- S_{att}/S_{att}^{max}; where S_{att}^{max} [N_c M^{-1}] is the maximum solid phase concentration of attached colloids. In contrast, the random sequential adsorption (RSA) approach employs a ψ_{att} that is a nonlinear function of S_{att}.

Attachment theory has been used to predict colloid transport behavior for a wide variety of colloid and porous media characteristics. Little attention has been paid to the colloid and porous media parameter ranges that may limit attachment model applicability, because straining has been assumed *a priori* to be insignificant. The third and fourth terms on the right hand side of (2) accounts for colloid straining and colloid-colloid interaction, respectively. The influence of straining is modeled using a value of ψ_{str} that is a function of both depth and S_{str} as:

$$\psi_{str} = H\left(z - z_o\right)\left(1 - \frac{S_{str}}{S_{str}^{\max}}\right)\left[\frac{d_{50} + z - z_o}{d_{50}}\right]^{-\beta} \tag{3}$$

Here β [-] is a parameter that controls the shape of the colloid spatial distribution, $H(z\text{-}z_o)$ is the Heaviside function (0 for $z < z_o$ and 1 for $z \geq z_o$), z [L] is depth, z_o [L] is the depth from the column inlet or textural interface (layered systems), and S_{str}^{max} [N M^{-1}]is the maximum solid phase concentration of strained colloids. The second term on the right hand side of (3) accounts for filling and accessibility of straining sites in a manner similar to the Langmuirian blocking approach.

The fourth term on the right hand side of (2) is used to account for the interaction of colloids in solution and those retained by straining. Retention of strained colloids is hypothesized to be hindered (term is negative) at greater collision frequencies (higher concentrations) when there are repulsive colloid (aqueous phase) - colloid (strained)

interactions. Conversely, attractive interactions of colloids in solution and those retained on the solid phase produce greater straining and can be simulated using a positive value for the fourth term of (2). Colloid-colloid interactions (repulsive or attractive) will dependent on the colloid surface chemistry and the aqueous chemistry. Our approach assumes that the frequency of collisions is proportional to the colloid concentration in solution and the amount retained on the solid phase.

To account for size and anion exclusion, values of θ_w and the Darcy water velocity, q_w [L T^{-1}] are adjusted to account for accessibility by colloids according to:

$$\theta_{mw} = \theta_w - \varepsilon\gamma \tag{4}$$

$$q_{mw} = q_w k_{rmw} / k_{rw} \tag{5}$$

Here ε [-] is the porosity, γ [-] is the water saturation that is not accessible to mobile colloids, k_{rw} [-] is the water relative permeability, and k_{rmw} [-] is the colloid accessible water relative permeability. The ratio of q_{mw} and θ_{mw} yields the colloid accessible pore-water velocity. The value of k_{rw} is typically determined from capillary pressure data using a pore size distribution model. The value of k_{rmw} is determined using the model of *Burdine* [1953] by adjusting its limits of integration to reflect pore space accessible to colloids:

$$k_{rmw}(S_w) = S_w^2 \frac{\int_\gamma^{S_w} R(x)^2 dx}{\int_0^1 R(x)^2 dx} \qquad S_w > \gamma \tag{6}$$

Here S_w [-] is the water saturation, R [L] is the pore size, and x [-] is a dummy saturation variable of integration. When S_w is less than γ then the value of k_{rmw} is set equal to zero. The value of γ can be theoretically related to a critical pore radius for exclusion using the Laplace equation and a capillary pressure curve. The critical pore radius for exclusion is likely a function of many variables, including: colloid size and concentration, diffuse double layer thickness, surface roughness, and the presence of retained colloids on the grain and pore surfaces. Alternatively, the value of γ can be fitted to transport data and a critical pore radius for exclusion can be calculated according to the outlined procedure.

Example Simulations

This section presents example simulations and experimental data that illustrate the outlined model capabilities and processes. Figure 1 presents o served and simulated breakthrough curves (Figure 1a) and deposition profiles (Figure 1b) for 1 μm carboxyl latex microspheres in 150 μm Ottawa (quartz) sand. Simulations considered attachment and detachment (ψ_{att}=1, k_{str} = 0; and k_{ci} = 0), attachment and Langmuirian blocking (k_{det} = 0; k_{str} = 0; and k_{ci} = 0), straining and Langmuirian filling (k_{att} = 0; k_{det} = 0; and k_{ci} = 0), and straining and colloid interactions (k_{att} = 0; k_{det} = 0; and S_{str}/S_{str}^{max} = 1). Notice that the straining simulations provide a reasonable description of both transport and deposition data, whereas attachment simulations only accurately charactize the breakthrough curves. *Bradford et al*. [2003] present more physically realistic simulations that consider both attachment and straining.

Figure 1.

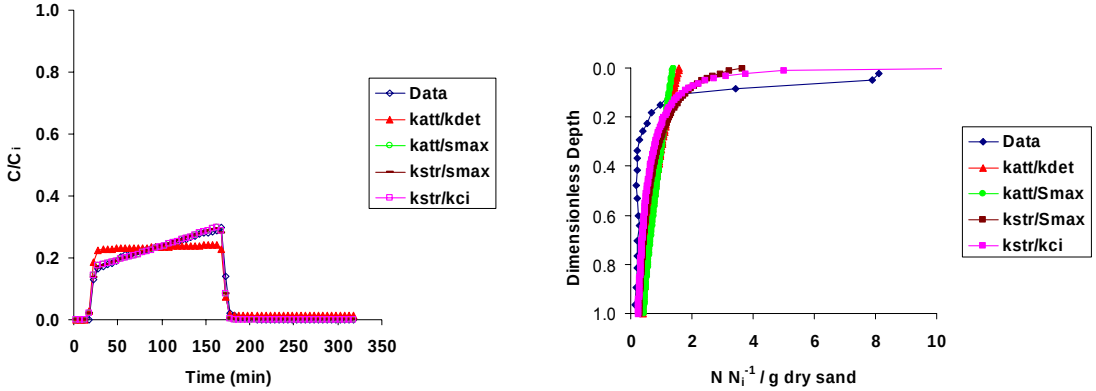

Figure 2 presents simulated breakthrough curves (Figure 2a) and deposition profiles (Figure 2b) when the straining parameters are fixed and the colloid interaction coefficient is varied. Observe that transport and deposition behavior is highly sensitive to this parameter, suggesting that colloid-colloid interactions will have an important role on straining behavior.

Figure 2.

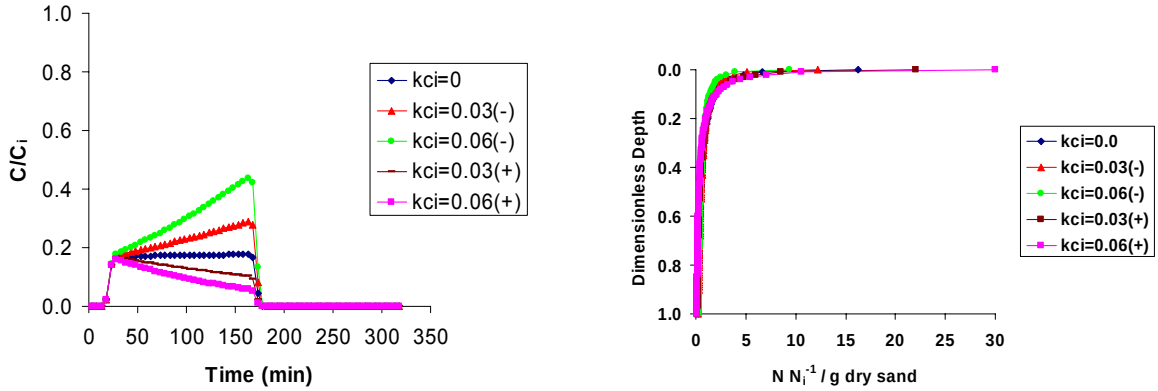

Figure 3 presents the predicted velocity enhancement (the ratio of the pore water velocity for mobile colloids compared to a conservative solute) for mobile colloids in a hypothetical soil for various values of S_w and γ. Observe that for $S_w>\gamma$ the velocity enhancement tends to increase with increasing values of γ and decreasing values of S_w. For $S_w<\gamma$ no colloids are mobile.

Figure 3.

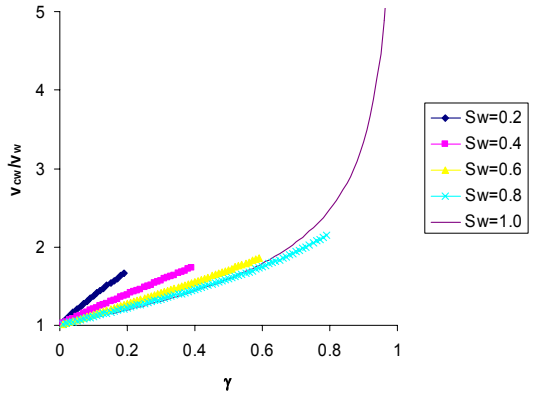

References

Bolster, C. H., A. L. Mills, G. M. Hornberger, and J. S. Herman. 1999. Spatial distribution of bacteria experiments in intact cores. Water Resour. Res. 35:1797-1807.

Bradford, S. A., S. R. Yates, M. Bettahar, and J. Simunek. 2002. Physical factors affecting the transport and fate of colloids in saturated porous media. Water Resour. Res. 38:1327, doi:10.1029/2002WR001340.

Bradford, S. A., J. Simunek, M. Bettahar, M. Th. van Genuchten, and S. R. Yates. 2003. Modeling colloid attachment, straining, and exclusion in saturated porous media. Environ. Sci. Technol. 37:2242-2250.

Bradford, S. A., M. Bettahar, J. Simunek, and M. Th. Van Genuchten. 2004. Straining and attachment of colloids in physically heterogeneous porous media. Vadose Zone J. 3:384-394.

Bradford, S. A., J. Simunek, M. Bettahar, Y. F. Tadassa, M. Th. Van Genuchten, and S. R. Yates. 2005. Straining of colloids at textural interfaces. Water Resour. Res., In press.

Burdine, N. T. 1953. Relative permeability calculations from pore size distribution data. Trans. Am. Inst. Min. Metall. Pet. Eng. 198:71-78.

Camesano, T. A., and B. E. Logan. 1998. Influence of fluid velocity and cell concentration on the transport of motile and nonmotile bacteria in porous media. Environ. Sci. Technol. *32* (11), 1699-1708.

Li, X., T. D. Scheibe, and W. P. Johnson. 2004. Apparent decreases in colloid deposition rate coefficient with distance of transport under unfavorable deposition conditions: a general phenomenon. Environ. Sci. Technol. *38* (21), 5616-5625.

Redman, J. A., S. B. Grant, T. M. Olson, and M. K. Estes. 2001. Pathogen filtration, heterogeneity, and the potable reuse of wastewater. Environ. Sci. Technol. *35* (9): 1798-1805.

Šimůnek, J., K. Huang, M. Šejna, and M. Th. van Genuchten, The HYDRUS-1D software package for simulating the one-dimensional movement of water, heat, and multiple solutes in variably-saturated media. Version 1.0, *IGWMC - TPS - 70,* International Ground Water Modeling Center, Colorado School of Mines, Golden, Colorado, 186pp., 1998.

Šimůnek, J., M. Th. van Genuchten, and M. Šejna, The HYDRUS-1D software package for simulating the one-dimensional movement of water, heat, and multiple solutes in variably-saturated media. Version 3.0, *HYDRUS Software Series 1*, Department of Environmental Sciences, University of California Riverside, Riverside, CA, 270pp., 2005.

Tufenkji, N., J. A. Redman, and M. Elimelech. 2003. Interpreting deposition patterns of microbial particles in laboratory-scale column experiments. Environ. Sci. Technol. *37*(3):616-623.

Tufenkji, N. and M. Elimelech. 2005a. Spatial distributions of Crypotsporidium oocysts in porous media: Evidence for dual model deposition. Environ. Sci. Technol., 39:3620-3629.

Tufenkji, N., and M. Elimelech. 2005b. Breakdown of colloid filtration theory: Role of the secondary energy minimum and surface charge heterogeneities. Langmuir, 21:841-852.

Effects of Canopy Shading and Irrigation on Soil Water Content and Temperature

Fares1 A., J. Šimůnek2, L.R. Parsons3, Th. M. van Genuchten4, and K.T. Morgan3
[1]University of Hawaii-Manoa, Email AFares@Hawaii.Edu
[2]University of California Riverside, [3]University of Florida, [4]USSL-USDA-ARS, Riverside, CA.

Abstract

Citrus root systems are exposed to different thermal and hydrologic conditions as a result of tree canopy shading and under-tree micro-irrigation. Because micro-sprinklers wet only part of the soil surface and are located under the tree, roots under the canopy usually receive more water than those outside the tree canopy. The combined effects of different soil temperature and water input on water redistribution under field conditions have not been fully studied in Florida sandy soils. The objective of this study was to investigate shading and irrigation effects on spatial distribution of water content and soil temperature at different soil depths. Real-time capacitance soil water sensors and thermocouples were used to monitor soil water content and temperature at depths of 0, 10, 20, 40, 80 and 150 cm. Weather parameters were monitored simultaneously at the same location. HYDRUS-2D, a two dimensional computer package for simulating movement of water, heat, and multiple solutes in variably saturated media, was used to simulate water flow and heat transport under such conditions. The predicted water contents and soil temperatures compared favorably with their corresponding observed parameters. In addition to its accuracy in simulating this system, HYDRUS-2D helped to improve the analysis of this research project.

Introduction

Citrus-tree root system is exposed to different thermal and hydrologic conditions as a result of tree canopy and under-tree microirrigation system. Thus, roots under the tree canopy are shaded by the canopy and receive irrigation water. In contrast, roots outside tree canopy are uncovered, receive full solar radiation, and only receive water from rain. Assuming isothermal conditions in studying water movement and root uptake could result in large errors.

Temperature plays an important role in the chemical, physical and biological functioning of a soil. Temperature gradients can cause water to move in the vapor phase from a hot site to a cold site. Water moves as a result of combined effects of temperature, water potential and solute concentration gradients. The movement of water under combined temperature and matric potential head gradient has been studied under wide ranges of soil and weather conditions over last four decades and have been reported (Philip and De Vries, 1957; Horton and Chung, 1991).

Numerical models, with varying complexities were developed to describe coupled heat, water and solute transfer (Nassar and Horton, 1992; Bear and Gilman, 1995 and Šimůnek et al., 1999). The combined effects of different soil temperature and water input under Florida sandy soils on water redistribution under field conditions has not been fully studied.

The objectives of this study were: i) to investigate, in the field, shading and irrigation effects on spatial distribution of water content and soil temperature at different soil depths (0, 10, 20, 40, 80 and 150 cm) and six field locations, ii) to use HYDRUS to simulated coupled water and heat transport.

Materials and Methods

The field study was conducted on a citrus grove of Hamlin orange trees (Citrus sinensis (L.) Osb.) on Swingle citrumelo (Citrus paradisi Macf. X Poncirus trifoliata (L.) Raf.) rootstock at the Water Conserv II, Avalon, Orange County, Florida. The soil is a Candler fine sand (hyperthermic, uncoated, Typic Quartzipsamments). Two replicates of three main locations within the tree canopy, at the dripline, and in the open between two tree rows were selected for measuring soil water

content and temperature. At each location, soil water contents were monitored at soil surface, and10, 20, 40, and 80 cm below soil surface at 30 min intervals. Air temperature, surface, and soil temperature at previously mentioned depths were monitored at the same time interval (30 minutes).

Simulations

HYDRUS-2D software package was used to simulate the movement of water and heat transport. A 1-D soil transect, 0.8 m deep, was used in this study. The Candler soil profile consists of very deep, excessively drained, rapidly permeable soils formed on thick beds of eolian or marine deposits of coarse-textured materials. Soil water release curves and their corresponding hydraulic conductivities are presented in Fares et al. (2000).

Results and Discussion

Figure 1 shows the rainfall data (A) that was measured on the research site and that was used as input for the simulations. There were several rainfall events during the first 10 days of the simulation period; however less rainfall was registered in the second part of this period. As a result, the soil water content showed at all depths fluctuated more frequently in the first part of the simulation as compared to the second part. The simulated and measured water contents at 10, 20 and 40 cm are shown in Fig. 1A, Fig. 1B and Fig. 1C, respectively. There is an excellent agreement between the measured simulated data at the 20 and 40 cm.

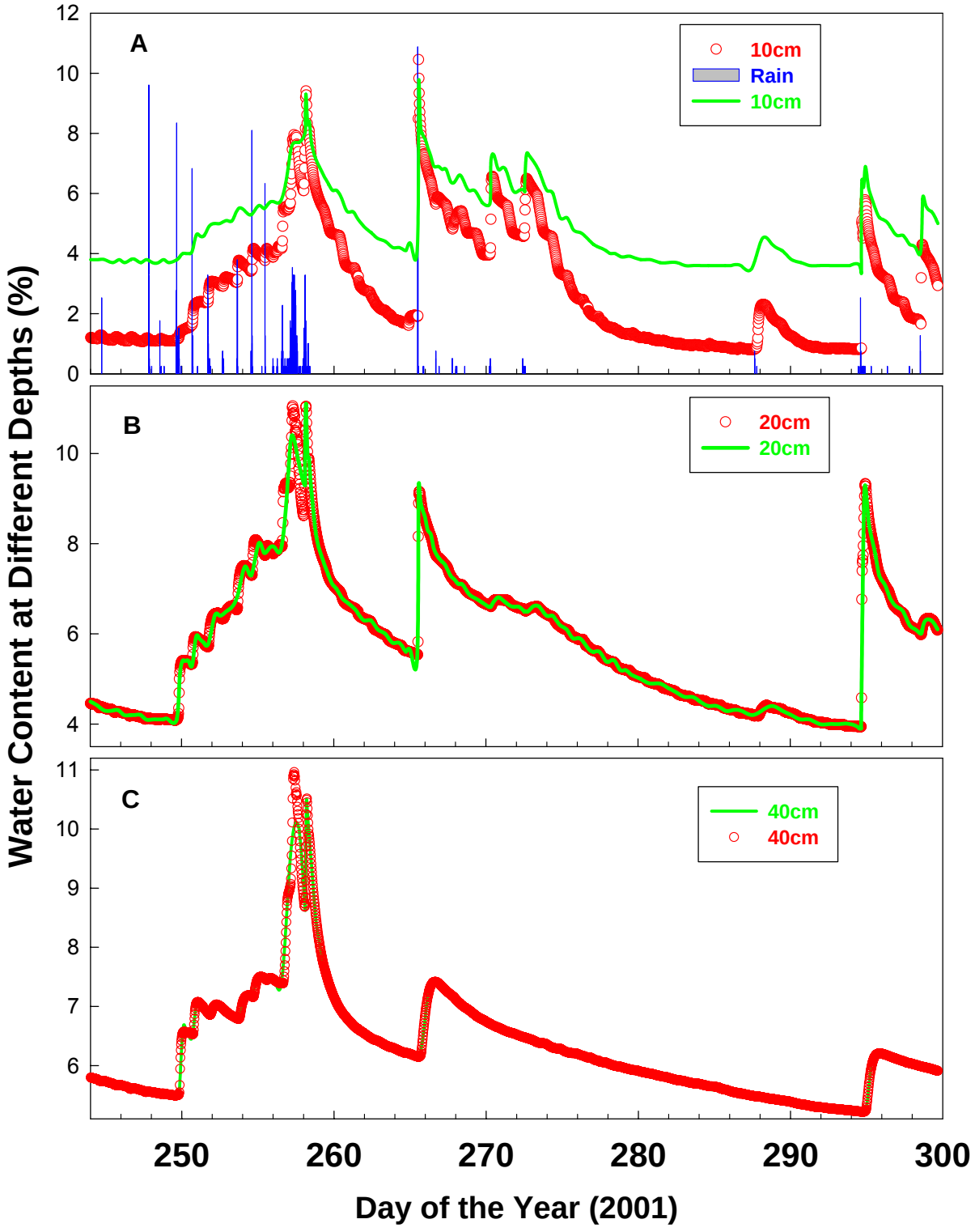

Fig. 1. Daily rainfall rates (solid bars, A), and measured (open circles) and simulated (lines) soil water contents at 10 cm (A), 20 cm (B), and 40 cm (C) depths.

Simulated and measured data of the soil temperatures at 40 and 80 cm depth are shown in Fig. 2A and Fig. 2B, respectively. Daily rainfall and daily net radiation measured outside the tree canopy in the open are shown in Fig. 2 A and 2B, respectively. The first 10 days of the simulation showed substantial decrease in the soil temperature at the two shown depths. This period was a rainy period with low net radiation values; thus, the lower the net radiation the sharper was the decrease in the soil temperatures. During this time of the year, rainfall in Florida occurs as a result of cold front spills that continue for days. During these cold fronts, there were almost overcast conditions that result in a substantial decrease of the net radiation.

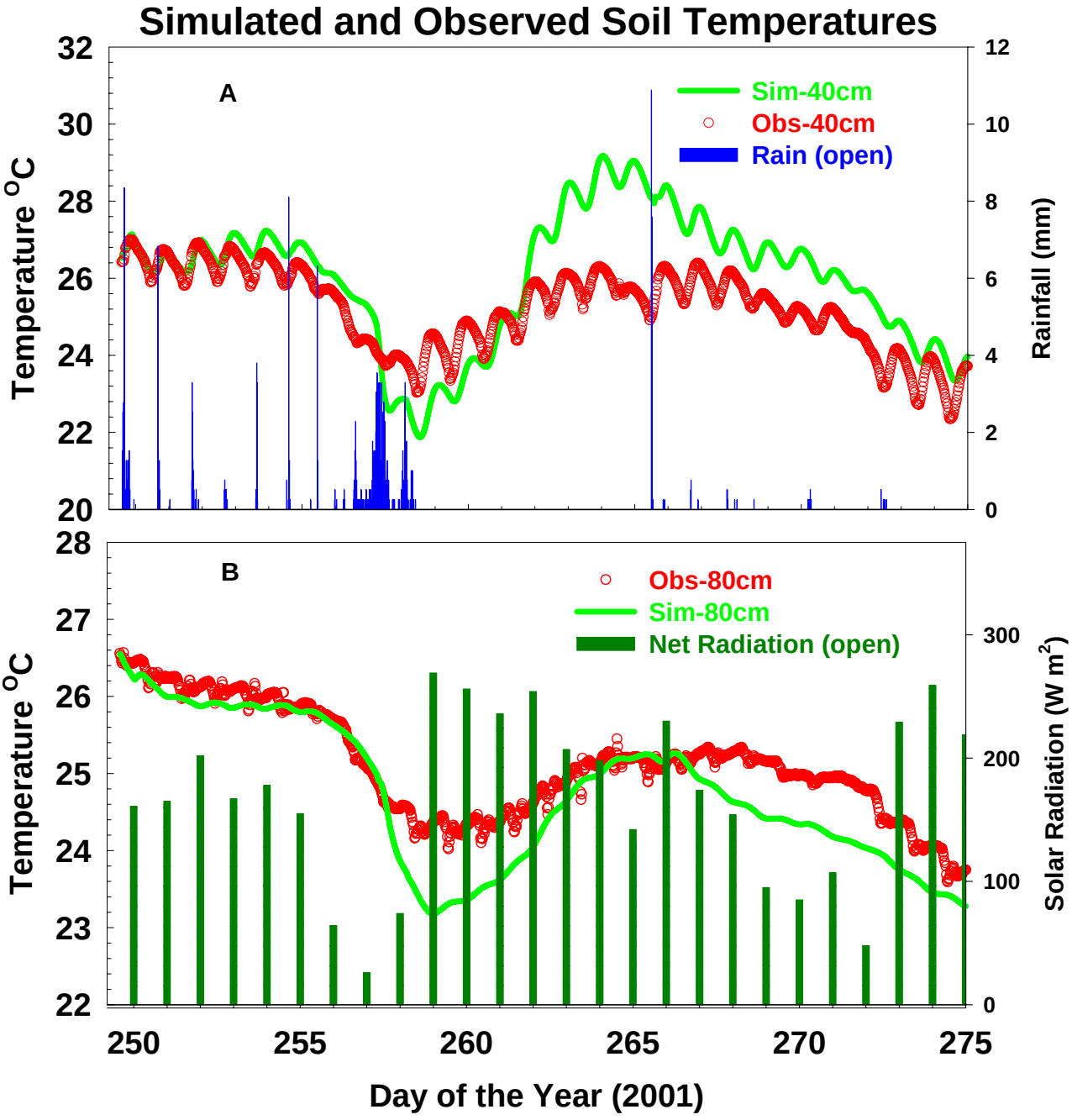

Fig. 2. Daily rainfall (A) and net radiation (B) rates (bar graphs), and measured (lines) and simulated (dots) soil temperatures at 40 cm (A) and 80 cm (B) depths.

The lowest soil temperatures were during the rainy and low net radiation days (days 256-258). This wet and overcast period was followed by a week of dry and clear sky conditions; during this period soil temperatures at both depths 40 and 80 cm increased substantially to over 26 and 25 ^{0}C, respectively. This period was followed by a cooling period with 11 mm rainfall event and substantial decrease in net radiation.

Despite the periodical decreases and increases in the soil temperature, there was an overall soil temperature decrease over this simulation period at both soil depths (Fig. 2 A and B). As expected, the amplitude of soil temperature decreased with depth as a result of the effect of damping depth. The predicted soil temperatures compared favorably with their corresponding observed data. Incoming solar radiation is the driving force of soil temperature fluctuations. Differences between simulated and measured soil temperatures as shown in (Fig. 2 A&B) are more pronounced during clear sky and warmer days. However, during relatively cooler days (overcast), differences between measured and simulated temperatures were the lowest.

References

1. Bear, J., and A. Gilman. 1995. Migration of salts in unsaturated zone caused by heating. Transp. Porous Media 19:139-156.
2. Fares, A., A.K. Alva., P. Nkedi-Kizza and M. A. Elrashidi. 2000. Determination of soil water physical properties under field conditions using capacitance probe and Guelph permeameter. Soil Sci. 165: 768-777.
3. Horton, R., and S.O. Chung. 1991. Soil heat flow. P. 397-438. In J. Hanks and J. Ritchie (ed.) Modeling plant and soil systems. Agron. Monogr. 31. ASA, CSSA, and SSSA, Madison, WI.
4. Nassar, I.N., and R. Horton. 1992. Simultaneous transfer of heat, water and solute in porous media: I. Theoretical development. Soil Sci. Soc. Am. J. 56:1350-1356.
5. Philip, J.R., and D.A. de Vries. 1957. Moisture movement in porous materials under temperature gradients. Trans. Am. Geophys. Union 38:222-232.
6. Šimůnek, J., and M. Th. van Genuchten. 1999. Using the HYDRUS-1D and HYDRUS-2D codes for estimating unsaturated soil hydraulic and solute transport parameters, in van Genuchten, M. Th., F. J. Leij, and L. Wu (eds.) *Characterization and Measurement of the Hydraulic Properties of Unsaturated Porous Media*, University of California, Riverside, CA, 1523-1536.
7. Šimůnek, J., M. Šejna, and M. Th. van Genuchten. 1999. The HYDRUS-2D software package for simulating to-dimensional movement of water, heat, and multiple solutes in variable saturated media. Version 2.0, IGWMC-TPS-53, International Ground Water Modeling Center, Colorado School of Mines, Golden, CO.
8. Vrugt, J. A., J. W. Hopmans, and J. Šimůnek. 2001. Calibration of a two-dimensional root water uptake model for a sprinkler-irrigated almond tree. Soil Sci. Soc. Am. J., 65(4):1027-1037.

Transport of sulfadiazine in soil

Anne Wehrhan[a,c], Roy Kasteel[a], Jirka Simunek[b], Joost Groeneweg[a], Harry Vereecken[a]
[a]Agrosphere Institute, ICG IV, Forschungszentrum Jülich GmbH, Germany;
[b]Department of Environmental Sciences, University of California, Riverside, US;
[c]e-mail: a.wehrhan@fz-juelich.de

Introduction

Among other veterinary pharmaceutical Sulfadiazine (SDZ) is a widely used antimicrobial substance in intensive livestock production to prevent and treat diseases (*Boxall et al.*, 2004; *Thiele-Bruhn*, 2003). Up to 40 % of the administered sulfonamides are eliminated as microbial active substances with the excretions (*Kroker*, 1983). Antibiotics such as sulfadiazine reach agricultural soils directly through grazing livestock or indirectly through the spreading of manure or sewage sludge on the field (*Jørgensen and Halling-Sørensen*, 2000). Knowledge about the fate of antibiotics in soil is crucial to assess the environmental risk of those compounds, including possible transport to groundwater.

Despite the assumed high mobility of SDZ in soil from its physicochemical properties (*Tolls*, 2001), SDZ was scarcely found in the leachate of column and plot studies and most of the applied SDZ was retained in the upper part of the soil (*Kreuzig and Höltge*, 2005). However, the fate of SDZ is not yet thoroughly investigated, partly because of analytical difficulties at the relevant low environmental concentration levels.

The objective of this study was to investigate the transport behavior of sulfadiazine in disturbed soil columns at a constant flow rate near saturation. Sulfadiazine was applied at different concentrations and for different pulse lengths. To identify relevant sorption processes, measured breakthrough curves and soil concentration profiles of sulfadiazine were fitted with a convective-dispersive transport model considering different sorption concepts. One, two and three sites sorption models were tested and their assumptions and limitations are discussed.

Materials and Methods

SDZ (Figure 1) belongs to the chemical group of sulfonamides and has a water solubility of 77 mg L^{-1}, a K_{OW} of 0.76 and two pK_a values at 1.6 and 6.5. The soil material (silty loam) was a mixed, sieved sample (2 mm) of the upper 30 cm of an Eutric Cambisol used as grassland near lake Greifensee, Switzerland, having an organic matter content of 3.3 % (mass) and a pH value of 6.1.

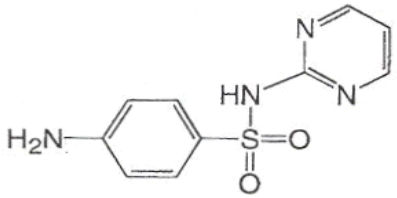

Figure 1: Chemical structure of SDZ. The ^{14}C-labelling is in the phenyl-ring.

The transport of ^{14}C labelled SDZ was investigated in disturbed soil columns (8.5 cm in diameter, 9 cm in height) at a constant flow rate near saturation. SDZ was applied in different concentrations (5.70 vs. 0.57 mg L^{-1}) for either a short or a long pulse duration (7 vs. 68 h). Breakthrough curves (BTC) of SDZ and the non-reactive tracer Cl^- where measured during 500 h. At the end of each experiment the concentration profile in the soil column was determined. Trace analysis of ^{14}C-SDZ in the water samples was done directly by liquid scintillation counting (LSC). For the soil samples total combustion was followed by LSC of the evolved and trapped $^{14}CO_2$.

The BTCs were fitted with a convective-dispersive transport model considering different sorption concepts to identify relevant sorption processes. These concepts were chosen according to the previously observed sorption behavior: In batch experiments sorption of SDZ is non-linear (Freundlich) and rate-limited. An apparent sorption equilibrium was reached only after 20 days, the desorption seems to be much slower. Time-dependent formation of non-extractable residues is frequently reported (*Kreuzig et al.*, 2003). Thus, the model needs to account for the concentration-dependent, rate-limited and possibly irreversible sorption processes.

An adapted version of HYDRUS-1D (*Simunek et al.*, 1998) was used to describe the transport experiments with SDZ. HYDRUS-1D is a finite element code which numerically solves the convection-dispersion equation. The possible solute-soil-water interaction models include one, two or three sorption sites, showing instantaneous sorption (linear or non-linear) or rate-limited reversible or irreversible sorption (Figure 2). Isotherm-based concepts were compared to the kinetic attachment/detachment concept, where all interactions are described by first-order rate processes.

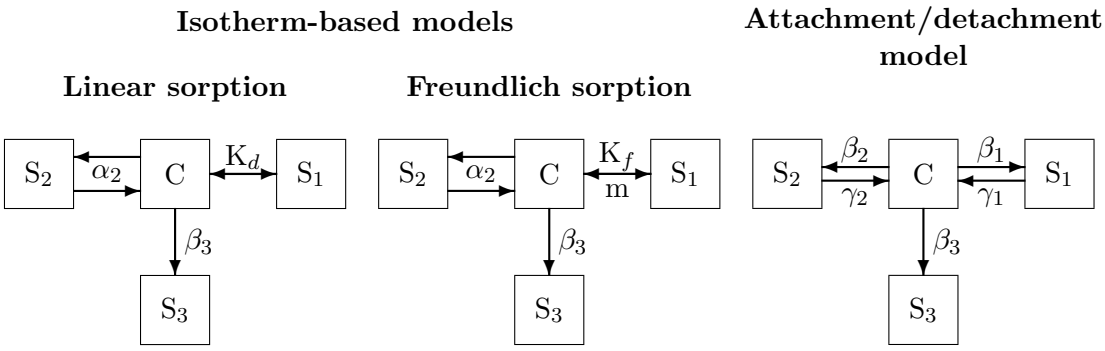

Figure 2: Applied solute-soil-water distribution concepts. The boxes labelled with C represent the liquid phase with the concentration C [M L^{-3}], the boxes S_1, S_2 and S_3 represent the three sorption sites with the respective concentrations S [M M^{-1}]. The arrows indicate the sorption process, where K_d is the distribution coefficient, K_f and m are the Freundlich coefficient and exponent, α is the reversible ad- and desorption rate [T^{-1}], β and γ are the one-way attachment and detachment rates [T^{-1}], respectively. Less complex versions of each model were derived by omitting one or two sorption sites.

Results

The BTCs are characterized by an early arrival of SDZ and an extended tailing (Figure 3(a)). The peak maxima of the different treatments were delayed relative to chloride by a factor of 2 to 5 and differed in the maximum concentration as well as the eluted mass fraction (18 % to 83 %) within the leaching period of experiments. Due to the ^{14}C-analysis the error in mass balances was as small

as 1 to 3 %. The way of application determined the fate of SDZ: (i) the longer the pulse duration and the higher the applied concentration, the more mass was leached, and (ii) the more mass was leached the later the peak concentration arrived.

The concentration profiles of SDZ for the columns with the long pulse applications show the highest concentrations at the top of the column, steadily decreasing towards the bottom (Figure 3(b)). In the column with the short pulse application the highest concentrations were found between 2 and 6 cm depth of the column.

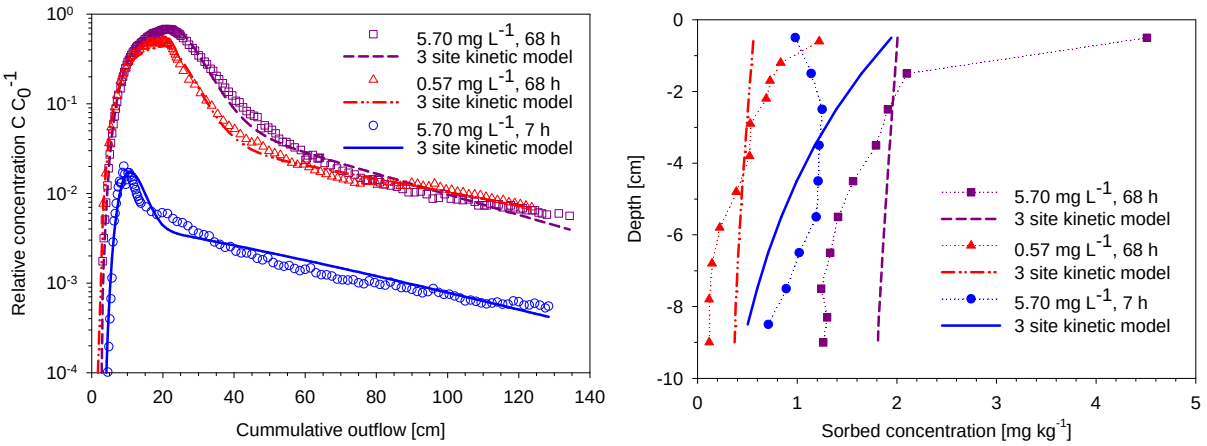

(a) (b)

Figure 3: Breakthrough curves (a) and soil concentration profiles of the residual ^{14}C concentrations (b) in the three columns. Measured data are represented by the symbols, modelled curves by the solid and dashed lines. Input concentration and pulse duration of the application scenarios are given in the legend. Note the logarithmic scale of the concentration axis for the BTCs.

The BTC of chloride were used to determine the water flow parameters volumetric water content and dispersivity. They were kept constant during the modelling of the reactive tracer. Simple equilibrium models overestimate the mobility of SDZ in soil, especially for lower application concentrations or short pulse applications. The extended tailing cannot be modelled with an one site equilibrium concept. Kinetic sorption processes allow both, an early breakthrough and a pronounced tailing. Irreversible sorption processes can account for the large mass fractions found in the soil column at the end of the experiment. Only the three site kinetic model with two reversible attachment/detachment sites and one irreversible site fitted the BTCs of all three experiments (Figure 3(a)). However, none of the models was able to describe the observed profiles (Figure 3(b)).

Conclusion

The major difficulties to fit the BTCs were the tailing and the mass recovery in the leachate. Only the complex three site kinetic sorption model with reversible and irreversible sorption sites is flexible enough to describe the observed BTCs under the variable application scenarios. Despite the good agreements for the BTCs, the observed and calculated concentration profiles in soil differed substantially. Therefore, common approaches for process identification on the basis of the main peak breakthrough without the observation of the tailing and the concentration profile are precarious.

As none of the models satisfactorily described the observed transport behavior of SDZ, the soil-water-SDZ system seems to be more complex than represented by the tested models. Due to the restricted analysis of ^{14}C only in this study, transformation of the applied SDZ cannot be ruled out. Transformation of SDZ in soil was observed by *Kreuzig and Höltge* (2005). In manure, one of the identified transformation products is even able to transform back into the parent compound (*Kroker*, 1983). In case transformation occurred in our experiments, the radio-chemical and mathematical analysis presented here described the effective behavior of the parent and possible transformation products. Because the active, re-transferable or unidentified transformation products can put the environment at an additional risk, such an effective description is still of interest.

References

Boxall, A. B. A., L. A. Fogg, P. A. Blackwell, P. Kay, E. J. Pemberton, and A. Croxford, Veterinary medicines in the environment, *Reviews of Environmental Contamination and Toxicology*, *180*, 1–91, 2004.

Jørgensen, S. E., and B. Halling-Sørensen, Drugs in the environment, *Chemosphere*, *40*, 691–699, 2000, Editorial.

Kreuzig, R., and S. Höltge, Investigations on the fate of sulfadiazine in manured soil: Laboratory experiments and test plot studies, *Environmental Toxicology and Chemistry*, *24*(4), 771–776, 2005.

Kreuzig, R., C. Kullmer, B. Matthies, S. Höltge, and H. Diekmann, Fate and behavior of pharmaceutical residues in soils, *Fresenius Environmental Bulletin*, *12*(6), 550–558, 2003.

Kroker, R., Aspects of the elimination of antibiotics after treatment of domestic animals, *Wissenschaft und Umwelt*, *4*, 305–308, 1983.

Simunek, J., M. Senja, and M. T. van Genuchten, *The HYDRUS-1D software package for simulating the one-dimensional movement of water, heat, and multiple solutes in variably saturated media. Version 2.0*, ICGWMC-TPS-70. International Ground Water Modeling Center, Colorado School of Mines, Golden, Colorado, 1998.

Thiele-Bruhn, S., Pharmaceutical antibiotic compounds in soil - A review, *Journal of Plant Nutrition and Soil Science*, *166*, 145–167, 2003.

Tolls, J., Sorption of veterinary pharmaceuticals in soils: A review, *Environmental Science and Technology*, *35*(17), 3397–3406, 2001.

Coupled reactive transport modelling based on the new biogeochemical code HP1

D. Jacques[(1)*], J. Šimůnek[(2)], D. Mallants[(1)] and M.Th. van Genuchten[(3)]

[(1)] Waste and Disposal Department, SCK•CEN, Boeretang 200, B-2400 Mol, Belgium
[(2)] Department of Environmental Sciences, A135 Bourns Hall, University of California Riverside, 900 University Avenue, Riverside, CA USA 92521
[(3)] George E. Brown, Jr. Salinity Laboratory, USDA, ARS, 450 W. Big Spring Rd, Riverside, CA USA 92507
* Corresponding author (djacques@sckcen.be)

The migration of many naturally occurring elements and contaminants in the subsurface is affected by a multitude of complex, interactive physical, chemical, mineralogical, geological, and biological processes. Cycles of precipitation and evaporation largely determine if contaminants remain near the soil surface. Changes in the chemical composition or pH of the soil solution may impact the retention of heavy metals on organic matter or iron oxides. Dissolution and precipitation of minerals generally buffer the transport of a solution with a different pH through the soil profile. Simulation of these and related processes requires a coupled reactive transport code that integrates the physical processes of water flow and advective-dispersive solute transport with a range of biogeochemical processes.

Recently, a new comprehensive simulation tool HP1 (HYDRUS1D-PHREEQC, Jacques and Šimůnek, 2005) was developed by coupling the HYDRUS-1D one-dimensional variably-saturated water flow and solute transport model (Šimůnek et al., 1998) with the PHREEQC geochemical code (Parkhurst and Appelo, 1999). The HP1 code incorporates modules simulating (1) transient water flow in variably-saturated media, (2) transport of multiple components, and (3) mixed equilibrium/kinetic geochemical reactions. The program numerically solves the Richards equation for variably-saturated water flow and advection-dispersion type equations for heat and solute transport. The flow equation incorporates a sink term to account for water uptake by plant roots. The heat transport equation considers transport due to conduction and convection with flowing water. The solute transport equations consider advective-dispersive transport in the liquid phase. The program can simulate a broad range of low-temperature biogeochemical reactions in water, soil and ground water systems including interactions with minerals, gases, exchangers, and sorption surfaces, based on thermodynamic equilibrium, kinetics, or mixed equilibrium-kinetic reactions. The program may be used to analyze water and solute movement in unsaturated, partially saturated, or fully saturated porous media. The flow region may be composed of nonuniform soils or sediments. Flow and transport can occur in the vertical, horizontal, or a generally inclined direction. The water flow part of the model can deal with prescribed head and flux boundaries, boundaries controlled by atmospheric conditions, as well as free drainage boundary conditions. The governing flow and transport equations were solved numerically using Galerkin-type linear finite element schemes. The coupled transport and reaction equations are solved by the non-iterative sequential approach. Its numerical accuracy was evaluated for a number of simulations under transient flow conditions (Jacques et al., 2005a). Graphical interfaces for both original

codes can be used with HP1 as well, enabling an easy generation of the input data and display of computational results.

HP1 is specifically developed for simulating water flow, transport and geochemical reactions in environmental soil quality problems. HP1 has been tested for a number of applications with other (less general) models (reported in Jacques and Šimůnek, 2005). Several studies (Jacques and Šimůnek, 2005, Jacques et al., 2003, Šimůnek et al., 2005) dealing with typical coupled transport phenomena demonstrated HP1's capabilities for environmental problems such as transport of heavy metals (Zn^{2+}, Pb^{2+}, and Cd^{2+}) subject to multiple cation exchange reactions, cadmium leaching in acid sandy soils, and transport of organic contaminants such as TNT or PCE (?)and its degradation products through soil.

We present here two examples: (1) Long term transient flow and transport of major cations and heavy metals in a soil profile (based on Jacques et al., 2005a), and (2) long term leaching of uranium from agricultural field soils following mineral fertilizer application (based on Jacques et al., 2005b,c) .

In the first example, transport of major cations and heavy metals in a soil profile under atmospheric boundary conditions is simulated. Two types of geochemical reactions are taken into account: (i) equilibrium aqueous speciation reactions (e.g. complexation reactions between Cd and Cl, (ii) and cation exchange reactions of both the major cations and the heavy metals. As will be illustrated, there is a strong interaction between water flow, water content, geochemical conditions (e.g. pH), speciation and mobility. For example, aqueous concentrations of the heavy metals increase significantly during summer near the soil surface. In other words, transient flow conditions also influence the bioavailability of heavy metals, since uptake processes by plants and soil micro-organisms are often concentration dependent (i.e., passive uptake of solutes together with uptake of water by roots, as well as active uptake which can be simulated with HP1 using Monod or Michealis-Menten kinetics). Moreover, the high heavy metal concentrations occur during periods with the highest (micro)biological activity during the year (the summer months). HP1 hence is thusa very useful tool for evaluating the effects of atmospheric boundary conditions on the long-term bioavailability and leaching of heavy metals in and from soils. While not further addressed here, such evaluations possibly could also account for the transport of colloids such as micro-organisms, humics or fulvics.

The second examples considers the transport of uranium (U) present in many mineral fertilizers, particularly (super)phosphates. Field soils that receive P-fertilizers accumulate U and thorium (Th) and their daughter nuclides, which eventually may leach to groundwater. Our objective was to numerically assess U migration in soils. Calculations were based on the new reactive transport model, HP1. In our simplified model, we account for interactions between U and organic matter, phosphate, and carbonate. Solid phase interactions were simulated by the combination of a cation exchange complex module (adsorption of major cations and U) and a surface complexation module (adsorption of cations and P). Furthermore, all geochemical processes were coupled with a model accounting for dynamic changes in the soil water content and the water flux. The capabilities of the code in calculating natural U fluxes to groundwater were illustrated using a semi-synthetic 200-year-long time series of climatological data for Belgium. Based on an average fertilizer application,

the input of phosphate and uranium in the soil was defined. In this example, the effect of the upper boundary condition (transient versus steady-state flow) on the migration and leaching of U was specifically addressed. Results showed that due to changing water content, water flow and, consequently, geochemical conditions (mainly pH changes), migration of U is faster under atmospheric boundary conditions than under steady-state flow.

HP1 is free software. Information on how to obtain HP1 can be found on www.sckcen.be\hp1 or by contacting one of the authors of this paper. A list of key publications is given in the references.

References

Jacques, D., Šimůnek, J., 2005. User manual of the multicomponent variably-saturated flow and transport model HP1: Description, Verification, and Examples (Version 1.0). SCK•CEN, Mol, Belgium, BLG-998, 79 p.

Jacques, D., J. Simunek, D. Mallants, and M.Th. van Genuchten, 2003. The HYDRUS-PHREEQC multicomponent transport model for variably-saturated porous media: Code verification and application. In '*Proceedings of MODFLOW and MORE 2003: Understanding through modeling'*, (Eds. E. Poeter, C. Zheng, M. Hill, and J. Doherty) MODFLOW and MORE 2003, September 16-19, 2003, International ground water modeling center, Colorado, Volume 1: 23-27

Jacques, D., Šimůnek, J., D. Mallants, and M.Th. van Genuchten, 2005a. HP1: A coupled numerical code for variably saturated water flow, solute transport and biogeochemistry in soil systems. Submitted to J. of Cont. Hydrol.

Jacques, D., Šimůnek, J., D. Mallants, and M.Th. van Genuchten, 2005b. Long term uranium migration in agricultural field soils following mineral P-fertilization. Proceedings of ICEM '05: The 10th International Conference on Radioactive Waste Management and Environmental Remediation, September 4 – 9, Glasgow, Schotland.

Jacques, D., Šimůnek, J., D. Mallants, and M.Th. van Genuchten, 2005c. Modelling uranium leaching from agricultural soils to groundwater as a criterion for comparison with complementary safety indicators. Proceedings of MRS05, Material Research Society 2005, Symposium on the Scientific Basis for Nuclear Waste Management, September 12-15, Ghent, Belgium.

Parkhurst, D.L., and C.A.J. Appelo, 1999. User's guide to PHREEQC (Version 2) – A computer program for speciation, batch-reaction, one-dimensional transport, and inverse geochemical calculations. Water-Resources Investigations, Report 99-4259, Denver, Co, USA, 312 pp.

Šimůnek, J., D. Jacques, M.Th. van Genuchten, and D. Mallants, 2005. Multicomponent geochemical transport modeling using the HYDRUS-1D computer software package. 2005 Summer Speciality conference, Institutions for sustainable watershed management: Reconciling physical and management ecology in the Asia-Pacific, American Water Resources Association, Hyatt Regency Waikiki Resort & Spa, Honolulu, HI, June 27-29 2005.

Šimůnek, J., M. Šejna, and M.Th. van Genuchten, 1998. The HYDRUS-1D software package for simulating the one-dimensional movement of water, heat, and multiple solutes in variably-saturated media. Version 2.0, IGWMC-TPS-70, International Ground Water Modeling Center, Colorado School of Mines, Golden, CO, 202 p.

The multi-component reactive transport module CW2D for subsurface flow constructed wetlands

Guenter Langergraber[1], Jirka Simunek[2]

[1] Institute of Sanitary Engineering and Water Pollution Control, BOKU - University of Natural Resources and Applied Life Sciences, Vienna, Muthgasse 18, A-1190 Vienna, Austria. *Guenter.Langergraber@boku.ac.at*
[2] Department of Environmental Sciences, University of California Riverside, Riverside, CA 92521, USA. *Jiri.Simunek@ucr.edu*

Abstract

Constructed wetlands (CWs) are becoming increasingly popular worldwide for removing organic matter, nutrients, trace elements, pathogens, or other pollutants from wastewater and/or runoff water. CWs represent a very complex mixture of water, substrate, plants, litter, and a variety of micro-organisms, in which a large number of simultaneous processes takes place. To describe this complex system of mutually dependent physical, chemical and biological reactions and chemical and biological compounds is almost impossible without the help of a numerical model that can consider the majority of these interactions. Water flow regime in subsurface vertical flow constructed wetlands is also highly dynamic, adding to the complexity of the overall system by requiring a transient variably-saturated flow model.

The multi-component reactive transport module CW2D, which is an extension of the variably-saturated water flow and solute transport program HYDRUS-2D (Simunek et al., 1999), includes biochemical transformation and degradation processes in subsurface flow constructed wetlands. The biochemical components defined in CW2D include dissolved oxygen, three fractions of organic matter (readily- and slowly-biodegradable, and inert), four nitrogen compounds (ammonium, nitrite, nitrate, and dinitrogen), inorganic phosphorus, and heterotrophic and autotrophic micro-organisms. Organic nitrogen and organic phosphorus were modelled as part of the organic matter. The biochemical degradation and transformation processes were based on Monod-type rate expressions. All process rates and diffusion coefficients were assumed to be temperature dependent. Heterotrophic bacteria were assumed to be responsible for hydrolysis, mineralization of organic matter (aerobic growth) and denitrification (anoxic growth). Autotrophic bacteria were assumed to be responsible for nitrification, which is modelled as a two-step process. Lysis was considered to be the sum of all decay and sink processes.

CW2D/HYDRUS-2D was developed to model processes in subsurface flow constructed wetlands intended for wastewater treatment. However, the model has already been successful applied to constructed wetlands for the treatment of combined sewer overflows (Dittmer et al., 2004; Henrichs et al., 2005). Possible future applications could also include a) constructed wetlands for other types of wastewater, such as industrial and agricultural wastewaters having compositions similar to municipal wastewater, b) infiltration of treated (waste)water into soil for groundwater recharge or other applications, c) carbon and nitrogen cycling in soils, d) processes in natural wetlands, and e) processes in riparian areas.

Implementation of CW2D into the HYDRUS-2D user interface

Pre-processing

To activate the CW2D module in the HYDRUS-2D graphical user interface the heading "CW2D" has to be written in the "Main Processes" window (Figure 1). The main changes are concentrated in the solute transport part. In the "Solute Transport" the number of solutes has to be set to 13 (12 CW2D module compounds and one non-reactive tracer compound, that is independent from the other 12 compounds). Figure 2 and Figure 3 show the two user interface windows for the CW2D model parameters.

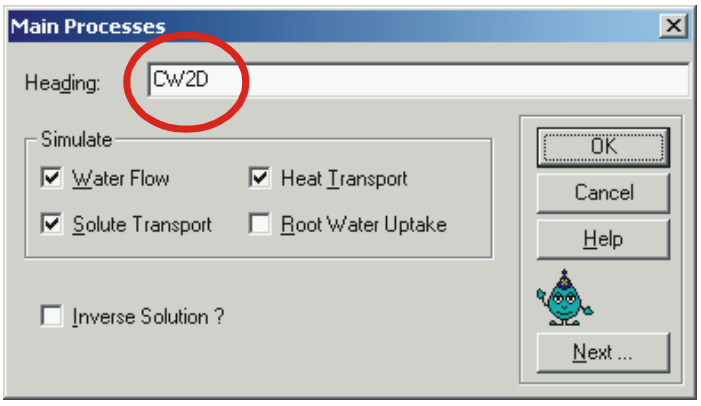

Figure 1: "Main Processes" window.

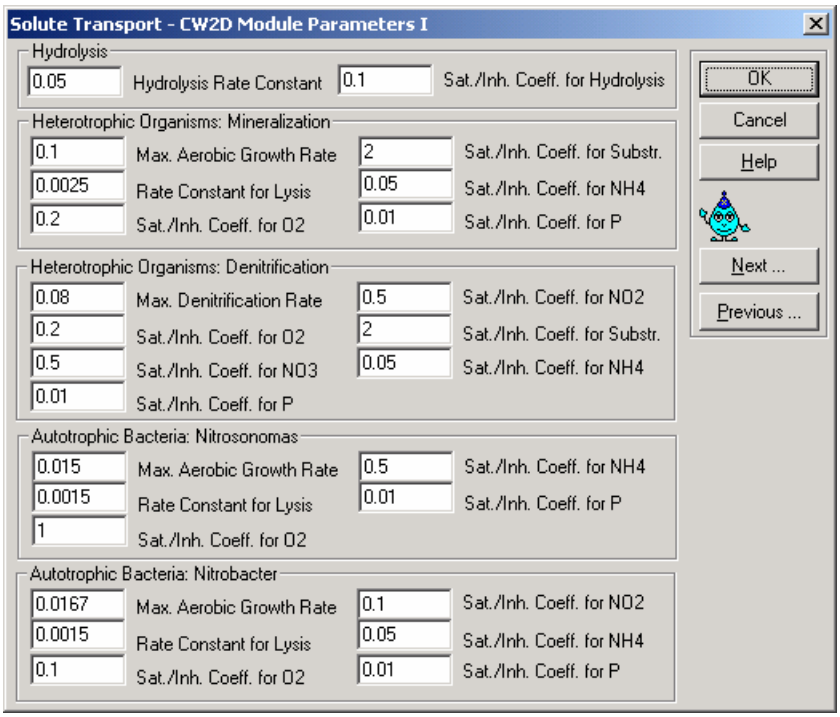

Figure 2: "Solute Transport – CW2D Model Parameters I" window (time unit: d).

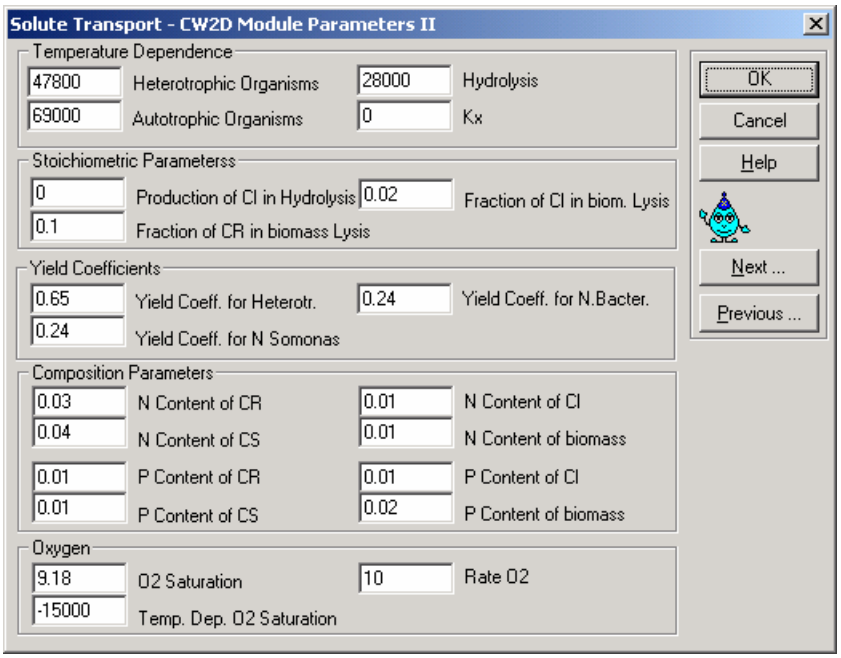

Figure 3: "Solute Transport – CW2D Model Parameters II" window (time unit: d).

Figure 4 shows the definition of the pressure head initial conditions in the "Boundary Conditions" window. Names of all compounds appear in the listbox in the left sidebar, with the "L" letter denoting the concentration in the liquid phase and "S" the concentration in the solid phase.

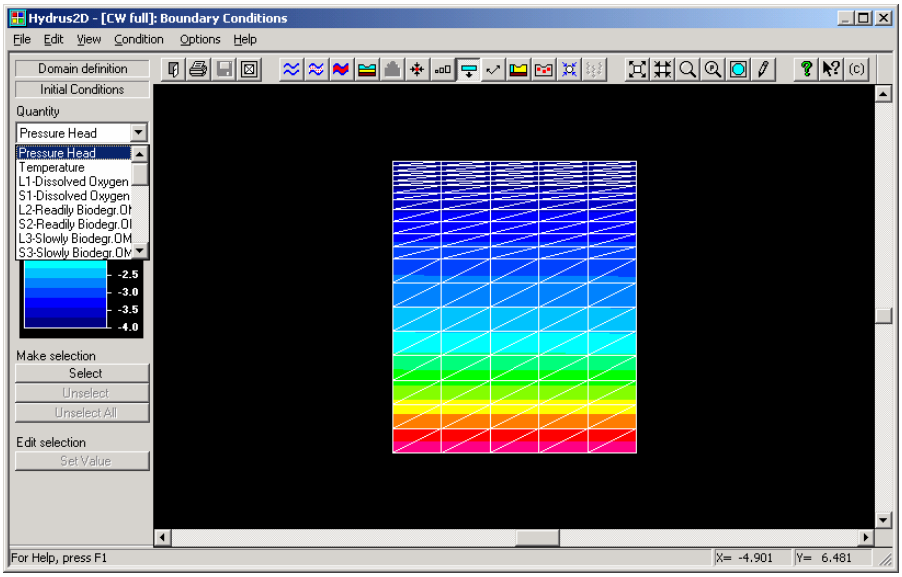

Figure 4: "Boundary Conditions" window – initial conditions.

Post-processing

Listboxes in the "Graphical Display of Results" window (not shown) and the "Observation Nodes" window (Figure 5) list names of all variables, including all biochemical compounds, that can be displayed.

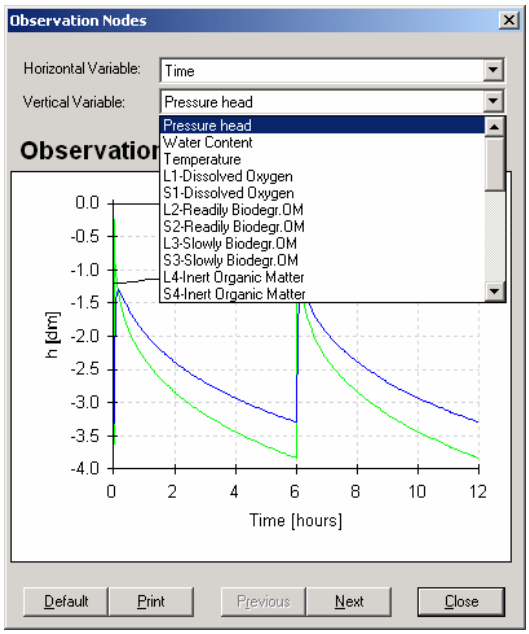

Figure 5: "Observation Nodes" window.

Publications:

Dittmer, U., Meyer, D., Langergraber, G. (2005): Simulation of a Subsurface Vertical Flow Constructed Wetland for CSO Treatment. *Water Science and Technology* 51(9), 225-232.

Henrichs M., Langergraber G., Uhl M. (2005): Modelling of organic matter degradation in constructed wetlands for treatment of combined sewer overflow. In: *Proceedings International Symposium on "Wetland Pollutant Dynamics and Control – WETPOL"*, 4-8 September 2005, Gent, Belgium.

Langergraber G. (2001): Development of a simulation tool for subsurface flow constructed wetlands. *Wiener Mitteilungen* 169, Vienna, Austria, 207p, ISBN 3-85234-060-8.

Langergraber, G. (2003): Simulation of subsurface flow constructed wetlands - Results and further research needs. *Water Science and Technology* 48(5), 157-166.

Langergraber, G. (2005a): The role of plant uptake on the removal of organic matter and nutrients in subsurface flow constructed wetlands – A simulation study. *Water Science and Technology* 51(9), 213-223.

Langergraber, G. (2005b): Simulation of the treatment performance of outdoor subsurface flow constructed wetlands in temperate climates. In: *Proceedings International Symposium on "Wetland Pollutant Dynamics and Control – WETPOL"*, 4-8 September 2005, Gent, Belgium.

Langergraber, G., Šimůnek, J. (2005): Modeling variably-saturated water flow and multi-component reactive transport in constructed wetlands. *Vadose Zone Journal (accepted)*.

Šimůnek, J., Šejna, M., van Genuchten, M.Th. (1999): The HYDRUS-2D software package for simulating two-dimensional movement of water, heat, and multiple solutes in variably saturated media. Version 2.0. *IGWMC - TPS - 53,* International Ground Water Modeling Center, Colorado School of Mines, Golden, Colorado, 251p.

Toscano, A., Langergraber, G., Consoli, S., Cirelli, G.L., Haberl, R. (2005): A simulation study for pilot-scale 2-stage subsurface flow constructed wetlands for wastewater treatment. In: *Proceedings International Symposium on "Wetland Pollutant Dynamics and Control – WETPOL"*, 4-8 September 2005, Gent, Belgium.

Numerical Analysis of One-Dimensional Coupled Water, Vapor and Heat Transport in the Vadose Zone using HYDRUS

Hirotaka Saito[1], Jiri Šimůnek[1], and Binayak P. Mohanty[2]
[1] Department of Environmental Sciences, University of California, Riverside, CA
[2] Biological and Agricultural Engineering, Texas A&M University, College Station, TX

ABSTRACT

Although it is well known that water and/or vapor flow and heat transport processes are closely coupled and strongly affect each other in the vadose zone of arid or semi-arid regions, their simultaneous interactions are rarely considered. In this study, we implemented in the HYDRUS-1D code the coupled movement of water, vapor, and heat in the subsurface, as well as interactions of these subsurface processes with the mass and energy balance at the soil surface. The code considers the movement of liquid water and water vapor in the subsurface to be driven by both pressure head (isothermal transport) and temperature (thermal transport) gradients. The heat transport module considers movement of soil heat by conduction, convection of sensible heat by water flow, transfer of latent heat by diffusion of water vapor, and transfer of sensible heat by diffusion of water vapor. The developed code allows a very flexible way of using various types of meteorological information at the soil-atmosphere interface for evaluating surface water and energy balance.

INTRODUCTION

The simultaneous movement of water, vapor and heat in the vadose zone of arid or semi-arid regions is of great interest in evaluating water and energy balance of subsurface environments for both agriculture and engineering applications. Although it is widely recognized that the movement of water, vapor, and heat are closely coupled and strongly affect each other, their mutual interactions are rarely considered in practical applications. The effect of heat transport on water flow is often neglected, arguably because of model complexity and a lack of data to fully parameterize the model, but partly also because of the unavailability of a user friendly simulation code.

The main objective of this study thus was to develop a numerical model for coupled water, vapor, and heat transport that, together with a surface water and energy balance, can be used to predict volumetric soil water contents and soil temperatures under field conditions. The goal was to develop a model that would provide much flexibility in accommodating various types of meteorological data that can be collected at various time intervals (daily, hourly, or other time intervals). The coupled movement of water, vapor, and heat in the subsurface, as well as an energy and water balance at the soil surface, was implemented in the HYDRUS-1D code (Šimůnek et al., 1998).

Model performance was subsequently evaluated by simulating continuous changes in water contents, temperatures, and fluxes in a bare field soil. The coupled model was compared against field soil temperature and water content data collected at different depths at a field site near the University of California Agricultural Experiment Station in Riverside, California, during the fall of 1995.

THEORY

Water and Vapor Flow

The governing equation for one-dimensional flow of water and vapor in a variably saturated rigid porous medium is given by the following mass conservation equation:

$$\frac{\partial \theta}{\partial t} = \frac{\partial}{\partial z}\left[K_{Lh}(h)\frac{\partial h}{\partial z} + K_{Lh}(h) + K_{LT}(h)\frac{\partial T}{\partial z} + K_{vh}\frac{\partial h}{\partial z} + K_{vT}\frac{\partial T}{\partial z}\right] - S$$
$$= \frac{\partial}{\partial z}\left[K_{Th}\frac{\partial h}{\partial z} + K_{Lh} + K_{TT}\frac{\partial T}{\partial z}\right] - S \qquad [1]$$

where θ is the total volumetric water content (-), h is the pressure head (L), T is the temperature (K), t is time (T), z is the spatial coordinate positive upward, S is a sink term, K_{Lh} (LT^{-1}) and K_{LT} ($L^2K^{-1}T^{-1}$) are the hydraulic conductivities for liquid phase fluxes due to gradient of h and T, respectively, K_{vh} (LT^{-1}) and K_{vT} ($L^2K^{-1}T^{-1}$) are the isothermal and thermal vapor hydraulic conductivities (Philip and de Vries, 1957), respectively, and K_{Th} (LT^{-1}) and K_{TT} ($L^2K^{-1}T^{-1}$) are the isothermal and thermal total hydraulic conductivities, respectively.

Heat Transport

The governing equation for the movement of energy in a variably saturated porous medium is given by the following energy conservation equation:

$$\frac{\partial C_p T}{\partial t} + L_0\frac{\partial \theta_v}{\partial t} = \frac{\partial}{\partial z}\left[\lambda(\theta)\frac{\partial T}{\partial z}\right] - C_w\frac{\partial q_L T}{\partial z} - L_0\frac{\partial q_v}{\partial z} - C_v\frac{\partial q_v T}{\partial z} - C_w S T \qquad [2]$$

where T is the temperature (K), θ_n is a volumetric fraction of solid phase (-), C_n, C_w, C_v and C_p are volumetric heat capacities ($Jm^{-3}K^{-1}$, $ML^{-1}T^{-2}K^{-1}$) of solid phase, liquid water, water vapor, and moist soil (de Vries, 1963) , respectively, L_0 is the volumetric latent heat of vaporization of water (Jm^{-3}, $ML^{-1}T^{-2}$), $\lambda(\theta)$ is the apparent thermal conductivity of soil ($Jm^{-1}s^{-1}K^{-1}$, $MLT^{-3}K^{-1}$), and q_L and q_v are flux densities of liquid water and water vapor (LT^{-1}), respectively.

Surface Energy Balance

Surface precipitation-irrigation-evaporation and heat fluxes are used as boundary conditions for water and vapor flow and heat transport, respectively. Evaporation and heat fluxes can be calculated precisely only from the surface mass and energy balance (e.g., van Bavel and Hillel, 1976):

$$R_n - H - LE - G = 0 \qquad [3]$$

where R_n is net radiation (Wm^{-2}, MT^{-3}), H is the sensible heat flux density (Wm^{-2}, MT^{-3}), LE is the latent heat flux density (Wm^{-2}, MT^{-3}), L is the latent heat (J kg^{-1}, L^2T^{-2}), E is the evaporation rate ($ML^{-2}T^{-1}$), and G is the surface heat flux density (Wm^{-2}, MT^{-3}). While R_n and G are positive downward, H and LE are positive upward. The modified version of HYDRUS-1D can either directly use measured continuous values of net radiation, R_n, and other meteorological variables, or it can calculate continuous vales from daily meteorological data (e.g., Saito et al., submitted).

Numerical Simulations

Study Site

Soil temperature and water content variations were measured near the soil-air interface at 20 and 40 minutes intervals, respectively, at depths of 2, 7, and 12 cm near the University of California Agricultural Experiment Station in Riverside, California, during the fall of 1995 (November 23, "day of year" or DOY 327, through December 5, DOY 339; Mohanty et al. 1998). The experimental field was irrigated twice during the measurement period on DOY 334 and DOY 335 with a sprinkler system. Daily standard meteorological information obtained from the weather station in Riverside was used. The soil at the experimental site was characterized as a Arlington fine sandy loam (coarse-loamy, mixed, thermic, Haplic Durixeralf).

Results

Soil water contents and soil temperatures at three different depths (2, 7, and 12 cm) at the experimental site were numerically simulated from DOY 328 to DOY 339 using the coupled water, vapor, and heat transport features implemented in HYDRUS 1D. Initial conditions were determined from measured values on DOY 328.

Fig. 1 shows measured and simulated water contents at the 2 cm depth. Predicted water contents follow the measured values fairly well during the entire simulation period. Rapid increases of the water content after irrigation on days 334 and 335 are predicted well. Fig. 2 depicts simulated and measured soil temperatures at the 7 cm depth. Both simulated and measured temperatures show typical sinusoidal diurnal behavior.

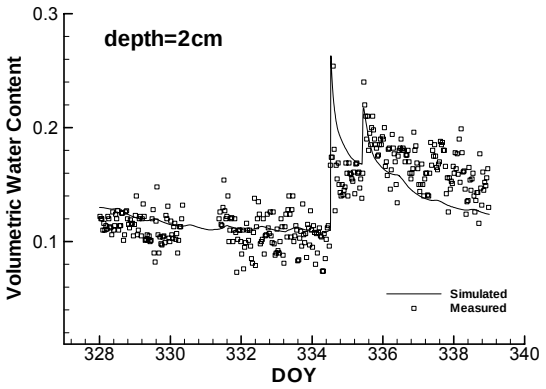

Fig. 1: Simulated (line) and measured (open circles) water content at 2 cm depth.

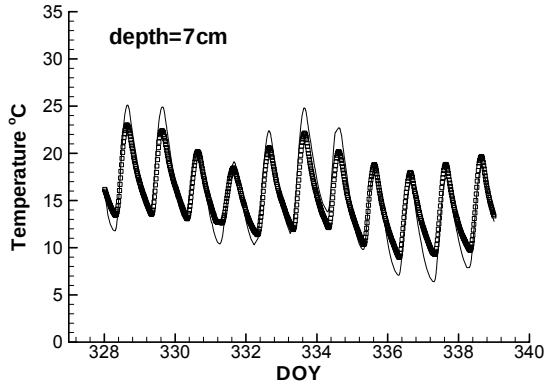

Fig. 2: Simulated (line) and measured (open circles) soil temperatures at 7 cm depth.

Depth profiles of simulated vapor fluxes and liquid water fluxes after irrigation are depicted in Fig. 3. Liquid water fluxes in the top layer are upward due to evaporation, while they are downward (i.e., negative fluxes) in the rest of the soil profile due to further infiltration and redistribution of irrigated water. Water vapor flows downward during the day across the soil profile due to temperature gradients, while it moves upward during the night. Vapor fluxes become much smaller after irrigation due to increased

gaseous tortuosity in the reduced soil air content. During the day, downward vapor fluxes thus transport latent heat to deeper depths, while during night the latent heat flux moves in the upward direction. Liquid water fluxes reflect mainly the water content distribution in the soil and not the temperature distribution. This coupled physical process thus indeed requires a mathematical/computer model that describes the coupled movement of water, vapor, and heat.

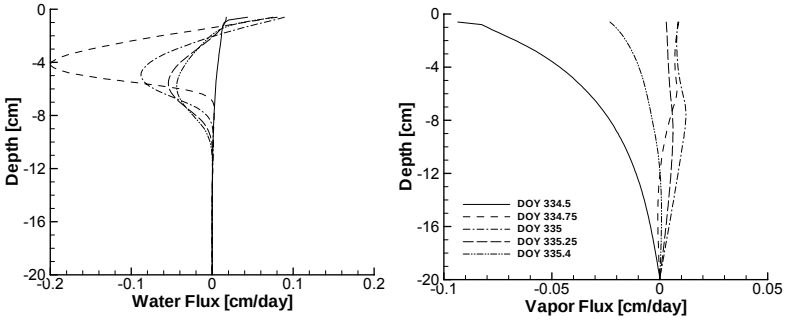

Fig. 3: Simulated vapor flux, and liquid water flux at noon of DOY 334, and 6, 12, 18, 24 hours after. Light irrigation was applied at noon of DOY 334.

This study demonstrates capabilities of the modified HYDRUS-1D program to simulate coupled water, vapor, and heat transport. Limited daily meteorological information can be used to predict soil temperatures and water contents reasonably well using the model.

Acknowledgements

This work was supported in part by SAHRA (Sustainability of semi-Arid Hydrology and Riparian Areas) under the STC Program of the National Science Foundation, Agreement No. EAR-9876800 and the Terrestrial Sciences Program of the Army Research Office (Terrestrial Processes and Landscape Dynamics and Terrestrial System Modeling and Model Integration). Mohanty acknowledges the support by NASA-Global Water and Energy Cycle grant NAG5-11702.

REFERENCES

[1] de Vries, D.A. 1963. The thermal properties of soils. p.210-235. *In* R.W. van Wijk (ed.) Physics of plant environment. North Holland, Amsterdam.

[2] Mohanty, B.P., P.J. Shouse, and M.T. van Genuchten. 1998. Spatio-temporal dynamics of water and heat in field soil. *Soil Tillage Res.* 47:133-143.

[3] Philip, J.R., and D.A. de Vries. 1957. Moisture movement in porous materials under temperature gradient. *Trans. Am. Geophys. Union.* 38:222-232.

[4] Saito, H., J. Šimůnek, and B.P. Mohanty. Using Surface Energy Balance and Limited Meteorological Information for Numerical Analysis of Coupled Water, Vapor and Heat Transport in the Vadose Zone*, Vadose Zone J.* Submitted.

[5] Šimůnek, J., M. Sejna, and M.T. van Genuchten. 1998. The HYDRUS-1D software package for simulating the one dimensional movement of water, heat, and multiple solutes in variably-saturated media. Version 2.0. IGWMC-TPS-70. International Groundwater Modeling Center, Colorado School of Mines, Golden, CO.

[6] van Bavel, C.H.M., and D.I. Hillel. 1976. Calculating potential and actual evaporation from a bare soil surface by simulation of concurrent flow of water and heat. *Agri. Meteorol.* 17:453-476.

Imprecise simulation of salt dynamic and balance – a Hydrus-1D flaw?

Irina Forkutsa and Rolf Sommer

Center for Development Research (ZEF), University of Bonn
Walter-Flex-Str.3, 53113 Bonn
Tel: +49 228 73 4636
e-mail: **forkutsa@yahoo.com**
web-page: http://www.zef.de

Introduction

The arid and semi-arid region of Khorezm in Uzbekistan is characterized by long and dry summers and short rainy/snowy winters; the agricultural production fully relies on irrigation. The development of huge-scale and massive irrigation schemes under conditions of improperly working drainage systems led to rising groundwater tables, drastically changing the local and regional hydrology. Salt accumulation in the root zone of the crops is an almost inevitable consequence adversely affecting crop growth. However over the past century farmers gained knowledge and experience how to manage the situation and use saline soil and partly saline water to produce crops. First of all, by applying high water amounts of water before the cropping period in March ("leaching") salts are washed out of the soil profile. Secondly, high amount of irrigation water might also temporarily decrease salt concentration in the root zone ("irrigation-leaching").

The objectives of this study was to estimate the water and salt balances as well as the capillary rise of saline shallow groundwater at irrigated field in Khiva district of the Khorezm region. In this paper the 2003-results of the salt balance estimation for one location at a sandy loam field are presented. To understand the processes of water flow and salt transport in soils of Khorezm, we applied Hydrus-1D.

Methods

A field experiment was conducted to monitor the water and salt distribution and to assess small-scale spatial differences. The research was focused on three points in a sandy loam field during the vegetation seasons of 2002 and 2003. The groundwater table and its salinity, the electrical conductivity of soil saturation paste (EC_p), and the gravimetric soil water content and soil tension were repeatedly determined at different depths along the field. A factor of 3.5 was used to convert EC_p into electrical conductivity of the saturated extract (EC_e). Furthermore, based on own data and regression analyses, a factor 0.042 was applied to convert EC_e into salt concentrations

(*TDS* in g 100 g^{-1} soil). Tensiometers were installed prior to the first irrigation event (16 July) and were kept in the sandy loam field until the end of the vegetation season (30 September). Meteorological data were monitored with a weather-station in the vicinity of the fields; applied water during three leaching and five irrigation events was quantified with Cipoletti weirs. Soil hydraulic properties were estimated from bulk density and soil texture with Rosetta DLL v.1.1. The single porosity model of Van Genuchten-Mualem with an air entry value of -2 cm was selected as the hydraulic model. The Van Genuchten parameters were inversely optimized based on tensiometers readings and volumetric soil moisture. The atmospheric boundary conditions with a surface layer and the groundwater table and its salinity were selected as upper and low boundary conditions. Solute transport and reaction parameters as the longitudinal dispersivity (L_{dis}) and the adsorption isotherm coefficient (K_d) were inversely optimized based on salt concentration along the 1m-depth soil profile and of groundwater. They were constrained to $1<L_{dis}\leq 1000$ and $0<k_d<0.35$.

The salt balance of the rooting zone can be calculated using two Hydrus output files: solute.out and nod_inf.out. The nod_inf.out file provides information about soil moisture, water fluxes and salt concentration of the simulated profile for any selected day. In the study two ways to calculate the salt balance were used:

(a) Method 1

Multiplying the soil moisture (θ; cm^3 cm^{-3}) with salt concentration (C; mg cm^{-3}) and the length of each particular soil increment between two consecutive nodes (z; cm) at a considered point in time (t) and adding it up over the rooting zone results in the amount of salt stored in the soil profile at that date. The difference between two consecutive dates reveals the amount of salt that has been added to, or was leached out of the rooting zone (ΔQ; mg cm^{-2}):

$$\Delta Q = \sum_{N=1}^{N} \left[\theta_i \cdot C_i \cdot \left(z_{i+1} - z_i\right)\right]_{t1} - \sum_{N=1}^{N} \left[\theta_i \cdot C_i \cdot \left(z_{i+1} - z_i\right)\right]_{t2} \qquad \text{Eq. 1}$$

(b) Method 2

Adding cumulative inputs (via irrigation [file solute.out] and/or upward movement of salts [file nod_inf.out]) and outputs of salts (via leaching [file nod_inf.out] at the bottom of the rooting zone) for a given period:

$$\Delta Q = \sum_{t1}^{t2} \left\{\left[C_{top} \cdot Flux_{top} \cdot \left((j+1) - j\right)\right] - \left[C_{bot} \cdot Flux_{bot} \cdot \left((j+1) - j\right)\right]\right\} \qquad \text{Eq. 2,}$$

whereas Flux is the flow of water (cm d^{-1}) and j and j+1 represent the current and next time levels of the simulation run.

Results and discussion

The model only poorly reproduced the rapid salt concentration fluctuations (Figure 1) during the simulation period from 13 February till 18 November (RMSE equal to 1.86 to 3.22 mg cm^{-3}).

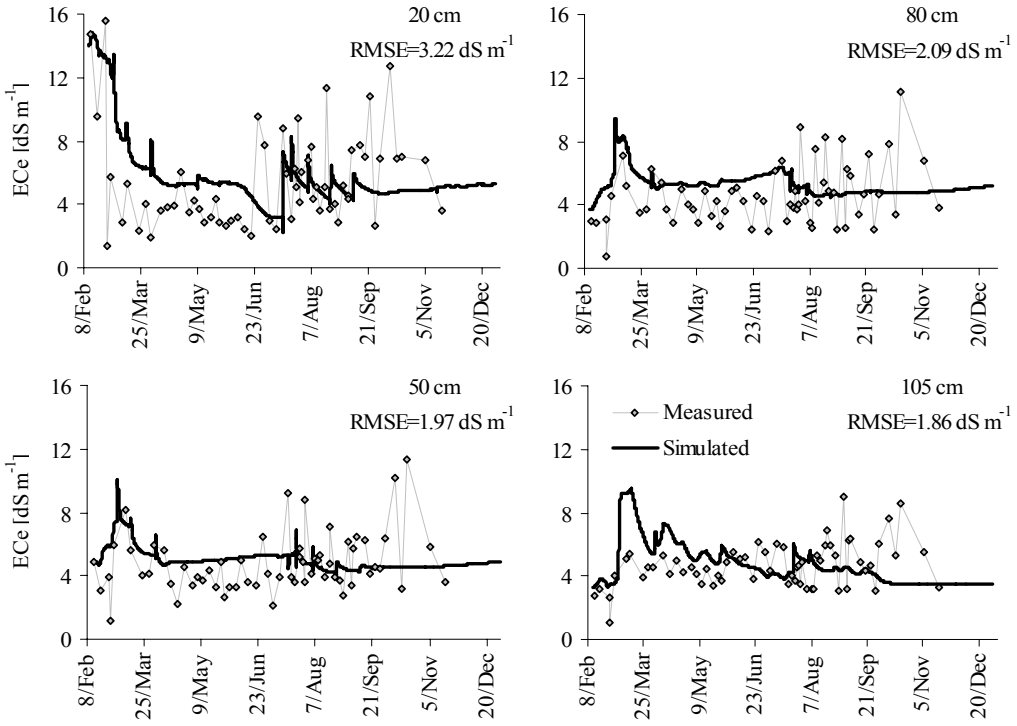

Figure 1 Comparison of measured and simulated electrical conductivity of saturated extract at different depths of sandy loam field in 2003 (middle location)

This might be due to wrong estimates of the solute transport and reaction parameters (L_{dis} and K_d), which are essential for the simulation of solute transport. Furthermore, there was strong influence from the saline groundwater (bottom boundary condition), which fluctuated comparatively less. Nevertheless, the simulation results of solute transport provided reasonable insight into seasonal salt balance of the monitored fields over the cotton root zone, because the simulated and observed salt concentration in the beginning and in the end of the simulation period were in good agreement.

Determining the salt balance of the rooting zones with the two different methods revealed some discrepancies (Table 1). Considering the whole season, the calculated

salt storage by method 2 was two times lower than with method 1, constituting 35 t ha^{-1} versus 18 t ha^{-1} of leached salts. The reasons for discrepancies between the two methods remain vague. A six-hour time step was used to compute the salt quantities according to equation 2. Thus a small rounding error in these calculations was tolerated (extrapolating momentary concentrations and fluxes). Nevertheless it should not amount to ~100 % deviation between these two applied methods. Possibly, discrepancies are the result of an accumulating – and thus emphasizing – mass-balance error when using off-rounded water fluxes or salt concentrations provided by the model.

Table 1 Salt balance [t ha^{-1} 90cm^{-1}] calculated by the two methods (eq. 1 and 2) of the sandy loamy field (middle location), 2003

Date	Method 1	Method 2	
	Salts stored	Salt input via leaching or irrigation	Salt outflow (drainage) at the bottom of profile
13-Feb	46.3	0.0	0.0
25-Apr	29.1	3.9	-42.2
04-Oct	25.8	7.3	-46.9
31-Dec	28.5	7.3	-42.2
Differences stored			
13 Feb - 25 Apr	-17.2	-38.3	
25 Apr - 4 Oct	-3.3	-1.3	
4 Oct - 31 Dec	2.7	4.7	
13 Feb - 31 Dec	-17.8	-34.9	

Conclusion

The solute transport simulation failed to mimic the rapid change in the observed soil salinity. Further research is necessary to detect the underlying causes. Additionally, there remains the need for checking the causes of mismatching salt balances calculated based on either salt-store or salt-in/outflow.

Application of Hydrus2D to derive a water balance in a karst dominated catchment

Manfred Fink & Marcel Wetzel
Institute of Geography, Department of Geoinformatics,
Friedrich-Schiller-University Jena, Loebdergraben 32, 07743 Jena

1. Introduction

The forest of the national park Hainich is one of the largest deciduous forest ecosystems in middle Europe. In the centre of the protected zone the forest is unmanaged since more then 50 years. The age of the trees goes up to 250 years. Therefore this site is used to determine, whether old woods are carbon sinks or they are in equilibrium.
Hence the Hainich was instrumented by a variety of sensors to measure carbon fluxes e.g. an eddy flux tower for the measurement of carbon dioxide exchange between forest and atmosphere. Resulted balances of carbon indicates a sink term of about 5 t carbon/ha*a for the whole system. This can not be explained by the measurements of storages and fluxes.
This result suggests to quantify the amount of carbon leaving the system as dissolved carbon related with the movement of water. While the hydrology in the study area is characterized by a karst system it is almost impossible to measure the discharge directly. We measure soil moisture with Frequency Domain Reflectrometry (FDR) probes to estimate the hydrologic fluxes of the Hainich site. To get a reasonable water balance we used the Hydru2D model.

2. Study area

The study area is located in the Hainich site in the western part of Thuringia, Germany. The altitude varies between 480 and 400 m above sea level. The annual average precipitation is approx. 700 mm. Annual average temperature ranges around 7° C. The geology is dominated by limestones with karstic phenomen. Soils developed from this bedrock are cambisols with a high content of clay (40 – 65 %) increased with soil depth. During events of high precipitation or snow melt the clay rich subsoil with its low hydraulic conductivity which leads to lateral subsurface flow. The forest is dominated by beech (Fagus sylvatica) combined with ash (Fraxsinus excelsior) and sycamore maple (Acer pseudoplatanus).

3. Measurement program

To study the water dynamics we instrumented hill slope catena in the study area with equipment for hydrological measurements. The measurement period was from August 2001 to November 2003. In particular we installed 13 FDR-Probes stations with 5 sensors in depths varying between 10 and 100 cm. At the valley bottom we installed one groundwater gauges which measures only periodic saturation. Additionally one runoff gauge was set up to measure the periodic stream (Figure 1). A rain gauge at every station was completed to measure trough fall. Observed data was recorded by data loggers with telemetry unit in a 5 minute interval. To characterize soils we accomplished field campaigns. Therefore we took samples for soil texture, organic carbon, bulk density, saturated hydraulic conductivity and soil porosity. These have been analysed in the laboratory. The observed data are used for model parameterization and validation.

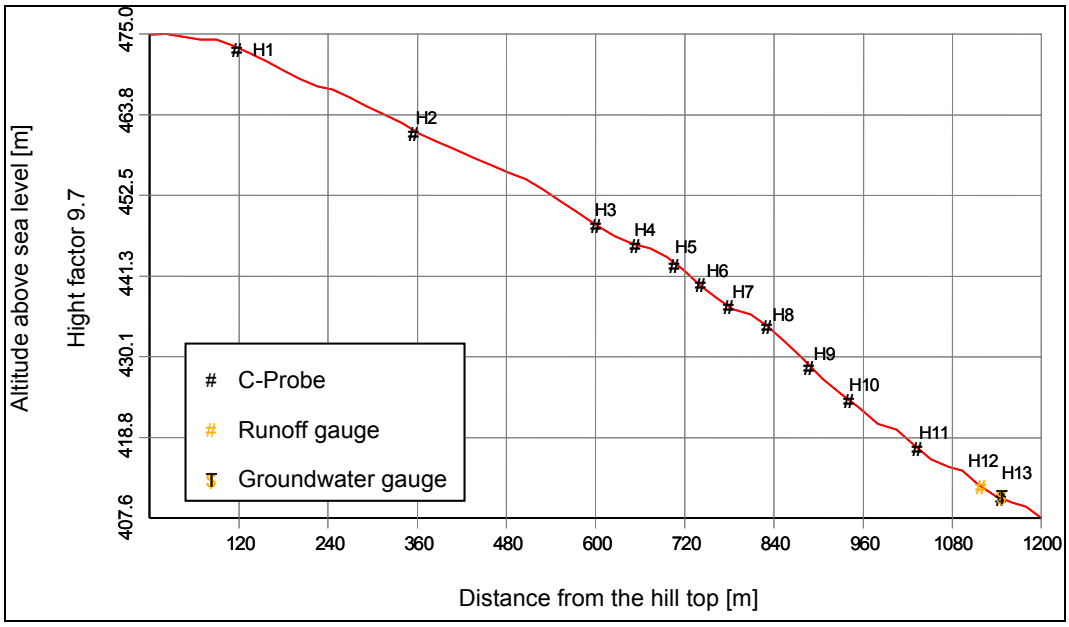

Figure 1: Profile of the instrumented hill slope catena.

4. Modelling

To model the soil water dynamics we used the vadose zone model Hydrus2D (Šimůnek & van Genuchten 1999). The model domain for the instrumented hill slope was 1137m long and the altitude difference was 64.5m which leads to a very gentle slope of 5.7%. The parameterized soil depth was 1.4 m at the upper hill, and 2 m in the valley. The domain consists of 246950 nodes (Figure 2).

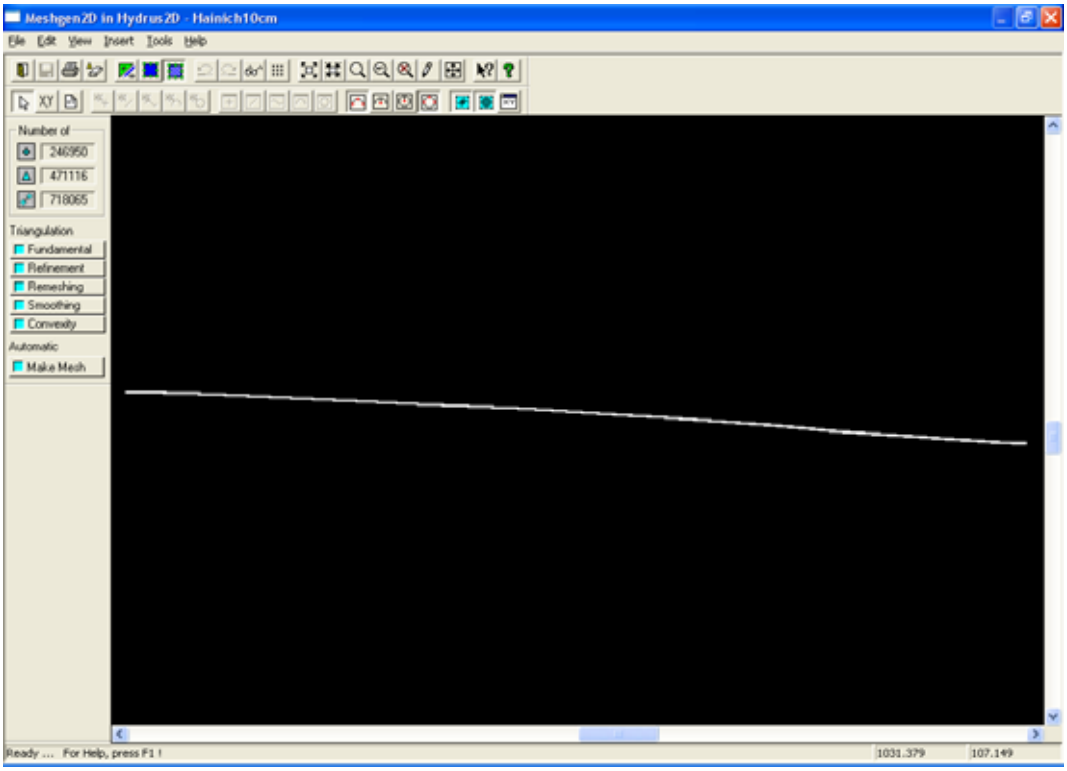

Figure 2: Hill slope representation of the test Site in Hydrus2D (Meshgen).

For parameterising the soil we used the van Genuchten (1980) model to adjustment the measured pF-Curves for three different soil horizons. The boundary conditions were defined as atmospheric boundary at the surface, no flux left at the hill top, seepage face right at the

valley bottom and free drainage as lower boundary condition. As climatic input we used data from an adjacent climate station. Evapotranspiration rates were calculated by using Penman Monteith method (Monteith 1975). We used the measured through fall and the measured precipitation from that climate station to derive the interception. Since Hydrus2D requires both evaporation and transpiration separately we divided the potential evapotranspiration through values from the literature (Brechtel 1973). To calculate the actual transpiration the S-Shape method (van Genuchten 1987) was used. The modification of precipitation due to snow dynamics was estimated according to a simple snow model (Bergström 1992). The model run included the time period from 1/2001 to 11/2003 on a hourly time step.

5. Results and discussion

The data of the measured soil water dynamics were used to validate the model. Figure 3 shows an example for the station H4 in the middle of the catena in the soild depth of 10 and 20 cm. The predicted curve is damped compared to the measured one. In contrast to this the coefficient of determination indicates a rather good fit. The damping in the predicted curve is caused by the fact that Hydrus2D only considers matrix flux. In these soils the macro pores are important because of the high clay content. This leads to soil cracks during the summer period. Additionally soil cracks were build due to a high biological activity. Given these natural conditions high soil moisture dynamic is observed. This can not be described by the model. Another problem was detected in spring 2003. Here an early drop of the predicted soil moisture is indicated. It can be marked that the model Hydrus2D is not able to follow up the effects of the frozen soil. Thereby actual soil moisture remains within the profile if comparing to modelling results. A further problem was that interflow could not has been simulated by Hydrus2D which was observed in the field. The reason for this might be the very gentle slope of the catena. Additionally the predictions for the stations in the valley are comparatively poor. It originates from laterally water flowing of the side slopes which can not be described by a 2 dimensional model.

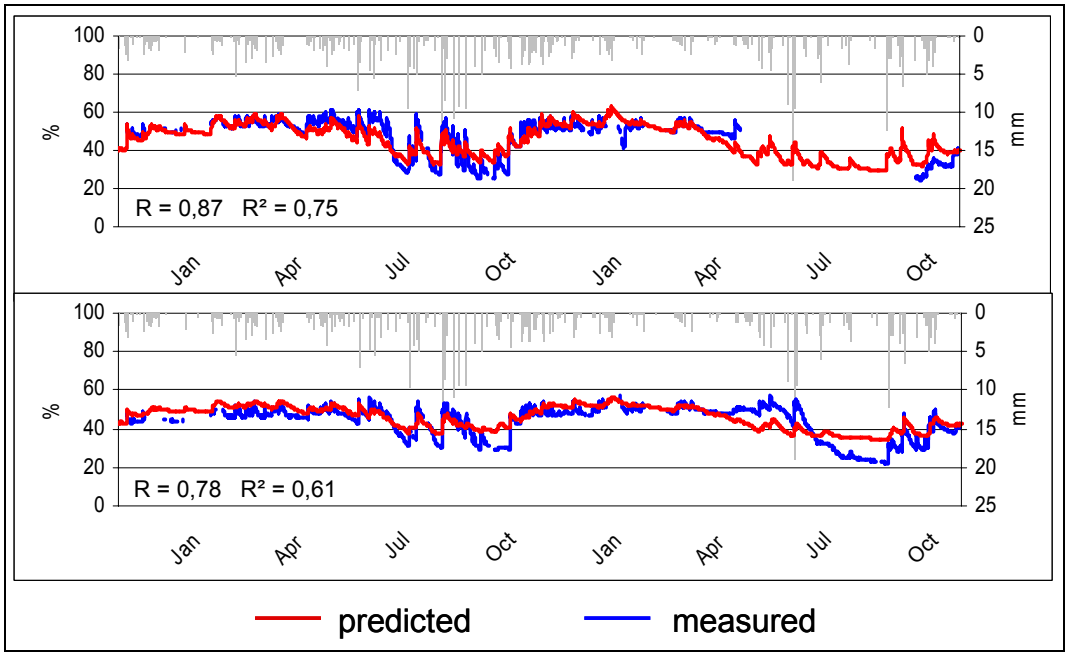

Figure 3: Measured and predicted soil moisture of station H4 in 10 and 20cm depth in the years 2002 and 2003. On the second X-axis hourly precipitation.

In spite of the shown problems we gain a reasonable water balance for the measured catena. Figure 4 shows typical characteristics for the components of the water balance. For example the discharge started in winter and reached a maximum in March which fits well to general

expectations. The characteristic of the transpiration during the vegetation period shows a typical dynamic as well. Consequently the modelled discharge is valid to be used for coupling solute carbon measurements for deriving carbon export rates (Fink et al. 2004).

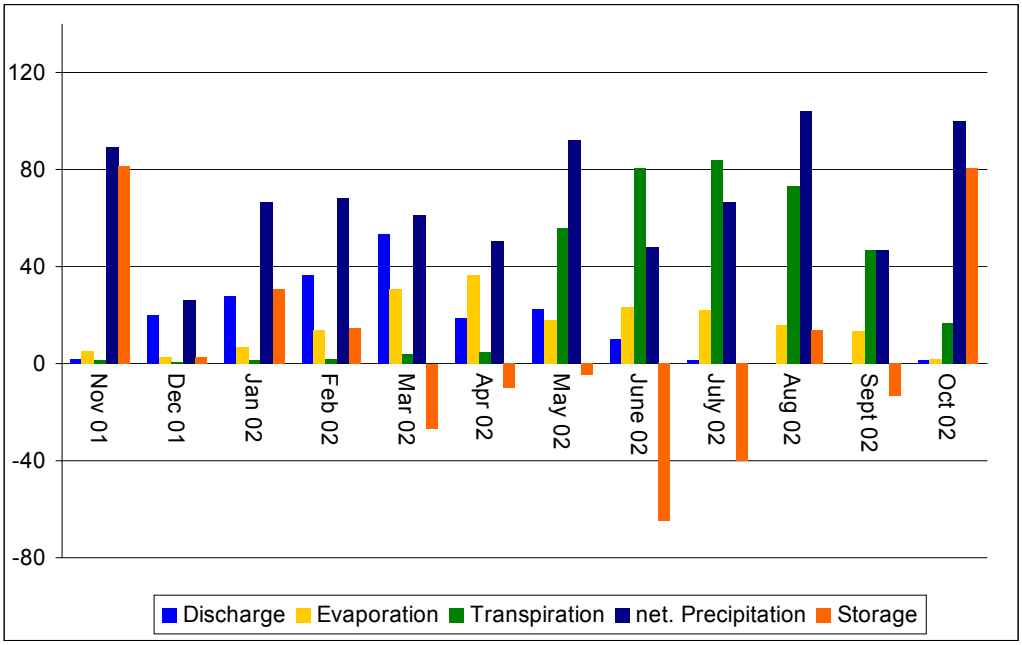

Figure 4: Monthly water balance in mm for the whole catena for the year 2002.

6. References

Bergström, S. (1992): The HBV model – its structure and applications.– SMHI, RH, 4, Norrköping, Sweden.

Brechtel, H.M. (1973): Ein methodischer Beitrag zur Quantifizierung des Einflusses von Waldbeständen verschiedener Baumarten und Altersklassen auf die Grundwasserneubildung in der Rhein-Main-Ebene.– Zeitschrift der Deutschen Geologischen Gesellschaft 124, 593–605.

Fink, M., Krause, P., Gleixner, G. & Flügel, W.A. (2004): Verknüpfung von Bodenfeuchte- und DOC – Messungen zur Abschätzung des Kohlenstofftransportes durch Wasser in einem Waldökosystem – Eine Fallstudie.– In: Bronstert, A. et al.: Wasser und Stofftransport in heterogenen Einzugsgebieten.– Forum für Hydrologie und Wasserbewirtschaftung, Heft 05.04, Band 2, 11–15.

Genuchten, M.T. van (1980): A closed-form equation for predicting the hydraulic conductivity of unsaturated soils.– SSSAJ 44, 892–898.

Genuchten, M.T. van (1987): A numerical model for water and solute movement in and below the root zone.– Research Report 121, USDA-ARS, US Salinity Laboratory, Riverside, California.

Šimůnek, J., Sejna, M. & van Genuchten, M.T. (1999): The HYDRUS-2D software package for simulating two-dimensional movement of water, heat, and multiple solutes in variably saturated media. Version 2.0.– IGWMC – TPS – 53, International Ground Water Modeling Center, Colorado School of Mines, Golden, Colorado.

Monteith, J.L. (1975): Vegetation and atmosphere, Vol. 1 Principles.– Academic Press, London.

Parameter estimation of soil hydraulic properties from tension infiltrometer data in Portugal

T. B. Ramos[1], M. Th. van Genuchten[2], M. C. Gonçalves[1], J. C. Martins[1] & F. P. Pires[1]

[1]Estação Agronómica Nacional, Quinta do Marquês, 2784-505 Oeiras, Portugal – Tel: (+351) 214 403 500 – Fax: (+351) 214 416 011 – E-mail: Tiago_Ramos@netcabo.pt
[2]George E. Brown, Jr. Salinity Laboratory, USDA-ARS, 450 W. Big Springs Road, Riverside, CA 92507-4617, USA.

INTRODUCTION

Mathematical models are increasingly used to address a broad range of variably-saturated flow and contaminant transport problems. Such simulations are generally based on numerical solutions of the Richards equation, which in turn require knowledge of the unsaturated soil hydraulic properties.

One of HYDRUS applications is the evaluation of the hydraulic properties by numerical inversion from tension disc infiltrometer data since Šimunek and van Genuchten (1996) proposed an alternative methodology to the traditional Wooding's (1968) analytical solution analysis for unconfined steady state infiltration from a disc. Šimunek and van Genuchten (1996) new approach consists in the formulation of the inverse problem and is based on minimization of a objective function, Φ, during the parameter estimation process. Minimization of the objective function Φ in HYDRUS-2D is accomplished using the Levenberg-Marquardt non-linear minimization method (Marquardt, 1963).

This brief document summarizes a recently submitted paper (Ramos *et al.*, 2005) where we further test the inverse modelling approach of Šimunek and van Genuchten (1996) by using the method to characterize the hydraulic properties of 4 field sites in Portugal. We also compare the resulting hydraulic properties with independent estimates using Wooding's analysis, and further interpret the results in terms of soil macroporosity measurements.

MATERIALS AND METHODS

The field tension infiltration experiments were carried out in Aljustrel and Alvalade (Alentejo), Portugal, using two experimental areas cropped with maize and irrigated with a center-pivot irrigation system. The infiltration experiments were performed on three different Gleyic Luvisols (LVgl), and on an Haplic Fluvisol (FLha) (soil classification according to ISSS-ISRIC-FAO, 1998).

Soil hydraulic properties were determined from undisturbed samples, collected from the superficial layers. The soil water retention curve was determined using suction tables with sand or kaolin for $h > -500$ cm and a pressure plate apparatus for $h < -1000$. The evaporation method was further used to simultaneously estimate both water retention and hydraulic conductivity data for $h > -1000$ cm.

The field tension infiltrometer measurements were performed twice at each location, designated as *Run A* and *Run B*. Both runs were carried out at a distance of about 1 m from each other using tension infiltrometers with the discs (having a radius of 20 cm) detached from the supply and tension control tubes. All four infiltration experiments were conducted with consecutive supply pressure heads of -15, -6, -3 and 0 cm. Readings of the water supply

tube were done visually. Figure 1 exemplifies a measurement cumulative infiltration rate versus time on LVgl 1. Using the capillary rise equation, the applied pressure heads correspond to the pore radii limiting the pore classes in the classification suggested by Watson and Luxmoore (1986).

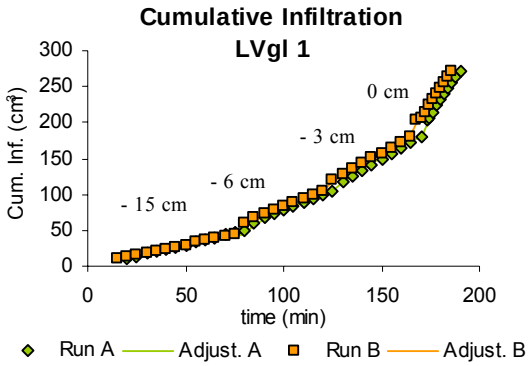

Figure 1. Measured cumulative infiltration rates at consecutive supply pressure heads of -15, -6, -3 and 0 cm for 4 superficial layers of one of the Gleyic Luvisols used in this study.

Disturbed gravimetric samples were taken to determine the initial and final water contents of the soils. The initial water content was determined at a different location from where the infiltration took place to avoid disturbance of the soil during the measurements. However, the final water content was determined under the disc membrane after reaching a steady flux for the last pressure head.

Following Šimunek *et al*. (1998a; 1998b), the objective function $\Phi(Q, \theta_i, \theta_f)$ was defined in terms of the measured cumulative infiltration data (Q) at multiple pressure heads, and the initial and final soil water contents (θ_i and θ_f, respectively), while the calculations and optimisation were carried out using HYDRUS-2D (Šimunek and van Genuchten, 1996). The weighting coefficients w_i in Eq. (1) for the different infiltration data points were all assumed to be 1 since the observation errors of each measurement are unknown. Although being a isolated entry in the optimisation, the final water content was given a weight of 10 to guarantee a reasonable effect on the final results relative to the cumulative infiltration data.

RESULTS AND CONCLUSIONS

Our study suggests that numerical inversion of tension infiltrometer data provides a relatively simple and reliable alternative method for determining the water retention and conductivity curves of unsaturated soils.

The water retention and conductivity curves obtained by numerical inversion closely matched the laboratory measured curves for the 4 superficial layers where the infiltration experiments were carried out (Figure 2). Hydraulic conductivities obtained with the inversely estimated Mualem-van Genuchten parameters also corresponded well with results obtained using Wooding's traditional approach of disc infiltrometer data following the methodology of Ankeny *et al.* (1991). This correspondence was further reflected by the very similar estimates of the macroporosity, mesoporosity 1, and mesoporosity 2 pore classes we calculated from the estimated $K(h)$ curves using the method of Watson and Luxmoore (1986).

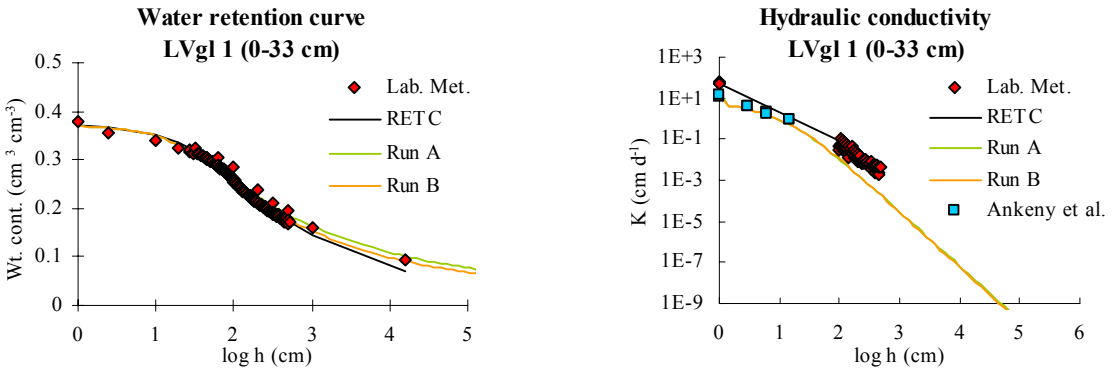

Figure 2 – Water retention $\theta(h)$ and hydraulic conductivity $K(h)$ curves obtained through numerical inversion of the measured tension disc infiltrometer data (Runs A and B), and by means of separate laboratory and field measurements after analysis with RETC. Results are for the surface layer of one of the Gleyic Luvisols (LVgl 1) used in the experiments.

One major limitation of the numerical inversion method is its extreme dependence of the field-measured water content values. The saturated water content θ_s estimated by numerical inversion in particular was very close to the final water content θ_f measured at the end of the infiltration tests, which indicates the extreme dependence of θ_s identification on the final water content value. While this situation was somewhat expected since a weighting coefficient of 10 was used for the final water content it does illustrate how poor estimates of θ_s can have a negative effect on the water retention curve. Some problems were found especially with the initial soil water content, which (unlike the final water content) cannot be determined at exactly the same location as where the tension infiltrometer measurements are carried out. Problems of soil spatial variably can become very important. This was shown in this study for the LVgl2 and LVgl3 field measurements which produced curves that deviated considerable from the laboratory derived curves (Figure 3).

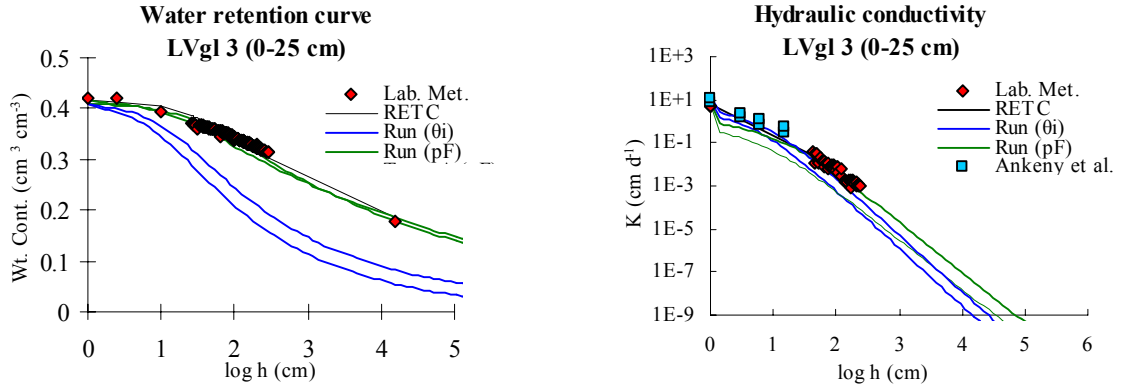

Figure 3 – Influence of a water content underestimation in the soil hydraulic curves determination [*Run* (θ_i)] and it's correction through the addition of water contents at 10 kPa and at 1500 kPa [*Run (pF)*] in the objective function.

Addressing essentially the same problem (i.e., to obtain a better description of the water characteristic in the dry region), Schwartz and Evett (2003) recently suggested that at least one independent measurement of $\theta(h)$ at a pressure head sufficiently less than the lowest h_0 in the objective function should be included in the objective function. To further test this, we re-ran the LVgl3 simulations, but now included measurements of $\theta(h)$ at pressure heads of -100 and –15,000, corresponding to pF values of 2 and 4.2, respectively. We obtained more reliable results when this independently measured water contents at -100 cm and -15000 cm

were added to the objective function. While this will require more time and effort (and additional equipment), and as such negate some of the advantages of numerical inversion methods (i.e., speed and ease of use), the results will be more reliable in the absence of having more complete laboratory data for comparison purposes.

REFERENCES

ISSS-ISRIC-FAO. 1998. *World Reference Base For Soil Resources*. World Soil Resources Report *84.* FAO, Rome, Italy.

Marquardt, D. W. 1963. An algorithm for least-squares estimation of non-linear parameters. *SIAM J. Appl. Math.*, 11: 431-441.

Ramos, T. B.; M. Th. van Genuchten, M. C. Gonçalves; J. C. Martins and F. P. Pires, 2005. Hydraulic properties evaluated by numerical inversion from tension disc infiltrometer data and using laboratory methods. *Vadose Zone Journal* (submitted June, 2005).

Schwartz, R. C. and S. R. Evett. 2003. Conjunctive use of tension infiltrometry and Time Domain Reflectometry for inverse estimation of soil hydraulic properties. *Vadose Zone Journal*, 2: 530-538.

Šimunek, J. and M. Th. van Genuchten. 1996. Estimating unsaturated soil hydraulic properties from tension disc infiltrometer data by numerical inversion. *Water Resour. Res.*, 32(9): 2683-2696.

Šimunek, J., R. Angulo-Jaramillo, M. G. Schaap, J. P. Vandervaere and M. Th. van Genuchten. 1998a. Using an inverse method to estimate the hydraulic properties of crusted soils from tension disc infiltrometer data. *Geoderma*, 86(1-2): 61-81.

Šimunek, J., D. Wang, P. J. Shouse and M. Th. van Genuchten. 1998b. Analysis of a field tension disc infiltrometer data by parameter estimation. *Int. Agrophysics*, 12: 167-180.

Van Genuchten, M. Th., F. J. Leij and S. R. Yates. 1991. *The RETC code for quantifying the hydraulic functions of unsaturated soils*. Environmental Protection Agency, United States.

Watson , K. W. and R. J. Luxmoore. 1986. Estimating macroporosity in a forest watershed by use of a tension infiltrometer *Soil Sci. Soc. Am. J.* 50: 578-582.

Wooding, R. A. 1968. Steady infiltration from large shallow circular pond. *Water Resour. Res.*, 4: 1259-1273.

Using HYDRUS to simulate water and solute transports in soil lysimeters

M. C. Gonçalves[1], J. Šimůnek[2], T. B. Ramos[1], J. C. Martins[1], M. J. Neves[1] & F. P. Pires[1]

[1]*Department of Soil Science, Estação Agronómica Nacional, Av.República 2784-505 Oeiras, Portugal*
[2]*Department of Environmental Sciences, University of California, Riverside, CA 92521, USA*

INTRODUCTION

A variety of analytical and numerical models have been developed in the past decades to predict water and/or solute transfer processes between the soil surface and the groundwater table. While many models quantifying solute transport in soils usually consider only one solute and severely simplify various chemical interactions, models such as HYDRUS consider multiple solutes and their mutual interactions.

HYDRUS has been recently updated to consider major ion chemistry [*Šimůnek et al.*, 2005]. This new module considers transport of major ions (Ca^{2+}, Mg^{2+}, Na^{+}, K^{+}, SO_4^{2-}, Cl^{-}) and various temperature dependent equilibrium chemical reactions between these ions, such as aqueous complexation, precipitation and dissolution of several solid phases (calcite, gypsum, dolomite, nesquohonite, hydromagnesite, and sepiolite), and cation exchange.

The two most important chemical reactions in our application were aqueous complexation and cation exchange. Equations for the aqueous complexation reaction can be obtained using the law of mass action.

Partitioning between the solid exchange phase and the solution phase (cation exchange reaction) is described in HYDRUS by the Gapon exchange equation [White and Zelazny, 1986] assuming that the cation exchange capacity (CEC) is constant and independent of pH.

The first objective of this study was to carry our field experiments to quantify salinisation and alkalisation risks of an Eutric Fluvisol irrigated with different quality waters in Alvalade-Sado (Alentejo), Portugal. The second objective was to evaluate the effectiveness of the HYDRUS-1D software package [*Šimůnek et al.*, 2005] to predict water contents and fluxes, and concentrations of individual ions, overall salinity, as well as SAR (sodium adsorption ratio) and ESP (exchangeable sodium percentage) indices under field conditions where salinisation may occur.

MATERIAL AND METHODS

The quantification of salinisation and alkalisation hazards in a soil irrigated with four different water qualities (Table 1) was carried out in Alvalade do Sado, Alentejo, Portugal. Three soil monoliths (1.2 m^2 x 1.0 m deep) were constructed in a Eutric Fluvisol (ISSS-ISRIC-FAO, 1998). The monoliths were laterally isolated with plastic to prevent lateral water and solute fluxes and subjected to atmospheric conditions at the top and free drainage at the bottom. The soil monoliths were covered by annual spontaneous vegetation. TDR probes and ceramic cups were installed in each soil monolith in two replicates at depths of 10, 30, 50 and 70 cm.

The monoliths were manually irrigated in years from 2001 to 2004 during the regular irrigation period between May and September. Application depths were 10 mm each, for a total of 500 mm per year. The monoliths were exposed to natural atmospheric conditions (rainfall and evapotranspiration) during the rest of the year. Due to variable Mediterranean conditions, there were large differences in cumulative rainfall during the time period between

September and May, which corresponds with the soil's leaching cycle. Irrigation water compositions, named *A*, *B* and *C* according to the monolith to which they were applied, are described in Table 1. The waters used in the experiment were produced by adding increased concentrations of NaCl, $CaCl_2$ and $MgCl_2$ to the water *A* available in the region, with a ratio of Ca:Mg = 1:2.

Table 1. Ionic composition of irrigation waters applied to the soil monoliths and their classification according to US Salinity Laboratory (Richards, 1954).

Monolith		EC	SAR	Ca^{2+}	Mg^{2+}	Na^{+}	Cl^{-}	USSL
		dS m^{-1}	$(meq\ L^{-1})^{0.5}$	meq L^{-1}				classification
Waters I	A	0.3	1.0	1.00	1.00	1.00	5.00	C2-S1
	B	0.8	3.0	1.28	2.56	4.16	11.82	C3-S1
	C	1.6	6.0	1.93	3.86	10.21	21.79	C3-S2
Waters II	A'	0.8	1.5	1.85	3.65	2.5	13.5	C3-S1
	B'	1.6	3.0	3.16	6.32	6.52	25.48	C3-S1
	C'	3.2	6.0	5.1	10.2	16.7	47.3	C4-S2

Soil solutions were collected from ceramic cups and soil water contents were monitored using TDRs at four depths twice a week during the irrigation periods and once a week during remaining months. At the beginning of the experiment, at the end of each irrigation period, and after the following winters, soil samples were collected at 5 depths (0-20, 20-40, 40-60, 60-80, 80-100 cm) to measure the exchangeable cations, and the cation exchange capacity (CEC).

Evapotranspiration, soil hydraulic properties, solute transport parameters and many physical and chemical analysis like soil texture, dry bulk density, concentrations of soluble cations (Na^{+}, Ca^{2+}, Mg^{2+}), electrical conductivity (ECe), and cation exchange capacity (CEC) were determined during the extend of the field experiment, in order to satisfy the considerable input data needed to evaluate the effectiveness of the HYDRUS-1D software package [*Šimůnek et al.*, 2005].

RESULTS AND CONCLUSIONS

The use of irrigation waters with EC up to 1.6 dS m^{-1} during the time period from May 2001 to September 2004 did not lead to salinisation/alkalization of the medium textured Fluvisol due to its favourable hydraulic characteristics and the winter precipitations. The rainfall water leached the salts accumulated during the irrigation period down to a depth of l50 cm. Irrigation with water having EC of 3.2 dS m^{-1} can cause significant soil salinisation and alkalisation. After two irrigation cycles (in 2003 and 2004) EC of the soil solution increased to about 12 dS m^{-1}, SAR to about 8 $(meq\ L^{-1})^{0.5}$, and ESP to 17% in the surface soil horizon (0-20 cm). Although the winter rainfall leached most salts from the surface layers, this was not sufficient to restore the soil to its initial conditions bellow the depth of 40 cm. EC values reached 3 dS m^{-1}, SAR 7 $(meq\ L^{-1})^{0.5}$ and ESP 9% at a depth of 50 cm in March 2004, immediately after the third rainfall season.

HYDRUS-1D has successfully simulated water regime, as well as the effects of different irrigation waters on the geochemistry of the studied Fluvissol (Figures 1 to 3). The correspondence between observed and simulated variables is remarkable, considering that simulations were carried out to predict field measurements over a considerable time period (4 years) without any calibration, with all input variables (i.e., soil hydraulic properties, solute transport parameters, atmospheric demand, Gapon constants, physical and chemical characteristics of the soil, LAI and root depth) measured independently. The agreement

between measure and simulated values was the best for soluble sodium concentrations (R^2=0.7980; n=1091 observations), SAR (R^2=0.8645 n=1180) and ESP (R^2=0.7338 n=105), while water contents (R^2=0.6033; n=1180), ECs (R^2=0.6505 n=1043), and soluble magnesium (R^2=0.6323 n=1056) and calcium concentrations (R^2=0.6219 n=1015) were predicted slightly less well.

Our study shows that HYDRUS-1D can become a very powerful tool in irrigation management, for predicting the effects of irrigation water quality on the soil and groundwater quality, and for implementing better irrigation and fertilization practices [e.g., *Gärdenäs et al*., 2005], which is particularly important when designing new irrigation areas. Models such as HYDRUS-1D, after their proper calibration and validation, should be used to establish sound irrigation policies and to mitigate environmental risks.

A complete description of this study can be found in Gonçalves *et al*. (2005).

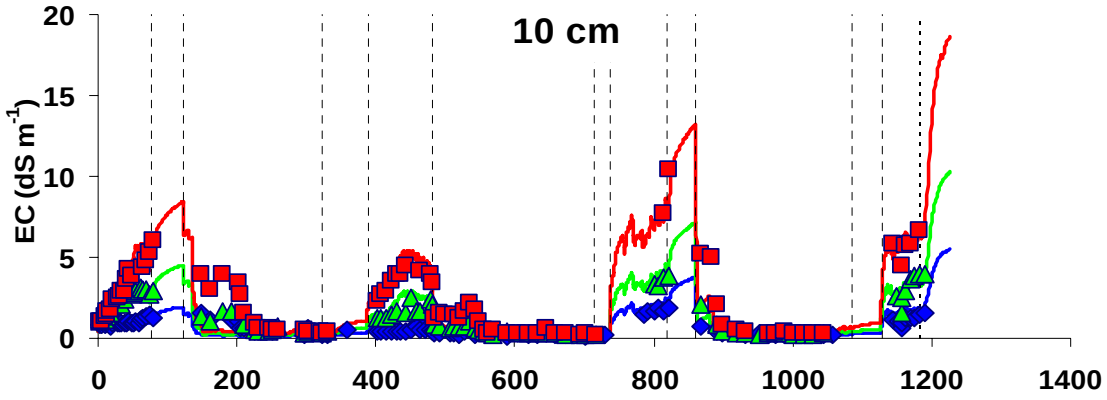

Figure 1 – Measured and simulated soil solution electrical conductivities at 10 cm depth in the three monoliths A, B, and C.

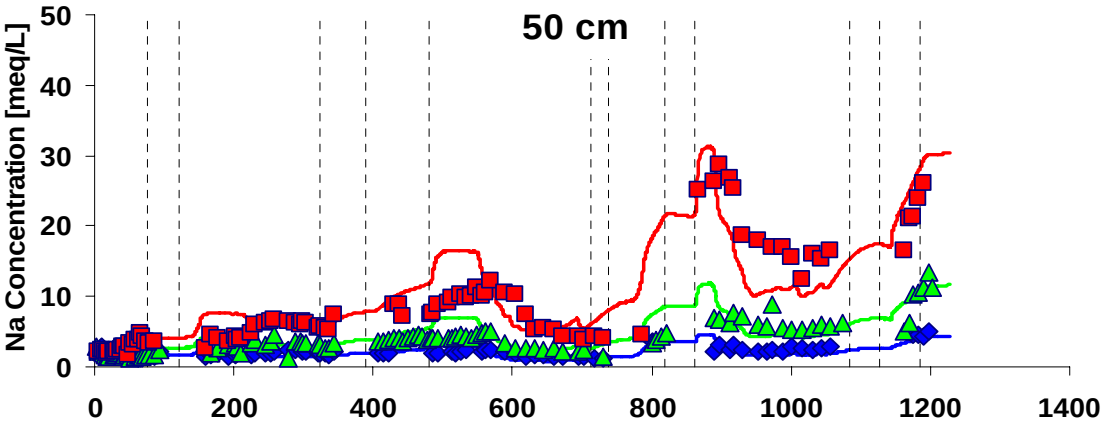

Figure 2 – Measured and simulated soluble sodium at 50 cm depth in the three monoliths A, B, and C.

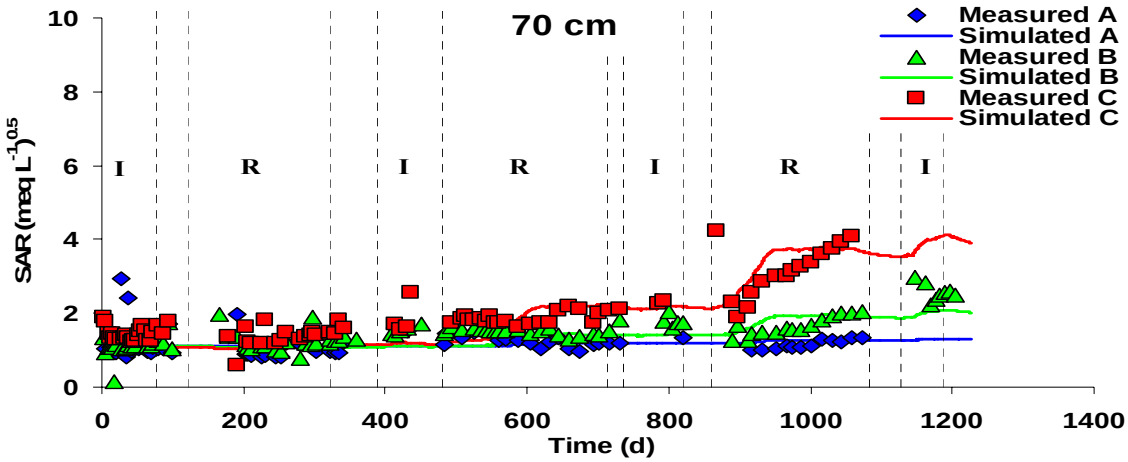

Figure 3 – Sodium adsorption ratios measured and simulated at 70 cm depth in the three monoliths A, B, and C. I and R correspond to the irrigation and rainfall periods, respectively.

REFERENCES

Gärdenäs, A., Hopmans, J. W., B. R. Hanson, and J. Šimůnek, 2005. Two-dimensional modeling of nitrate leaching for various fertigation scenarios under micro-irrigation, *Agric. Water Management, 74*, 219-242.

Gonçalves, M. C., J. Šimůnek; T. B. Ramos, J. C. Martins, M. J. Neves and F. P. Pires, 2005. Multicomponent solute transport in soil lysimeters irrigated with different quality waters *Water Resour. Res*., (submitted July, 2005).

Richards, L. A., 1954. *Diagnosis and Improvement of Saline and Alkali Soils*, USDA Handbook *60*, Washington, USA.

Šimůnek, J., M. Th. van Genuchten, and M. Šejna, 2005. The HYDRUS-1D software package for simulating the one-dimensional movement of water, heat, and multiple solutes in variably-saturated media. Version 3.0, *HYDRUS Software Series 1*, Department of Environmental Sciences, University of California Riverside, Riverside, CA, 270pp.

White, N. L., and L. M. Zelazny, 1986. Charge properties in soil colloids. in *Soil Physical Chemistry*, edited by D. L. Sparks , CRC Press, Boca Raton, Florida.

Multi-step outflow experiments to link soil hydraulic properties with electrical characteristics

H.-M. Münch[1], A. Kemna[1], M. Herbst[1], E. Zimmermann[2], H. Vereecken[1]

[1] Agrosphere Institute (ICG-IV), Forschungszentrum Jülich GmbH, 52425 Jülich, Germany
[2] Central Institute for Electronics (ZEL), Forschungszentrum Jülich GmbH, 52425 Jülich, Germany

Introduction

The electrical conduction and polarisation properties of soils include structure and state information dependent on flow and transport parameters. Electrical polarisation phenomena, measured with the Spectral Induced Polarisation (SIP) method, are caused by the electro-diffusive interaction of the soil matrix with the pore fluid. The polarisation depends e.g. on the pore size, on the electrical conductivity of the pore fluid as well as on saturation (e.g. Münch et al., 2005; Binley et al., 2005). Here we present results from SIP measurements which were conducted in conjunction with multi-step outflow (MSO) experiments to examine relationships between soil hydraulic properties and electrical characteristics.

Experimental Setup

In order to jointly measure SIP characteristics and hydraulic properties we established a new laboratory measurement setup (Fig. 1): Two electrodes (porous bronze discs) were used to inject an electric current in the frequency range 1 mHz to 42 kHz into the specimen. The difference of the electric potential between two further electrodes was measured. The main target value was the phase shift, φ [rad], between current and voltage which depends on the applied frequency (a sinusoidal wave form was used). For the variation of water saturation and further the determination of the unsaturated hydraulic properties a MSO facility was used. The advantage of this against evaporative drying to adjust the water content is that an almost constant value of the electrical conductivity σ_w [S / m] of the pore fluid can be maintained. A pressure head was applied at the top of the column, and the outflow into a burette was measured. After reaching an equilibrium the pressure

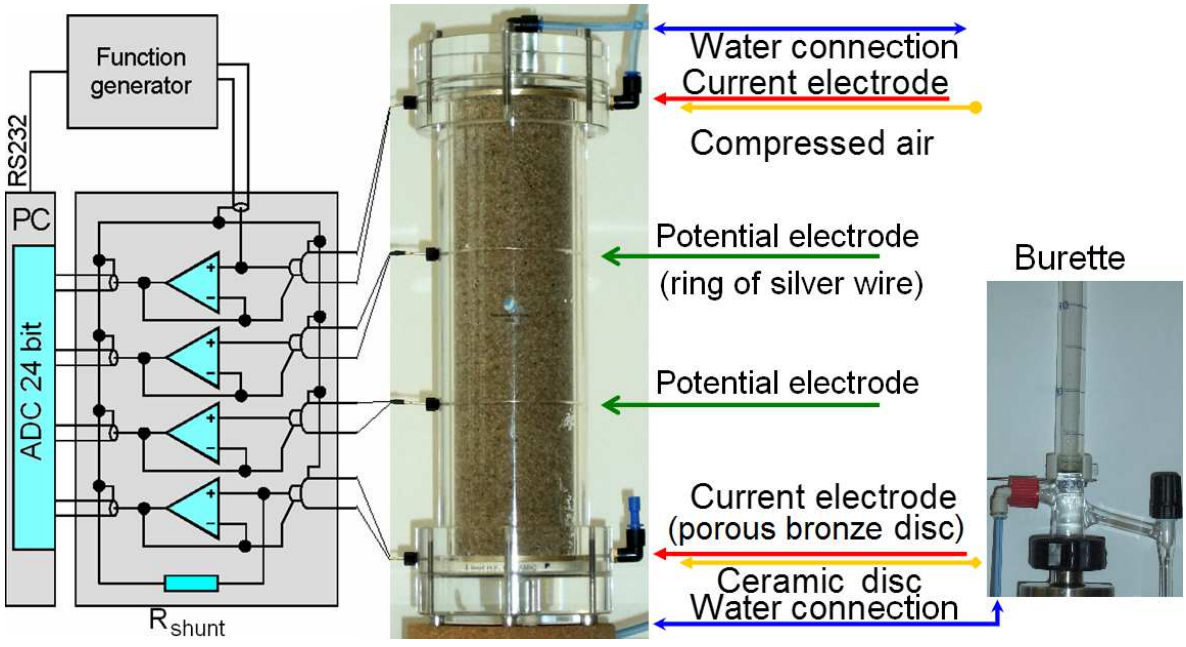

Figure 1: Experimental setup showing measurement electronics, column, and burette.

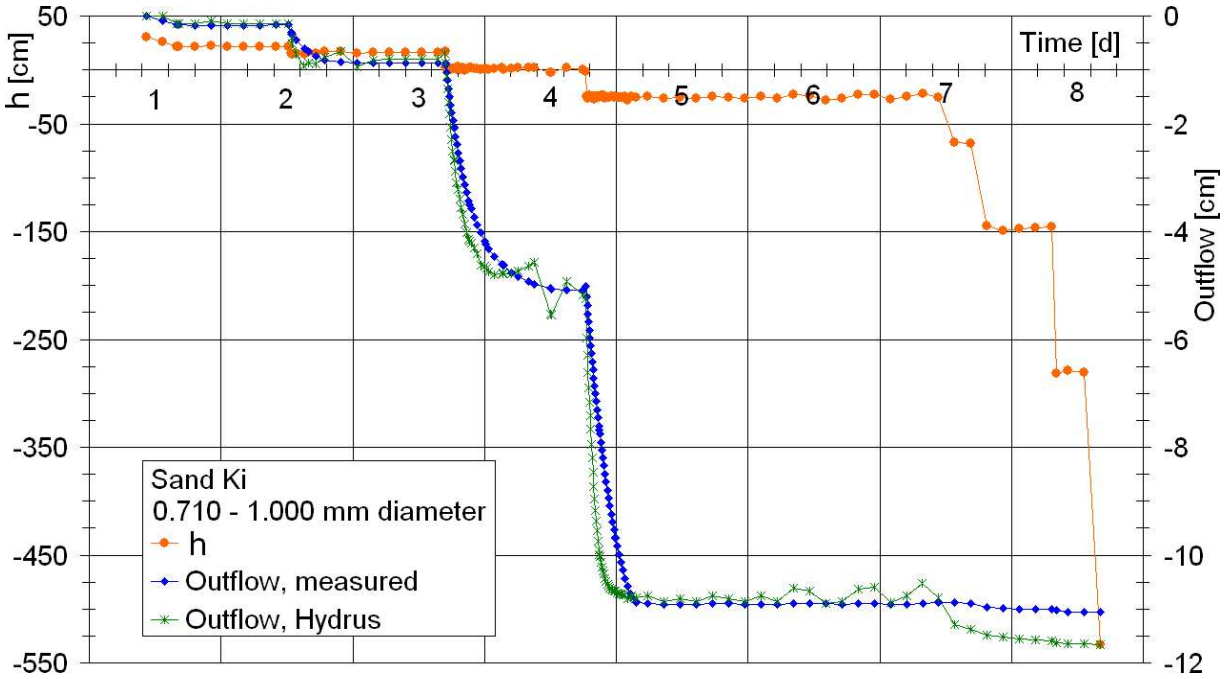

Figure 2: Example of MSO data showing applied pressure h, resultant outflow, and HYDRUS-1D fit.

was increased. It is possible to invert from the corresponding data the hydraulic properties with the HYDRUS-1D program of SIMUNEK ET AL. (2005). For this the pressure P_{top} at the top of the column had to be transformed into suction at its bottom: $h_{\text{bottom}}\,[\text{cm}] = -\left(P_{\text{top}}\,[\text{bar}] \cdot 1019.716\frac{\text{cm}}{\text{bar}} - H_{\text{water column in the burette}}\,[\text{cm}]\right) + h_{\text{bronze}}\,[\text{cm}] + h_{\text{ceramic disk}}\,[\text{cm}] + h_{\text{soil}}\,[\text{cm}]$. The outflow was measured as pressure of the water column in the burette and converted into water height H [cm] and volume V [ml]. For the use of HYDRUS-1D V has to be converted into a normalised outflow $Y\ [\text{cm}^3\,\text{cm}^{-2}] = V \cdot 1\frac{\text{cm}^3}{\text{ml}} \cdot A^{-1}$, where $A = \pi r^2$ denotes the area and r [cm] the radius of the bottom of the column. Fig. 2 shows the measured outflow as well as the applied pressure head for an exemplary sample.

Data Analysis

The phase spectrum was analysed by fitting an overlaying Cole-Cole model (COLE & COLE, 1941; KEMNA, 2000) to the impedance data, where impedance

$$Z(\omega) = R_0\left[1 - \sum_x m_{\text{cc}_x}\left(1 - \frac{1}{1 + (i\omega\tau_x)^{c_x}}\right)\right] \quad [\Omega\,\text{m}]$$

and $\varphi(\omega) = \arctan\frac{\text{Im}(Z(\omega))}{\text{Re}(Z(\omega))}$. The multi-Cole-Cole fit yields the parameters relaxation time τ [s], chargeability m_{cc} [−], and Cole-Cole exponent c [−] for each individual dispersion term as well as DC resistivity R_0 [Ω m]. According to theory, the relaxation time τ is connected to a characteristic spatial dimension l [m], e.g. $l = \sqrt{4D\tau}$ (TITOV ET AL., 2002) with diffusion coefficient D [$\text{m}^2\,\text{s}^{-1}$]. For example the effective hydraulic radius r_{eff} [m] is linked to the hydraulic permeability $k \propto r_{eff}^2$ by the Kozeny-Carman model (CARMAN, 1956). The inverse of the Cole-Cole exponent c is a measure of the flatness of the phase spectrum, and we consider c^{-1} as an indicator for the pore size distribution index n. The Cole-Cole parameter m_{cc} is a measure of the electrical polarisability, which depends on

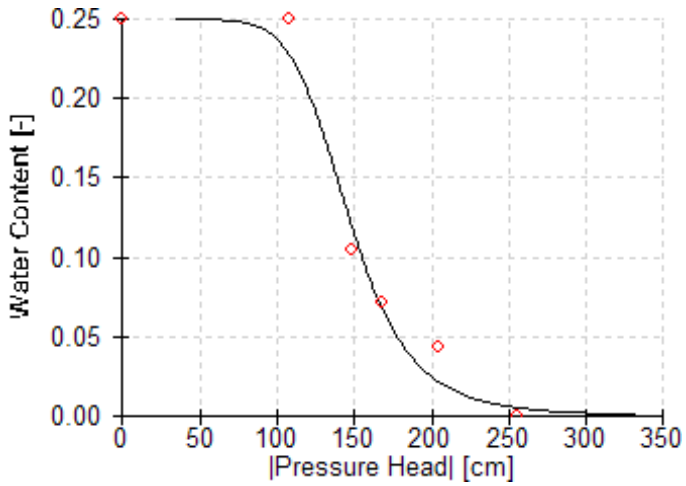

Figure 3: Retention function of one of the used bronze electrodes.

specific surface, clay content, and cation exchange capacity (e.g. BÖRNER & SCHÖN, 1991). Further it is $R_0^{-1} \sim \sigma_w S_e^{n_{Archie}}$ (ARCHIE, 1942), where S_e denotes the effective saturation and $n_{Archie} \approx 2$ the saturation exponent.

The HYDRUS-1D program allows to invert the MSO data (time t [s], applied pressure head h, outflow Y) for the parameters characterizing the soil hydraulic properties (Fig. 2). The water content is given as $\theta(h) = \theta_r + \frac{\theta_s - \theta_r}{(1+|\alpha h|^n)^m}$, and further it is (VAN GENUCHTEN, 1980)

$$K(h) = K_s \cdot \frac{\left[1 - (\alpha|h|)^{n-1}\left(1 + (\alpha|h|)^n\right)^{-m}\right]^2}{\left[1 + (\alpha|h|)^n\right]^{ml}}$$

where θ_r and θ_s denote the residual and the saturated water content, respectively, h [cm] the pressure head, $K(h)$ [cm / d] the unsaturated and K_s [cm / d] the saturated hydraulic conductivity, α [cm^{-1}] is the inverse of the air-entry value, n as well as m are form parameters related to the pore size distribution, and l is the tortuosity. In order to reduce the number of unknown parameters we set $m = 1 - 1/n$, $l = 1/2$, and $\theta_r = 0$, leading to $S_e(h) = \theta(h)/\theta_s = \left(1 + (\alpha|h|)^n\right)^{\frac{1-n}{n}}$. Knowing K_s, S_e, and m (or n) now allows to calculate $K(h)$. For all materials (soil, bronze disc, ceramic disc) the saturated water content θ_s and hydraulic conductivity K_s were measured. The remaining hydraulic properties of the ceramic disc were taken from OBERDÖRSTER (2005). For the bronze discs we computed α and n from measured retention values with RetC (VAN GENUCHTEN ET AL., 1991) from the HYDRUS package (Fig. 3). The HYDRUS-1D fit yields the pore size distribution index n and the bubbling pressure α^{-1} from which the unsaturated hydraulic conductivity can be calculated.

Results

The analysis outlined above made it possible to examine the relation between the hydraulic properties and the characteristic electrical parameters. Fig. 4 shows the relation between K, τ, and S_e for the investigated samples with different grain sizes. The relaxation times for the different grain sizes differ systematically over the considered saturation range. For a value of effective saturation it is possible to determine a relationship between hydraulic conductivity and relaxation time, the closer inspection of which will be subject of future work.

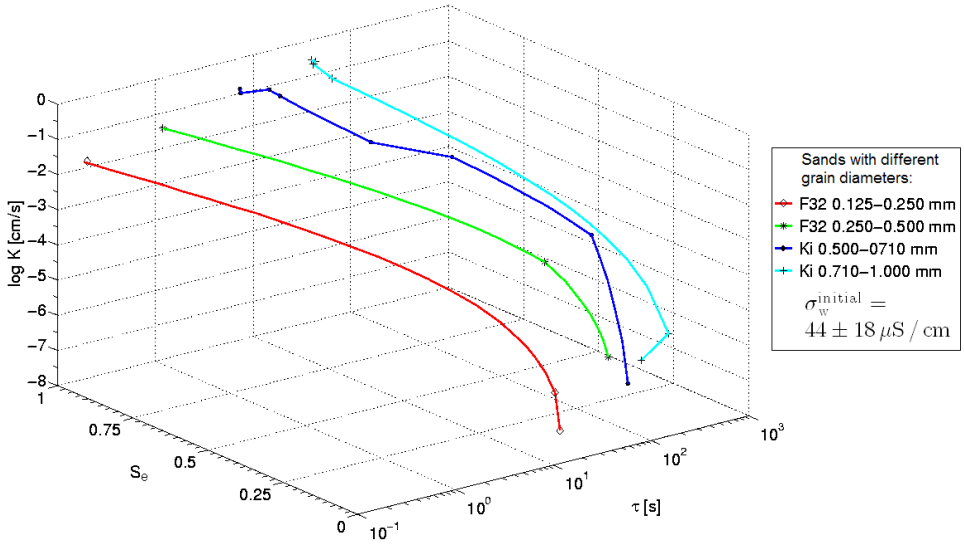

Figure 4: Relationship between hydraulic conductivity K, relaxation time τ, and effective saturation S_e for sand samples with different grain sizes.

References

Archie, G. E. (1942): The electrical resistivity log as an aid in determining some reservoir characteristics. *Trans. Am. Inst. Min., Met. & Petr. Eng.*, **146**, 54–62.

Binley, A., Slater, L. D., Fukes, M., & Cassiani, G. (2005): The relationship between spectral induced polarization and hydraulic properties of saturated and unsaturated sandstone, *Water Res. Res.*, in press.

Börner, F. D., Schön, J. H. (1991): A relation between the quadrature component of electrical conductivity and the specific surface area of sedimentary rocks, *The Log Analyst*, **32**, 612–613.

Carman, P. C. (1956): Flow of gases through porous media. Butterworths, London.

Cole, K. S., & Cole, R. H. (1941): Dispersion and absorption in dielectrics, *J. Chem. Phys.*, **9**, 341–351.

Kemna, A. (2000): Tomographic inversion of complex resistivity - theory and application. Ph. D. thesis, Bochum University, ISBN: 3934366929.

Münch, H.-M., Kemna, A., Titov, K., Zimmermann, E., & Vereecken, H. (2005): Dependence of the spectral induced polarization response of sands on salinity, grain size and saturation, *Geophys. Res. Abstr.*, **7**, 02645.

Oberdörster, Ch. (2005): personal communication, see also Oberdörster, Ch. (2004): Überprüfung des Mualem-Friedman-Modells durch Messung des Wassergehalts und der elektrischen Leitfähigkeit in Bodensäulen mittels TDR unter transienten Bedingungen, Diplomarbeit, Univ. Bonn.

Simunek, J., van Genuchten, M. Th., & Sejna, M. (2005): HYDRUS-1D, V3.00, Code for simulating the one-dimensional movement of water, heat and multiple solutes in variably-saturated porous media, Riverside (USA).

van Genuchten, M. Th. (1980): A closed-form equation for predicting the hydraulic conductivity of unsaturated soils, *Soil Sci. Soc. Am. J.*, **44**, 892–898.

van Genuchten, M. Th., Simunek, J., Leij, F. J., & Sejna, M. (1991): RetC, V6.0, Code for quantifying the hydraulic functions of unsaturated soils, Riverside (USA).

Titov, K., Komarov, V., Tarasov, V., & Levitski, A. (2002): Theoretical and experimental study of time domain-induced polarization in water-saturated sands, *J. Applied Geophys.*, **50**, 417–433.

PARSWMS: a parallelized version of SWMS_3D

Javaux, M., Hardelauf, H., Gottschalk S., Herbst, M., Vanderborght, J. and H. Vereecken

1. Introduction

There is currently a need for large-scale models representing the water flow and solute transport processes at large scale. Among the numerous approaches dealing with this problem, distributed modeling based on Richards'equation is one of the most popular. Yet, a key issue of the distributed modeling is the maximum grid resolution at which the model is valid. Theoretically, the grid resolution should be of the same order of magnitude as the Darcy (or elementary representative volume) scale, that is between 10^{-2} -10^{0} m. Thus, when large-scale problems have to be faced, the major drawback of fine grid models is the enormous demand for computational time and resources (Harter and Hopmans, 2004). The speed and efficiency of current models have therefore to be improved. The paralellization of the code is one possible way to decrease the computational time by distributing a complex large geometry problem over multiple processors working in parallel.

2. Code principles

The PARSWMS code is based on the SWMS_3D code (Simunek et al., 1995). Most of the subroutines, functions and variable names have been kept the same whereas some changes were made to parallelize the code. First the programming language was switched from FORTRAN to C++ , which allows for dynamic allocation of all variables, i.e. there is no need to redefine array sizes. Also the output was slightly modified. Basically, the code gives one series of output files per processor. Therefore, a post-processing is needed to merge all the data together after running. Though, note that the input files are the same as in SMWS_3D.

The new code is based on MPI (Message-Passing Interface), a library specification for message-passing, which provides source-code portability and allows efficient implementation across a range of computer architectures. MPI is a free software for LINUX or UNIX, which

needs to be installed on the working machine, and which provides several libraries for parallel computing.

The partitioning of the problem is automatically performed based on the PARMETIS library. With the aid of this library the partitioning process itself is parallelised, partitioning could be made dynamically (adapted at each time step), can be carried out for irregular grids, and the parallel code can be run on heterogeneous cluster of processors. Currently the partitioning is static, in the sense that this is done once at the beginning of the run. The algorithm optimizes the partitioning between processors based on weights given by the user to different subdomains, by minimizing the surface of the subvolumes on each processor as well as the connection numbers between processors.

The solution of the system of linear equations is achieved for the nodes of the subvolume allocated on each processor. The PETSc toolbox was used since it allows the user to choose between a large range of solvers or preconditionners able to deal with linear and non-linear problems. Therefore, the solver implemented in PARSWMS is different to SWMS_3D, and could be further optimized.

The PARSWMS code can be compiled and run on any network (or even uni-processor) of LINUX or UNIX workstations or on specialized parallel hardware as long as the MPI, PETSc and PARMETIS freewares are installed.

3. Applications and results

A first release of the code is working and it performance is currently evaluated. Several points are particularly investigated: (1) the code is submitted to a benchmarking developed for testing numerical codes (Vanderborght et al., 2005), (ii) the code is compared with the current SWMS_3D code in terms of performance and results, and (iii) the performance of the code in terms of computational time is evaluated, i.e., the time scaling of several computationally-demanding problems is studied on a massive parallel system.

First results confirm that SWMS_3D and PARSWMS give convergent simulations for most cases, under several benchmarking scenarios for water and solute. Figure 1 shows the time scaling for a steady-state solute transport scenario through a soil cylinder with 500.000 nodes. Tests were made on 1 to 128 processors and there was a linear relationship between the log10 number of nodes and the log10 time reduction with a slope around 0,9.

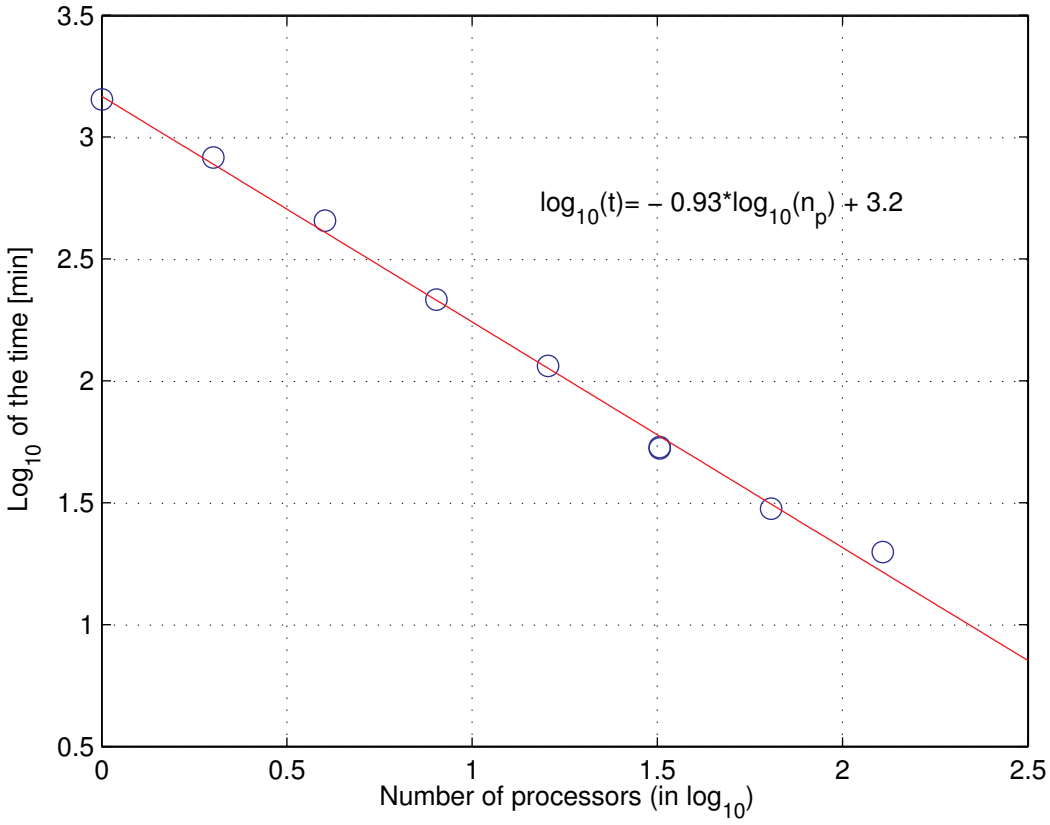

Fig. 1.:Ttime scaling for solute transport scenario with 492264 nodes

4. References

Harter, T and J. W. Hopmans. 2004. Role of vadose-zone flow processes in regional-scale hydrology: review, opportunities and challenges. In Unsaturated-zone modeling. Progress, challenges and applications, edited by Feddes, R. A., G. H. De Rooij, and J. C. Van Dam Wageningen Frontis Series. Dordrecht, The Netherlands: Kluwer Academic Publisher.

Simunek, J., K. Huang, and M. Th. Van Genuchten. 1995. The SWMS_3D code for simulating water flow and solute transport in three-dimensional variably-saturated media. Version 1.0. Research Report n°139. Riverside, California. U. S. Salinity Laboratory. Agricultural Research Service. U.S. Department of Agriculture.

Vanderborght, J., R. Kasteel, M. Herbst, M. Javaux, D. Thiery, M. Vanclooster, C. Mouvet, and H. Vereecken. 2005. A Test of Numerical Models for Simulating Flow and Transport in Soils Using Analytical Solutions. Vadose zone journal. 4:206-221.

Non-equilibrium Isoproturon Transport in Structured Soil Columns: Experiments and Model Analysis

J. Maximilian Köhne[*1], Sigrid Köhne[1], and Jirka Šimůnek[2]

[1] Institute for Land Use, Faculty for Land Use and Agricultural Sciences, University Rostock, Justus-von-Liebig-Weg 6, 18044 Rostock, Germany, max.koehne@uni-rostock.de, sigrid.koehne@uni-rostock.de; [2] University of California, Riverside, Dept. of Environmental Sciences, 900 University Avenue, A135 Bourns Hall, Riverside, CA 92521, jiri.simunek@ucr.edu; [*] *Presenter*

Introduction

Model predictions of pesticide transport in structured soils are complicated by multiple processes acting concurrently. In this study, the hydraulic, physical, and chemical nonequilibrium (HNE, PNE, and CNE) processes governing isoproturon transport under variably-saturated flow conditions were analyzed. Objectives were (i) to investigate the applicability of model parameters obtained from inverse analysis of transient water flow and Br^- transport, and from equilibrium or kinetic batch isoproturon sorption experiments, for the forward simulation of isoproturon transport during variably-saturated flow, and (ii) to detect potential differences in isoproturon sorption for the PFPs and the matrix domains.

Materials and Methods

An undisturbed soil column (14.7 cm diameter, 15 cm long) was extracted from a loamy Ap horizon (2% clay, 44% silt, 54% sand, 1.8% organic carbon, bulk density 1.4 g cm^{-3}) with subangular aggregate structure (Meyer-Windel, 1998). Bromide (Br^-) and isoproturon (IPU, 3-(4-isoprpylphenyl)-1,1-dimethylurea) were applied to the soil column which was then irrigated at a rate of 1 cm h^{-1} for 3 h. Two more irrigations at the same rate and duration followed in weekly intervals. Nonlinear (Freundlich) equilibrium and two-site kinetic sorption parameters were determined for IPU using batch experiments. The observed water flow and Br^- transport were inversely simulated using mobile-immobile model (MIM), dual-permeability model with equilibrium sorption (DPM) or with kinetic sorption (DP-KM), and combined triple-porosity model (DP-MIM), all implemented in HYDRUS-1D (Šimůnek et al., 1998, 2003, Pot et al., 2005, Köhne et al., 2005).

Results

The MIM, DPM, and DP-MIM inverse simulation results for water flow and Br^- transport in the Ap soil column are displayed in Figure 1. Observed bulk soil water contents varying between 0.3 and 0.36 (Fig. 1a), pressure heads between -60 and 0 cm (Fig. 1b), and cumulative outflow (Fig. 1c) for three intermittent irrigation events were more or less matched by all three models. Simulated Br^- BTCs were within fluctuations of measured concentrations up to 7.5 days (Fig. 1d). Both the early but low Br^- peak of 5.5 mg L^{-1}, corresponding to only 0.5% of the applied concentration of 1000 mgL^{-1}, and the shape of the

Br^- BTC were delineated by all model approaches. The late-time low Br^- concentrations observed after two weeks could be most accurately captured using the DP-MIM (Fig. 1d). The assumption of the two pore domains was a suitable concept to describe Br^- leaching at HNE and PNE, at least during the first two irrigation events. The accurate match of Br^- concentrations after two weeks using the DP-MIM suggests that the late-time Br^- transport was dominated by diffusive transfer into the microporosity subdomain of the matrix that acted as a sink for Br^-.

For isoproturon, Figure 2 shows the measured BTC together with simulation results using various forward (Fig. 2a) and inverse (Fig. 2b,c,d) modeling approaches. The IPU breakthrough displayed a somewhat similar shape as the Br^- breakthrough, but at much lower concentrations below 0.2 mg L^{-1} (0.08% of the applied 254 mgL^{-1}). The simultaneous start of the BTCs for Br^- and IPU at relatively low peak concentrations suggested (weak) preferential flow conditions. The lower peak concentrations for IPU than for Br^- can be explained with sorption of IPU. The MIM forward approach predicted zero concentrations for all times and is not shown in Fig. 2a. While none of the forward modeling approaches closely approximated the observed IPU breakthrough, the DP-KM was the only approach that predicted an early concentration increase (Fig. 2a). Fitting the fraction of sorption sites in equilibrium with the mobile, f_{mo} (MIM), or fracture, f_f (DPM), domains improved results for the two-domain equilibrium sorption approaches and enabled them to almost match the early IPU peak (Fig. 2b). Note that we refer to DPM with optimized parameter f_f as DPMf in Fig. 2b and that we use similar notation for other inverse optimizations. IPU concentrations at one week were overestimated with DPM, but were matched well when the first-order degradation constant, μ, was additionally fitted (Fig. 2b). MIM slightly underestimated IPU concentrations after one week, which could not be compensated by additionally fitting μ (not shown). The match of the early IPU peak was further improved using inverse DP-KM approaches assuming HNE, PNE, and CNE (Fig. 2c). Predictions of the measured early IPU concentration increase (Fig. 2c) improved in the same order. The DP-MIM approach with the inverse estimation of f_f failed to describe IPU concentrations, but approximations improved when fitting f_f and μ; or f_f, μ and β (Fig. 2d). Furthermore we note that we obtained similar values for the fraction of sorption sites f_{mo} (= 0.056) for MIM and corresponding global values f_f w_f (=0.04 to 0.06) for DPM and DP-MIM, which can be explained with the comparable mathematical structure of the two models. The simultaneous inverse estimation of f_f, $\omega_{c,f}$, and μ in the DP-KM$f\omega\mu$ approach decreased f_f from 0.375 (batch test value for the bulk soil) to 0.187, increased the sorption rate coefficient in the fracture pore system, $\omega_{c,f}$, from 0.105 (batch test) to 0.756 d^{-1}, and increased μ from 0.046 to 0.32 d^{-1}, corresponding to a short half-life of 2.2 days. The total IPU mass loss after 14.2 days was slightly underestimated with the DP-KM$f\omega\mu$ approach. While the observed mass loss was 0.090 mg or 7.1 % of 1.27 mg IPU applied, the simulated mass loss was 0.074 mg or 5.8 %. Although the agreement between DP-KM and observed IPU concentrations was further improved by fitting the Freundlich isotherm exponent β together with f_f, ω_c, and μ, resulting parameter values appeared to be unrealistically high. Overall, the DP-KM$f\omega\mu$ approach was deemed to give the best representation of the IPU breakthrough.

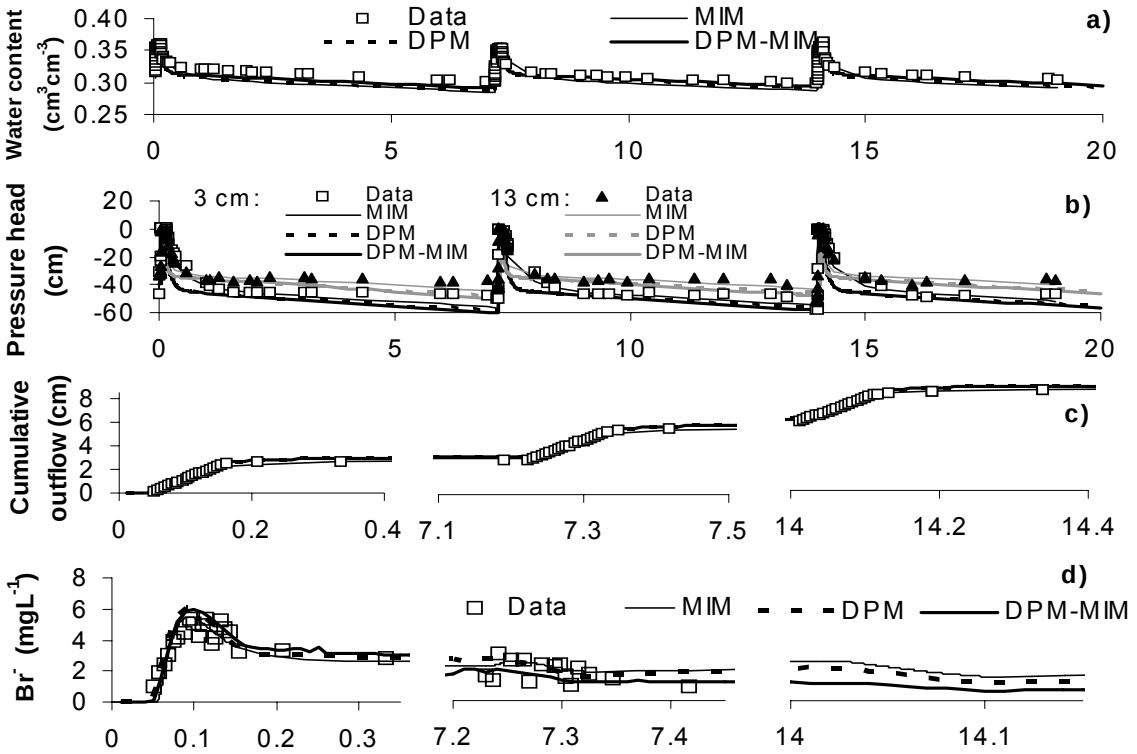

Figure 1. Water flow and bromide (Br^-) transport data and simulation results using the mobile-immobile model (MIM), dual-permeability model (DPM), and the dual-permeability triple-porosity model (DP-MIM), a) water contents, b) pressure heads at 3 and 13 cm depths, c) cumulative outflow, and d) Br^- effluent concentrations.

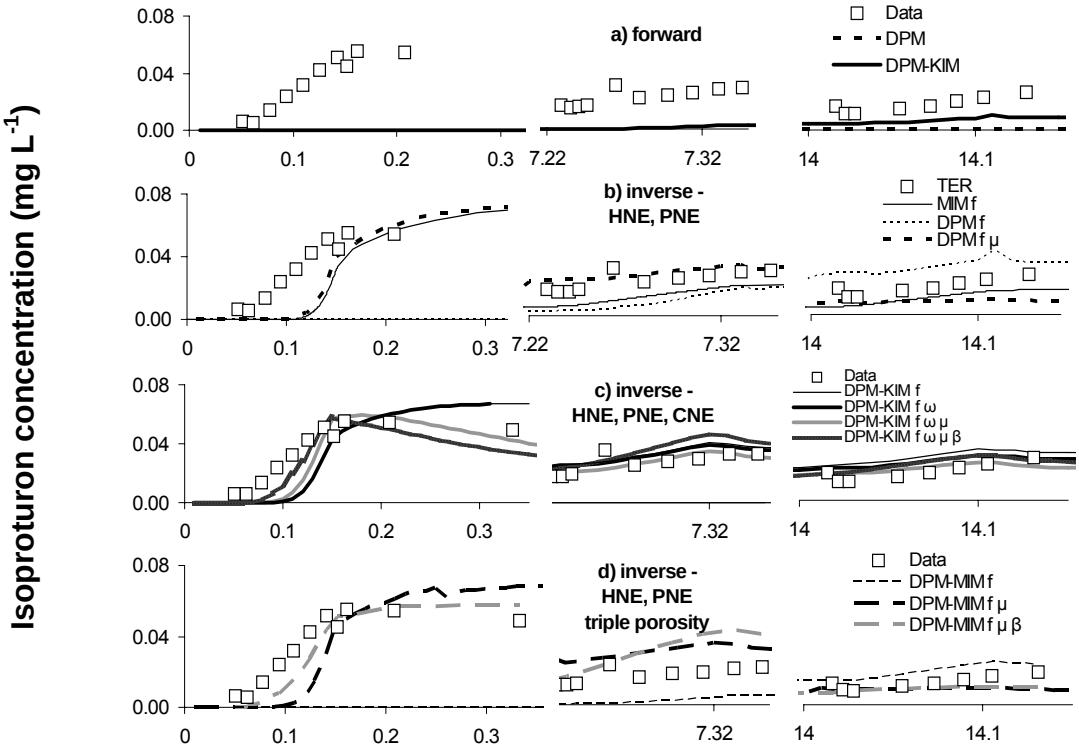

Figure 2. Isoproturon (IPU) transport data and simulation results using the mobile-immobile model (MIM), dual-permeability model (DPM), dual-permeability kinetic sorption model (DP-KM), and the dual-permeability triple-porosity model (DP-MIM), a) forward simulations, and b), c, d) different inverse simulations.

Conclusions

The improved DP-KM predictions of the isoproturon concentrations using the batch two-site kinetic sorption parameters (as compared to using batch equilibrium sorption parameters) indicated that kinetic sorption was a relevant process for preferential isoproturon leaching in the Ap soil column. The inverse DP-KM approach revealed that kinetic sorption was different in the matrix and fracture pore system, which cannot be derived from batch tests on the bulk soil. A good description of the isoproturon BTC was obtained with the inverse DP-KM approach when fitting three parameters: the fraction of equilibrium sorption sites in the fracture pore region, f_f, the first-order kinetic sorption coefficient in the fracture pore region, $\omega_{c,f}$, and the first-order decay constant in the liquid phase of both pore regions, μ. A smaller magnitude of f_f as compared to values derived from batch tests suggests that sorption in the fracture pore region was time-dependent, as compared to being largely at equilibrium in the matrix. The larger magnitude of $\omega_{c,f}$ indicated that kinetic sorption in the fracture pore system was relatively fast. Large decay rates, μ, for the bulk soil are in accordance with results of previous studies in laboratory column transport experiments. However, as was suggested already by Pot et al. (2005), high degradation rates may partly reflect irreversible sorption. Overall, modeling our data was successful and permitted identification of different processes involved in multi-process isoproturon transport under variably saturated flow conditions.

References

Meyer-Windel, S. (1998). Transport processes of bromide and isoproturons under steady-state and transient flow conditions. PhD-dissertation, Schriftenreihe Institut für Wasserwirtschaft und Landschaftsökologie der Christian-Albrechts-Universität zu Kiel, 28, 113pp.

Köhne, J.M., Köhne, S., and J. Šimůnek (2005). Multi-Process Herbicide Transport in Structured Soil Columns: Experiments and Model Analysis, submitted to Journal of Contaminant Hydrology.

Pot, V., Šimůnek, J., Benoit, P., Coquet, Y., Yra, A., and M.-J. Matrinez Cordón (2005). Impact of rainfall intensity on the transport of two isoproturons in undisturbed grassed filter strip soil cores, J. Contam. Hydrol., accepted.

Šimůnek, J., M. Šejna, and M. T. van Genuchten (1998). The HYDRUS-1D software package for simulating the one-dimensional movement of water, heat, and multiple solutes in variably-saturated media, Version 2.0, *IGWMC - TPS - 70,* International Ground Water Modeling Center, Colorado School of Mines, Golden, Colorado, 202pp.

Šimůnek, J., N.J. Jarvis, M.T. van Genuchten, and A. Gärdenäs (2003). Review and comparison of models for describing nonequilibrium and preferential flow and transport in the vadose zone. J. Hydrol. 272, 14-35.

Numerical Analysis of Soil Limiting Flow from Subsurface Sources

Naftali Lazarovitch[1,2], Jiri Šimůnek[2], Martinus Th. van Genuchten[3] and Uri Shani[1]

[1] Dept. of Soil and Water Sciences, Faculty of Agriculture, Food and Environmental Quality Sciences, Hebrew Univ. of Jerusalem, Rehovot, Israel. lazarovi@agri.huji.ac.il
[2] Dept. of Environmental Sciences, Univ. of California, Riverside, CA USA.
[3] George E. Brown, Jr. Salinity Laboratory, USDA, ARS, Riverside, CA, USA.

Abstract

The infiltration rate of water from a subsurface cavity is affected by many factors, including the pressure in the cavity, its size and geometry, and the hydraulic properties of the surrounding soil. When a predetermined discharge of a subsurface source (e.g. a subsurface emitter) is larger than the soil infiltration capacity, the pressure head in the source outlet increases and becomes positive. The increased pressure may significantly reduce the source discharge rate. The main objective of this study was to develop a system-dependent boundary condition that describes this process while considering the source characteristics, and to implement this boundary condition into HYDRUS-2D software package. The updated numerical model was validated against transient experimental data. Good agreement was found between transient cavity pressures measured in laboratory experiments and those calculated using the updated numerical model.

Introduction

When a predetermined discharge from a subsurface source (e.g. a subsurface emitter) is larger than the soil infiltration capacity, the pressure head in the source outlet increases and becomes positive (Shani et al., 1996). This pressure buildup in the soil reduces the pressure difference across the source and, subsequently, decreases the source discharge rate. Warrick and Shani (1996) showed that the reduction in the pressure difference is larger for soils having a lower hydraulic conductivity and that the positive pressure in the vicinity of the source increases rapidly at the beginning of the infiltration event and approaches a final value after only several minutes. The source discharge is also affected by the source characteristics and the cavity size of the source outlet (Shani et al., 1996). Analytical solutions for water flow from a subsurface cavity are available for calculating spatial distributions of the pressure head in the soil, ψ [L]. However, since these solutions were derived only for steady-state water flow conditions (Philip, 1992; Ben-Gal et al., 2004; Lazarovitch et al., 2005a,b), the models can be applied only to relatively long infiltration events. The models are also restricted to Gardner's (1958) hydraulic conductivity function, which represents an important simplification of the dependence of the hydraulic conductivity on the pressure head. Since numerical models can implement any model for the soil hydraulic properties and are applicable to transient conditions, they can overcome many of the restrictions imposed by analytical models. The objectives of this study were to a) implement into a transient numerical model a system-dependent boundary condition that describes infiltration from subsurface sources and considers the source characteristic curves, b) evaluate the dependence of the transient source discharge rate on the soil and source hydraulic properties, c) carry out laboratory experiments involving transient water flow from subsurface water sources, and d) compare the experimental results with those obtained with the a modified version of the HYDRUS-2D software package of Šimůnek et al. (1999).

Theory

Warrick and Shani (1996) suggested the following relationship between the source discharge, Q [L^3T^{-1}], and the inlet pressure of the source (P_{in} [L]):

$$Q = Q_0\left(\frac{P_{in} - \psi_s}{P_{in}}\right)^c \qquad [1]$$

where ψ_s [L] is the pressure head at the source-soil interface, often called the back pressure, Q_0 [L^3T^{-1}] is the nominal discharge of the source for an inlet pressure P_{in} of 10 m and a back pressure equal to zero, and c [-] is an empirical constant that reflects the flow characteristics within the emitter. Normally, c = 0.5 corresponds to a turbulent flow emitter and c = 1 to a laminar one.

In our analysis we used a numerical solution of the Richards' equation as implemented in the HYDRUS-2D code for axisymmetric flow. In addition to existing boundary conditions that available in HYDRUS-2D code, Eq. [1] was implemented as a new system-dependent boundary condition. This boundary condition allows calculation of the source discharge while considering properties of the source, and the inlet and back pressures:

$$Q = Q_0\left(\frac{P_{in} - \psi_s}{P_{in}}\right)^c = -\int_\Gamma K\left(\frac{\partial\psi}{\partial r} + \frac{\partial\psi}{\partial z} - \delta_{iz}\right)n_i d\Gamma \qquad [2]$$

where δ_{iz} is the Kronecker delta [-], Γ is the boundary of the source, and n_i are the components of the outward unit vector normal to the boundary. At each time step during the calculations, the discharge rate was adjusted while ψ_s was calculated by averaging pressure heads (from the previous time step) around the subsurface source:

$$\overline{\psi_S} = \frac{1}{\Gamma}\cdot\int_\Gamma \psi_S d\Gamma \qquad [3]$$

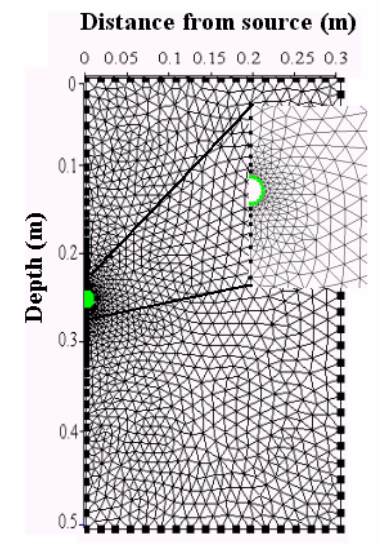

Figure 1. Finite element grid and flow domain. Water flows from the half sphere on the left (zoomed). Boundary condition [1] is specified on the sphere surface, while zero flux conditions are applied to the other boundaries.

Application

An axisymmetrical three-dimensional flow domain was selected as shown schematically in Fig. 1. The flow domain (50 x 30 cm) was discretized into 1183 triangular finite elements with triangles significantly smaller around the source and then smoothly increasing with distance from the source. Except for the free drainage boundary condition at the bottom of the flow domain and the source boundary condition [2] at the source-soil interface, all boundaries were subjected to zero flow conditions.

Laboratory drip irrigation experiments were carried out with a non-compensated dripper packed inside a perforated plastic sphere (the source) with a radius of 0.01 m. The source was connected to a flexible tube and buried 0.25 m deep in a Magal clay loam soil. Sources with nominal discharges Q_0 of 4 and 8 L h^{-1} were used, while a value of 0.5 for c in [1] was assumed for all sources. Hereafter we denote the source by its Q_0 value.

The saturated hydraulic conductivity was estimated using the horizontal soil column constant head method (Hillel, 1971), while the retention curve $\theta(\psi)$ was determined using a ceramic plate suction cell apparatus (Klute, 1986). The Mualem-van Genuchten soil hydraulic model (van Genuchten, 1980) was fitted to the data using the RETC least-square optimization program of van Genuchten et al. (1991) to obtain the following values for the soil hydraulic parameters: α=3.01 m^{-1}, n=1.57, K_s = $3.47 \cdot 10^{-6}$ ms^{-1}, θ_r=0.05, and θ_s=0.51.

The subsurface source was connected to a Mariotte apparatus that maintained a constant input pressure, P_{in}. The discharge Q was measured by weighing the Mariotte apparatus. A pressure transducer was inserted into the source to measure the pressure head in the source cavity. The initial water content was measured at several points and depths using TDR.

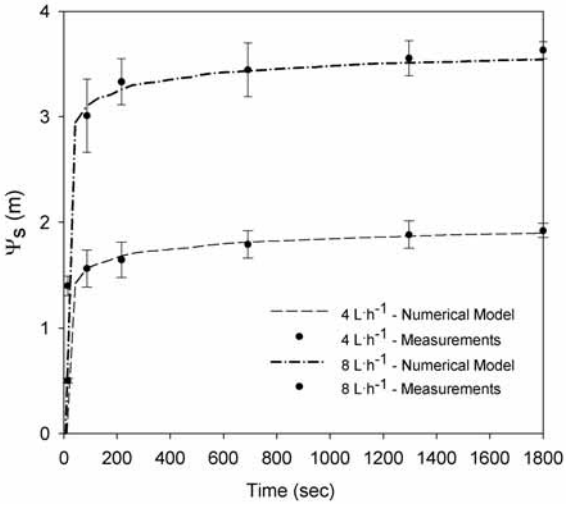

Figure 2. Measured (triangles and circles) and calculated (lines) soil pressure heads as a function of time for two subsurface sources (4 and 8 $L \cdot h^{-1}$) in the Magal clay loam with the source radius r_0 of 0.01 m and the inlet

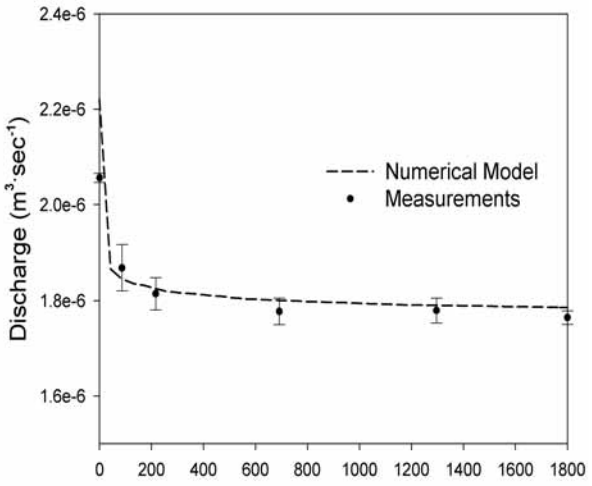

Figure 3. Measured (triangles) and calculated (lines) discharge from a subsurface source as a function of time for an 8 $L \cdot h^{-1}$ source and the Magal clay loam with the source radius r_0 of 0.01 m and the inlet pressure P_{in} of 10 m.

Measured and calculated back pressures ψ_s as a function of time for two sources with nominal discharge rates Q_0 of 4 and 8 L h^{-1} are presented in Fig. 2 for a radius r_0 of 0.01 m and an inlet pressure P_{in} of 10 m. The initial water content was considered to be constant (0.07) throughout the flow domain. For both sources ψ_s increased rapidly during the first 10 to 15 minutes, but then gradually approached a final value as time proceeded. The final value of ψ_s was 2 and 3.7 m for the 4 and 8 L h^{-1} sources, respectively. Notice the excellent agreement between the measurements and the calculations.

The transient decrease in the source discharge is depicted in Fig. 3 for a nominal discharge Q_0 of 8 L h^{-1}, an inlet pressure P_{in} of 10 m, and a radius r_0 of 0.01 m. Following an increase in ψ_s from zero to 3.7 m (Fig. 2), the pressure difference between the soil back pressure and the source inlet decreased, and the discharge rate decreased from $2.22 \cdot 10^{-6}$ m^3 s^{-1} to $1.73 \cdot 10^{-6}$ $m^3 \cdot s^{-1}$. HYDRUS-2D predicted the measurements again very well. The results presented in Fig. 3 demonstrate the transient nature of the subsurface source discharge and the significant decrease in discharge due to development of the back pressure.

Conclusions

Good agreement was found between transient back pressures measured in the laboratory experiment and those calculated using the updated HYDRUS-2D numerical model. The modified model allows the use of any hydraulic model for soil and source properties, simulation of both short and long duration infiltration events, and consideration of various source geometrical shapes. The modified numerical model also enables complex processes in the root zone involving short-time irrigation and root water uptake.

Previous infiltration models that describe transient flow from subsurface sources neglect the possibility that the soil hydraulic properties will limit the infiltration capacity. This phenomenon can lead to an increase in the water pressure head at the source, and hence a lower source discharge rate. If neglected, the dependence of the subsurface source discharge on the soil hydraulic properties can lead to smaller than designed irrigation volumes when the irrigation amount is preset by time, and consequently to considerable non-uniformity in water application rates (Warrick and Shani, 1996).

References

Ben Gal, A., N. Lazarovitch, and U. Shani. 2004. Subsurface drip irrigation in gravel filled cavities. Vadose Zone J. 2004 3: 1407-1413.

Gardner, W. R. 1958. Some steady-state solutions of the unsaturated moisture flow equation with application to evaporation from a water table. Soil Sci., V. 85, P. 228-232.

Hillel, D. 1971. Soil and Water Physical Principles and Processes. Academic Press, New York. pp 82–83,106–107,228–230.

Klute, A. 1986. Water retention:Laboratory methods.In Methods of Soil Analysis,Part 1 2nd edition.Ed.A Klute. pp 635–662.ASA Inc.,Madison,WI.

Lazarovitch, N. J., J. Šimůnek, and U. Shani. 2005. System dependent boundary condition for water flow from subsurface source, Soil Sci. Soc. Am. J., 69, 46-51.

Lazarovitch, N., Thompson, L.T., Warrick, A.W. and Shani, U. Soil Hydraulic Properties Effecting Discharge Uniformity of Subsurface Drip Irrigation. Submitted to J. Irrig. and Drain. Eng.

Philip, J. R. 1992. What happens near a quasi-linear point source? Water Resour. Res., V. 28, P.47-52.

Šimůnek, J., M. Sejna, and M. T. van Genuchten, 1999. The HYDRUS-2D software package for simulating two-dimensional movement of water, heat, and multiple solutes in variably saturated media, Version 2.0, Rep. IGWMC-TPS-53, 251 pp., Int. Ground Water Model. Cent., Colo. Sch. of Mines, Golden.

Shani, U., Xue, S., Gordin-Katz, R. and Warrick, A. W. 1996. Soil limiting flow from subsurface emitters. 1: Pressure measurements . J. Irrig. and Drain. Eng. 122(5), P. 291-295.

van Genuchten, M.Th. 1980. A closed-form equation for predicting the hydraulic conductivity of unsaturated soils. Soil Sci. Soc. Am. J. 44:892-898.

van Genuchten, M.Th., F.J. Leij, and S.R. Yates. 1991. The RETC code for quantifying the hydraulic functions of unsaturated soils. USEPA Rep. 600/2-91-065 (IAGDW1293-3-934). U.S. Salinity Laboratory, USDA-ARS, Riverside, CA.

Warrick, A.W. and Shani, U. 1996. Soil limiting flow from subsurface emitters. 2: Effect on uniformity. J. Irrig. and Drain. Eng. 122(5), P. 296-300.

Modelling groundwater - surface water interactions in Dutch fens

Paul P. Schot and Stefan C. Dekker

Department of Environmental Sciences
COPERNICUS Institute for Sustainable Development and Innovation
Utrecht University
P.O. Box 80.115, 3508TC Utrecht
The Netherlands
p.schot@geo.uu.nl

Introduction

Wetland ecosystems in the Netherlands are heavily influenced by human interventions. From the twelfth century onward, the wetlands have increasingly been drained for agricultural purposes. Systems of connected drainage canals (ditches) were dug to create polders in which the surface water levels were artificially controlled using windmills to discharge excess water. Nowadays most wetland areas are drained and predominantly used for dairy farming.
A number of wetland remnants within the agricultural land use matrix presently are designated as protected nature reserves. However, they still contain the drainage canals in which surface water levels are artificially adjusted to the needs of the surrounding agricultural areas. Amongst the protected nature reserves are fen wetlands which are characterised by a species rich vegetation and high biodiversity. Inflow of nutrient poor, alkaline groundwater is generally seen as a prerequisite for the development of this species rich fen vegetation (e.g. Wheeler and Shaw, 1995).
However, drainage and groundwater abstraction have affected the hydrological functioning of the fens. These human interventions may lead to the development of so-called rainwater lenses in the upper groundwater of fens, which prevent upward seeping alkaline groundwater from reaching the fen root zone (fig. 1). This threatens the conservation of the species rich vegetation.
As a basis for conservation and restoration of fen biodiversity, numerical groundwater flow simulations were performed for a case area in the Netherlands, in order to provide insight in rainwater lens dynamics.

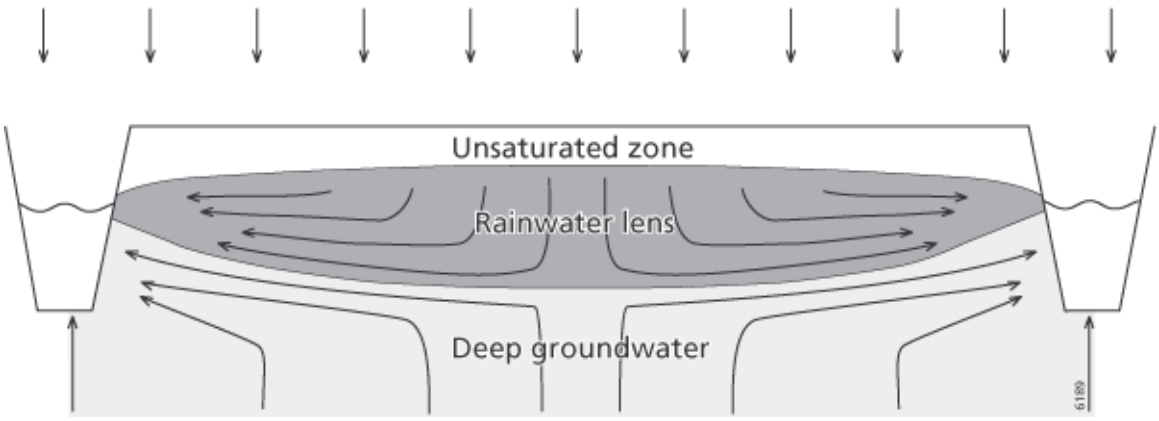

Figure 1. Schematic representation of a rainwater lens on top of upwelling groundwater.

Method

The numerical two-dimensional unsaturated-saturated groundwater flow and transport model Hydrus-2D (Simunek et al., 1999) was used to simulate the form of rainwater lenses characteristic for the case area, as a function of hydrological boundary conditions and geology.
A two-dimensional section representative for the fen remnants area was modelled. The section is perpendicular to the parallel drainage canals that are characteristic of the polders in the case area. Left and right model boundaries represent flow lines located halfway two drainage canals making them no flow boundaries. The atmospheric upper model boundary automatically switches between Dirichlet and Neumann boundary conditions if minimum or maximum surface pressure head is reached. The lower model boundary was defined as a constant flux boundary assuring upward seepage at all times. The model drainage canals have a free drainage face above the fixed surface water level, while a fixed head boundary applies below the surface water level. The model was set to instantly remove exfiltrating groundwater at the soil surface (e.g. surface runoff) when the phreatic water level exceeds the soil surface. Ponding was not considered. Permeabilities of the sandy aquifer and semi-confining peat and clay layers are representative for the sediments in the case area and the aquifer is considered homogenous and isotropic.

The model was used to provide insight in rainwater lens dynamics as a function of drainage canal water levels, upward groundwater inflow fluxes and the thickness of semi-confining layers. Table 1 presents boundary conditions for the steady state simulations. Thicknesses of the semi-confining layer of 0, 1 and 2 m were simulated.

Table 1. *Boundary conditions for the steady state simulations. (W and S = weak and strong drainage; – and + = low and high upward groundwater flux)*

Run	**Drainage canal water level** (m NAP)	**Lower boundary upward flux** (mm d^{-1})
W+	-0.30	10
W-	-0.30	5
S+	-0.60	10
S-	-0.60	5

Results

The simulations indicate that drainage canal surface water levels mainly affect the phreatic level in the fens, while groundwater inflow fluxes mainly affect the thickness of the rainwater lens. Increasing thickness of a semi-confining surface layer results in a rise in phreatic level. As soon as the phreatic level reaches the soil surface the rainwater lens may split in two as a result of groundwater discharge windows, which come into existence in the centre of the parcel.

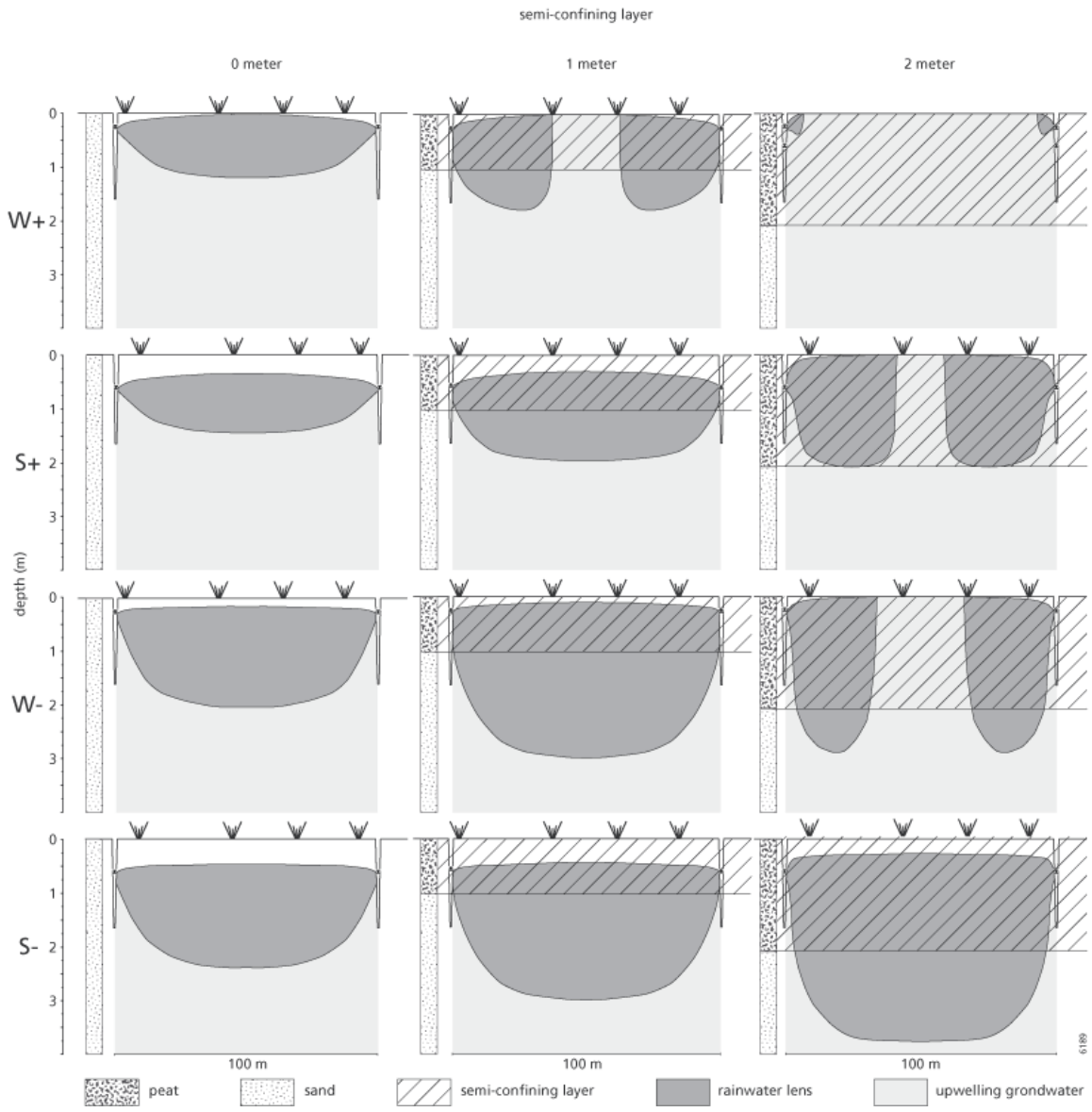

Figure 2. Yearly average form of the rainwater lens as a function of:

- *weak and strong drainage (W and S) and groundwater inflow flux (- and +) (vertical axis);*
- *presence of a semi-confining surface layer (0, 1 and 2 meter) (horizontal axis).*

For W-, W+, S-, S+ see table 1. (source: Schot et al, 2004)

Discussion

Most simulations show rainwater lens thicknesses well exceeding rooting depths of fen plants. This is inconsistent with the fact that fen vegetation is still found in nature reserves for which the simulations are considered representative. Chemical buffer processes in the soil may explain this inconsistency, masking an acidification process under way. As buffer capacities will become exhausted over time, acidification and fen

deterioration will occur at a certain future moment. To arrive at more definite conclusions about this hypothesis, our simulations of steady-state convective groundwater flow need to be supplemented by transient modelling of groundwater flow, as well as of hydrochemical processes in rainwater lenses, followed by verification at actual field locations. These activities are presently underway.

References

Schot, P.P., Dekker, S.C. and Poot, A.. The dynamic form of rainwater lenses in drained fens. *Journal of Hydrology*, 293 (2004) pp. 74-84.

Simunek, J., Sejna, M. and Van Genuchten, M.T., 1999. *The HYDRUS2D software package for simulating the two-dimensional movement of water, heat, and multiple solutes in variably-saturate media*. U.S. Salinity Laboratory, USDA/ARS, Riverside, California, pp. 227.

Wheeler, B.D. and Shaw, S.C., 1995. A focus on fens - Controls on the composition of fen vegetation in relation to restoration. In: B.D. Wheeler, S.C. Shaw, W.J. Fojt and R.A. Robertson (Editors), *Restoration of temperate wetlands*, Chichester, Wiley, pp. 33-48.

Chlorotoluron transport in the soil profile affected by non-equilibrium flow

Radka Kodešová[1], Martin Kočárek [1], Jiří Šimůnek[2], Josef Kozák[1]
[1] Czech University of Agriculture in Prague, Department of Soil Science and Geology, Kamýcká 129, 16521 Prague, Czech Republic, kodesova@af.czu.cz, kocarek@af.czu.cz, kozak@af.czu.cz
[2]University of California Riverside, Department of Environmental Sciences, Riverside, CA 92521, USA, jiri.simunek@usr.edu

Introduction

Non-equilibrium water flow and contaminant transport in soil porous media are frequently observed phenomena. Numerical models that assume bi-modal soil porous systems have been developed to describe non-equilibrium flow and solute transport. Single-porosity, dual-porosity and dual-permeability models in HYDRUS-1D (Šimůnek et al., 1998, 2003) were applied in this study to estimate soil hydraulic parameters from laboratory multi-step outflow experiment via numerical inversion and to simulate chlorotoluron transport in the soil profile that was experimentally studied in the field.

Materials and Methods

The transport of chlorotoluron in the soil profile was studied under field conditions. The herbicide Syncuran was applied on a four square meter plot using an application rate of 2.5 kg/ha of active ingredient. Chlorotoluron dissolves in water, adsorbs on soil particles and degrades with time. Soil samples were taken after 6, 14, 22 and 36 days to study the residual chlorotoluron distribution in the soil profile.

The soil was defined as Greyic Phaozem. The soil profile was divided into two layers: 0-35 cm and 35-80 cm. The soil hydraulic properties were defined as follows. The multi-step outflow experiments (van Dam et al., 1994) were performed on the 100 cm^3 undisturbed soil samples (A,B,C,D) using the 15, 30, 70, 130 and 210 cm pressure head steps. The pressure head steps and the soil-water contents obtained from the final soil-water contents and water balances in the soil samples provide data points of the soil-water retention curves. The code HYDRUS-1D (Šimůnek et al., 1998, 2003) and the numerical inversion (Hopmans et al., 2002) were used to analyze the cumulative outflow and the soil-water retention data points to obtain hydraulic parameters characterizing different soil-water flow models: the single-porosity model, the dual-porosity model, and the dual-permeability model. In all cases limited sets of parameters had to be optimized to ensure unique results.

The chlorotoluron transport under field conditions was simulated using the single-porosity, dual-porosity, and dual-permeability models in HYDRUS-1D. The top boundary condition was defined using daily precipitation and potential transpiration rates. Given the root zone depth of 20 cm, a Feddes model in HYDRUS-1D with parameters defined for wheat was applied to simulate the root water uptake. The bottom boundary condition was defined as a free drainage. The bulk densities were 1.5 g/cm^3 and 1.55 g/cm^3 for the first and second layers, respectively. The Freundlich adsorption isotherm was measured for the first layer: k_F = 2.73 and n_F = 1.33. Degradation rate 0.002 day^{-1} was estimated from the herbicide content 36 days after the herbicide application (Kočárek et al., 2005). Degradation was assumed to occur in both water and solid phases. The reasons were previously discussed in Kodešová et al.

(2004) for Chermozem. The longitudinal dispersivity was set to 2 cm for the single- and dual-porosity models, and 2 and 1 cm in matrix and macropore domain, respectively, for the dual-permeability model. The molecular diffusion was 1 cm^2day^{-1} in all cases.

Results and Discussion

Soil hydraulic parameters (van Genuchten, 1980) for the single-porosity model obtained using the numerical inversion of the cumulative outflow and soil-water retention curve data are shown in Tab. 1. Values of θ_s were obtained from the water balance in the soil samples.

Soil hydraulic parameters for the dual-porosity model obtained using the numerical inversion of cumulative outflow and soil-water retention curve data are shown in Tab. 2. Values of $\theta_{r,t}$, $\theta_{s,t}$ (t = total), α_m and n_m (m = mobile domain) are equal to values of θ_r, θ_s, α and n for the single-porosity model. Values of $\theta_{r,im}$ and $\theta_{s,im}$ (im = immobile domain) were estimated. ω_w is the water transfer coefficient between the immobile and mobile domains.

Table 1: Soil hydraulic parameters – single-porosity model.

	θ_r [cm^3cm^{-3}]	θ_s [cm^3cm^{-3}]	α [cm^{-1}]	n	K_s [cm/day]
A (1 - 35)	0.293	0.391*	0.0141	1.891	1.061
B (1 - 35)	0.306	0.389*	0.0101	2.289	0.382
C (35 - 80)	0.126	0.413*	0.0140	1.255	20.40
D (35 - 80)	0.000	0.410*	0.0145	1.145	10.78

* not optimized

Table 2: Soil hydraulic parameters – dual-porosity model.

	$\theta_{r,t}$ / $\theta_{r,im}$ [cm^3cm^{-3}]	$\theta_{s,t}$ / $\theta_{s,im}$ [cm^3cm^{-3}]	α_m [cm^{-1}]	n_m	$K_{s,m}$ [cm/day]	ω_w [day^{-1}]
A (1 - 35)	0.293* / 0.293*	0.391* / 0.320*	0.0141*	1.891*	1.020	$5.86\ 10^{-5}$
B (1 - 35)	0.306* / 0.306*	0.389* / 0.320*	0.0101*	2.289*	0.334	$2.25\ 10^{-4}$
C (35 - 80)	0.126* / 0.126*	0.413* / 0.250*	0.0140*	1.255*	19.92	$4.85\ 10^{-5}$
D (35 - 80)	0.000* / 0.000*	0.410* / 0.250*	0.0145*	1.145*	12.48	$9.07\ 10^{-4}$

* not optimized

Table 3: Soil hydraulic parameters – dual-permeability model.

	$\theta_{r,f}$ / $\theta_{r,m}$ [cm^3cm^{-3}]	$\theta_{s,f}$ / $\theta_{s,m}$ [cm^3cm^{-3}]	α_f / α_m [cm^{-1}]	n_f / n_m	$K_{s,f}$ / $K_{s,m}$ [cm/day]
A (1 - 35)	0* / 0.293*	0.450* / 0.391*	0.023 / 0.0037	3* / 2.990	9.720* / 0.012
B (1 - 35)	-	-	-	-	-
C (35 - 80)	0* / 0.126*	0.450* / 0.413*	0.030 / 0.0028	3* / 1.689	187.2* / 0.142
D (35 - 80)	0* / 0.000*	0.450* / 0.410*	0.022 / 0.0027	3* / 1.237	98.88* / 0.219

* not optimized

Soil hydraulic parameters for the dual-permeability model obtained using the numerical inversion of cumulative outflow data are shown in Tab. 3. Following parameters defining the structure of matrix (m) and macropore (f) domains were used in all cases: $w = 0.1$, $\beta = 15$, $d = 0.3$ cm, $\gamma_w = 0.4$. Values of $\theta_{r,m}$ *a* $\theta_{s,m}$ are equal to values of θ_r and θ_s for the single-porosity model. Values of $\theta_{r,f}$, $\theta_{s,f}$ a n_f were estimated. Values of $K_{s,f}$ were determined based on the

following assumptions: 0.9 $K_{s,m}$ + 0.1 $K_{s,f}$ equals to K_s for the single-porosity model and $K_{s,f}$ values are hundred times larger then initial estimates of $K_{s,m}$ values. Experimental data for the sample B could not be successfully analyzed using this model. In other three cases the sum of soil-water retention curves of both domains multiplied by corresponding ratios of each domain follow the measured soil-water retention data points.

The hydraulic parameters obtained for the soil samples A and C were used to simulate chlorotoluron transport in the two-layered soil profile. Calculated chlorotoluron concentrations 6, 14, 22 and 36 days after the application are shown in Fig. 1a for the single-porosity model, in Fig. 1b for the dual-porosity model and in Fig. 1c for the dual-permeability model. Measured chlorotoluron concentrations are shown in Fig. 1d.

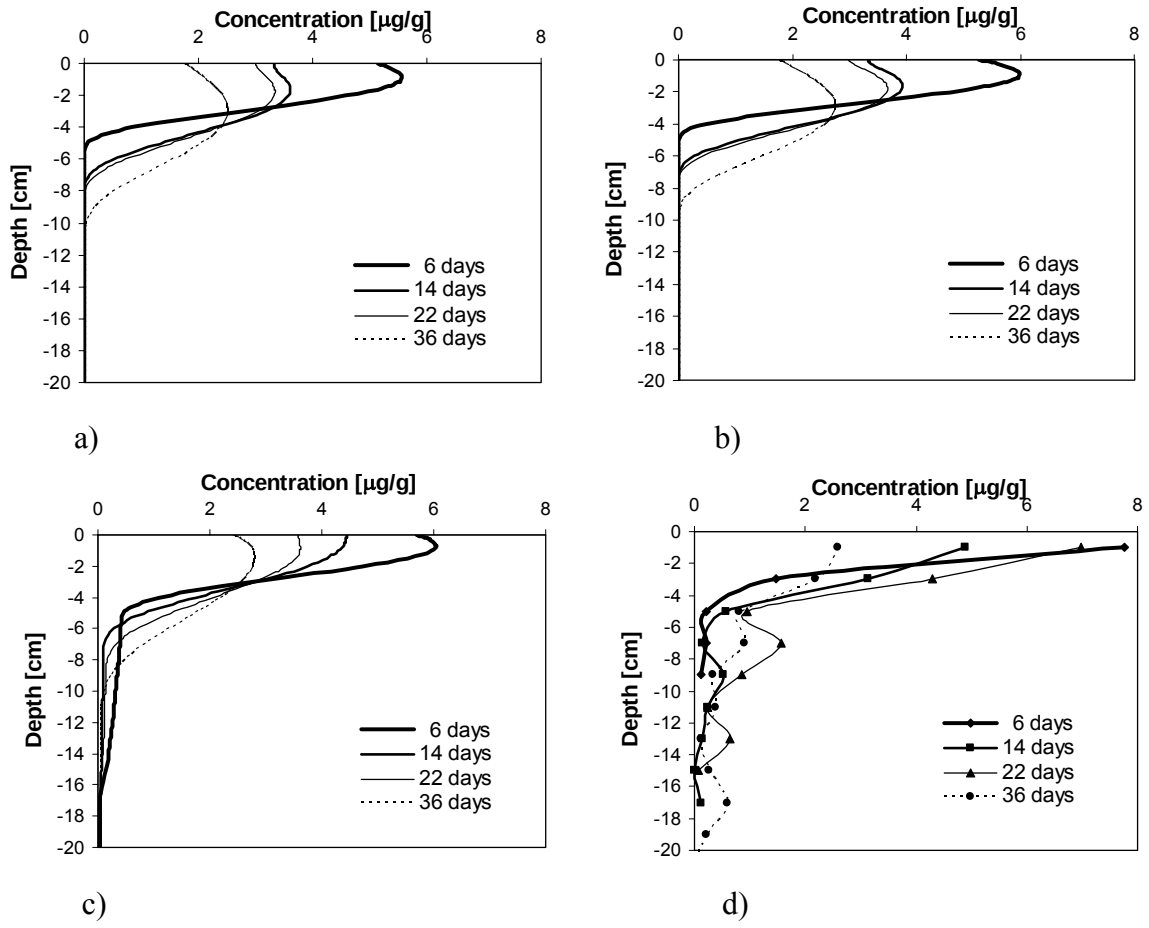

Figure 1. Chlorotoluron distribution in the soil profile a) single-porosity model, b) dual-porosity model, c) dual-permeability model, d) measured values (averages from 3 sampling positions).

Figs. 1a and 1b show that immobile water in the dual-porosity system had only a little impact on the solute transport. Solute moved to a depth of 10 cm in the single-porosity system compared to 9 cm in the dual-porosity system. In the case of the dual-permeability system solute moved to a depth of 60 cm (depth not shown in Fig. 1c). Comparison of all simulated and measured chlorotoluron distributions makes obvious that the results of the dual-permeability model correspond more to the measured values then the other two models due to the fact that observed herbicide transport was highly affected by a preferential flow. It should be mentioned that the measured total chlorotoluron contents in the soil profile 22nd day after

the herbicide application is higher then the total chlorotoluron concentrations measured on 6th and 14th day. This may be due to an uneven distribution of chlorotoluron on the soil surface, herbicide transport through the preferential paths and its deviation from the vertical axes. Observed oscillations of chlorotoluron concentrations in depths of 6 – 20 cm were probably caused by preferential flow (quick solute penetration to deeper depths) and solute accumulation due to the disconnection of preferential pathways. This phenomenon was not considered in the model.

Conclusions

It is shown that, despite having very similar total soil hydraulic prosperities for different flow models, the simulated chlorotoluron transport is different. Observed chlorotoluron transport was affected by preferential flow. Therefore chlorotoluron concentrations in the soil profile simulated using the dual-permeability model are closer to observed values then those calculated with the other two models. The impact of different definitions of the soil porous system as single-porosity or dual-permeability systems with the similar total soil hydraulic properties was previously discussed for Chernozem in Kodešová et al. (2005). The dual-permeability model is a powerful tool describing preferential flow and transport.

Acknowledgement

Authors acknowledge the financial support of the Czech Grant Agency GA CR No. 103/05/2143. Thanks are due to K. Němeček for his help with the fieldwork and O. Drábek for the chemical analysis.

References

Hopmans, J. W., Šimůnek, J., Romano, N., Durner, W. (2002): Inverse methods, in Methods of Soil Analysis, Soil Science Society of America, Inc. Madison, Wis., 963-1008.

Kočárek, M., Kodešová R., Kozák, J., Drábek, O., Vacek, O. (2005): Chlorotoluron behaviour in five different soil types. Plant, Soil and Environment, 51 (7), 304-309.

Kodešová, R., Kozák, J., Vacek, O. (2004): Field and numerical study of chlorotoluron transport in the soil profile, Plant, Soil and Environment, 50 (8): 333-338.

Kodešová, R., Kozák, J., Šimůnek, J., Vacek, O. (2005): Single and dual-permeability model of chlorotoluron transport in the soil profile. Plant, Soil and Environment, 51 (7), 310-315.

Šimůnek J., Šejna M., van Genuchten M. Th. (1998): The HYDRUS-1D software package for simulating the one-dimensional movement of water, heat and multiple solutes in variably-saturated media. Version 2.0. IGWMC-TPS-53. International Ground Water Modeling Center, Colorado School of Mines, Golden, CO.

Šimůnek J., Jarvis N. J., van Genuchten M. Th., Gärdenäs A. (2003): Review and comparison of models for describing non-equilibrium and preferential flow and transport in the vadose zone, Journal of Hydrology, 272, 14-35.

van Dam, J. C., Stricker, N. M., and Droogers, P. (1994): Inverse method to determine soil hydraulic functions from multistep outflow experiments. Soil Sci. Soc. Am. J., 58, 647-652.

van Genuchten M. Th. (1980): A closed-form equation for predicting the hydraulic conductivity of unsaturated soils. Soil Sci. Soc. Am. J., 44: 892-898.

Simulating simultaneous nitrification and denitrification with a modified 2D-mobile immobile model.

Sigrid Köhne[1*], Jiri Šimůnek[2], J. Maximilian Köhne[1] and Bernd Lennartz[1]

1 Introduction

Permanent grassland and cattle production characterize agriculture in many lowland regions with artificial drainage systems. In addition to mineral fertilizers, cattle manure is used as nitrogen (N) source in such areas. Whereas the manure carries about mostly ammonium (NH_4) as directly plant available N, mineral fertilizer N may contain nitrate (NO_3) or NH_4, or both.

Nitrification and denitrification are biological processes within the soil nitrogen cycle. Ammonium is oxidized to NO_3 by autotrophic nitrifying bacteria under aerobic conditions. Under anaerobic conditions, NO_3 may be used by heterotrophic denitrifying bacteria during respiration to be reduced into gaseous NO_2 or N_2. The facultative anaerobic denitrifying bacteria need a very low oxygen (O_2) concentration to accept NO_3 as terminal electron acceptor. In soils, very low O_2 concentrations are usually associated either with water saturation (Wilson and Bouwer 1997) or with spots of high decomposition (Nielsen et al. 1996, De Klein et al. 1996). Moreover, nitrification and denitrification depend on soil temperature and soil pH.

Because nitrification and denitrification proceed under contrasting redox conditions, they are regarded as separate processes with respect to time or location. Recently, there is increasing evidence that nitrification and denitrification occur simultaneously and in close vicinity to each other in the soil (Abassi and Adams 1998, De Klein et al. 1996, Nielsen et al. 1996, Zanner and Bloom 1995). Vertical Redox gradients across the first few centimetres from the surface resulted in parallel occurrence of nitrification and denitrification in a grass covered compacted soil (Abassi and Adams 1998). Anaerobic-aerobic interfaces may prevail at spots of high decomposition of organic matter or manure and can induce coupled nitrification-denitrification (Nielsen et al. 1996). The NH_4 released from such anaerobic spots to the neighbouring aerobic soil material was found to be nitrified at the anaerobic-aerobic interface, whereupon the nitrification product, NO_3, diffused back into the anaerobic spot to be denitrified (Nielsen et al, 1996). Similarly, De Klein et al. (1996) found that mineralization-induced O_2 consumption in combination with high water contents led to the development of denitrification zones within a basically aerated soil. Adjacent cells of aerobic and anaerobic conditions may also be caused by local variations in water contents and lead to simultaneous nitrification and denitrification in flooded soils (Lindau et al, 1988). Zanner and Bloom (1995) suspected anaerobic soil aggregate centres and aerobic inter-aggregate space (Fig. 1) to cause simultaneous nitrification and denitrification in soil.

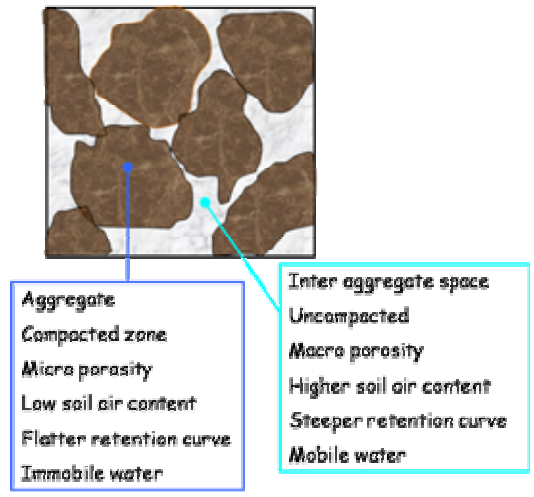

Fig 1: Small scale variation of soil properties in aggregated soils.

[1] Institute for Land Use, Faculty for Land use and Agricultural Sciences, University Rostock, Justus-von-Liebig-Weg 6,18044 Rostock, Germany, sigrid.koehne@uni-rostock.de, max.koehne@uni-rostock.de, bernd.lennartz@uni-rostock.de , * *Corresponding author*

[2] Dept. of Environmental Sciences, University of California, Riverside, 900 University Avenue, A135 Bourns Hall, Riverside, CA 92521, jiri.simunek@ucr.edu

The Infeld experimental station is situated in northern Germany and has been used to monitor, among others, NO_3 and NH_4 leaching losses via tile drains over decades. In a study about N leaching losses and N balance of the site under pasture, Spatz et al. (1989) found that the high amount of N-input by fertilizer is not recovered with the exported crop plus the N loss in drainage water. The authors conclude that a considerable amount of the fertilizer N is lost by denitrification.

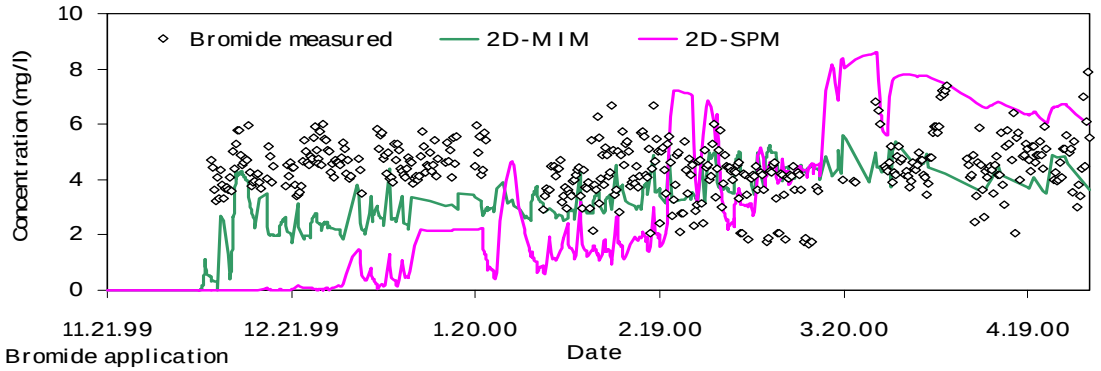

Fig. 2. Bromide concentrations in tile drainage water as compared to simulations with the 2D mobile immobile model (MIM) and the 2D single porosity model (SPM).

A tracer study performed at Infeld was analysed with different mobile immobile (MIM) and single porosity (SPM) models and revealed that transport through the soil towards drains was influenced by immobile water regions (Fig. 2). While the mobile regions accelerated bromide transport through the soil, the immobile regions acted as a sink for more than 60% of the surface applied tracer mass (Köhne et al. 2005).

Our hypothesis is that immobile regions hold high water contents over long periods and thus are more often anaerobic than the adjacent mobile water regions that change their water contents more dynamically in response to variable atmospheric conditions. Physically, the immobile regions may represent soil aggregates with rather small pores. The mobile regions may represent the inter-aggregate space. As with decomposition induced anaerobicity described above, NO_3 can be produced from added NH_4 in the aerated mobile regions, and then be transferred into the immobile regions (aggregates) where the reductive denitrification process is taking place. During dry and sufficiently warm periods, nitrification can also occur within the unsaturated immobile region.

The basic idea of this study is to investigate long term nitrate transport as affected by both immobilization and metabolization. To follow the objective, we extended the 2D-MIM, as implemented in HYDRUS-2D, with a relatively simple nitrogen metabolism model, where the nitrogen reaction rates in each, the mobile and immobile regions, are functions of bulk soil temperature and the mobile and immobile water contents, respectively.

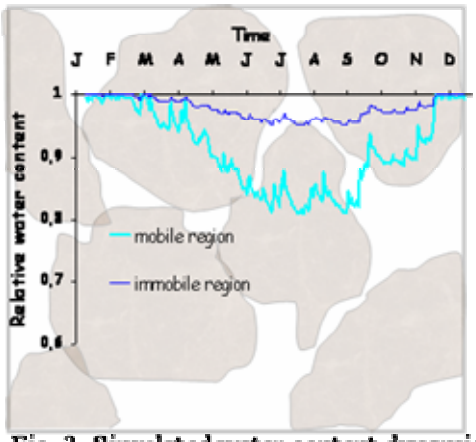

Fig. 3. Simulated water content dynamics in mobile and immobile regions at 15 cm soil depth.

2 Extension of the 2D-MIM

Figure 3 shows exemplary water contents in mobile and immobile regions as simulated with the HYDRUS-2D MIM. The simulation is based on model parameters as given in Köhne et al (2005) for the Infeld plot B. The water contents of the mobile region reach a

lower saturation than those of the immobile region. Fig. 4 is an extension of Fig. 3 that shows the implementation of simultaneous aerobic and anaerobic processes. Nitrification and denitrification were calculated as first order processes with potential rates μ' and μ, respectively, and response functions considering the effects of soil moisture.

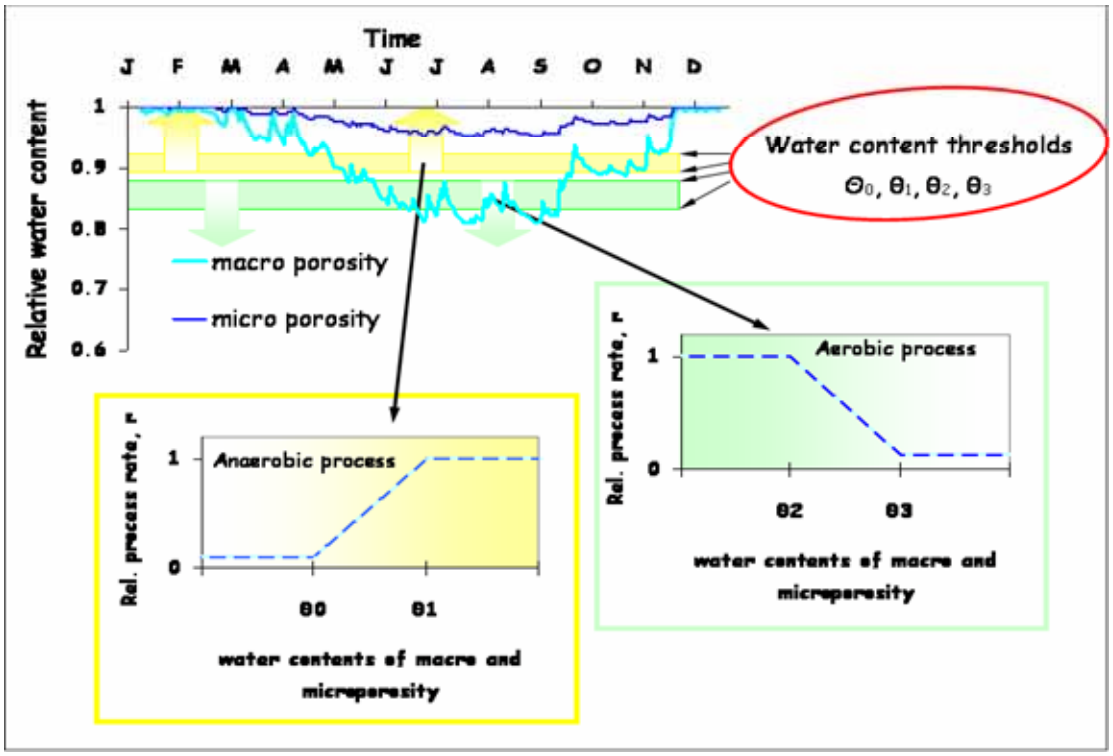

Fig. 4. Coupling the dual porosity concept with water content dependent processes rates to obtain simultaneous occurrence of aerobic and anaerobic processes.

The response functions for the aerobic and anaerobic processes are depicted in the green and yellow frames of Fig. 4, respectively. Under aerobic conditions, denitrification is reduced to a minimal rate of r_{min0} times μ. The relative rate r increases linearly from r_{min0} to 1 over a water content range between θ_0 and θ_1. In a similar way, relative nitrification rates reduce from 1 to r_{min1} over the range specified by θ_2 and θ_3. The soil moisture response functions are separately defined for each, mobile and immobile water contents. Besides the soil region moistures, temperature dependence of the process rates was considered (not shown in Fig. 4).

3 First simulation results

Fig. 5 shows simulations of NO_3 concentrations in drain outflow (symbols) and in the mobile and immobile region at the drain (light and dark lines, respectively) as compared to the 12-year measurements at the Infeld site. Simulation 1 and 2 are based on N transformations limited to the upper 25 cm (top soil) of the 2-m soil profil with 1 m tile drain depth and 18 m drain spacing. They differ in the water content thresholds with nitrification (denitrification) decreasing (increasing) between 93and 95 % saturation of both, the mobile and immobile zones for simulation 1 and between 90 and 93 % saturation of the regions for simulation 2. Simulation 3 allows for N transformations in the entire profile with the saturation thresholds set as in simulation 1. Increasing denitrification (by setting the thresholds in a lower saturation range) yields lower concentrations at the drain (compare simulations 1 and 2).

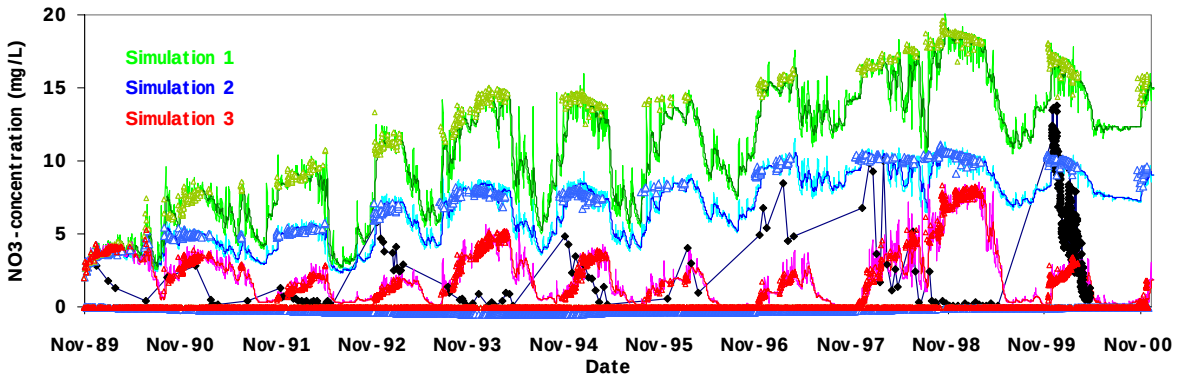

Fig. 5. Twelve year measurements of nitrate concentrations in tile drain outflow and simulations of NO3 concentrations in drain outflow (symbols) and in the mobile and immobile region at the drain (light and dark lines, respectively)

To allow for water content controlled denitrification in the entire profile (simulation 3), rather than in the upper 25 cm only, leads to zero-concentration at drain depth at the end of each drainage period as observed with the data. The dynamic NO_3 pattern across drainage seasons, with high concentrations at the start and low concentrations at the end of each drainage season, lies between simulations 2 (upper horizon is involved in N-metabolisms) and 3 (entire profile involved).

4 Conclusions

The NO_3concentrations measured for more than one decade in tile drainage water at the Infeld site seem to be governed by both physical non-equilibrium and N-transformations. The 2D-MIM model extended with water content dependent rate response functions for N-transformations in mobile and immobile regions could simulate simultaneous aerobic and anaerobic processes and could reproduce the principal observed NO_3 concentration pattern. Due to convective transport and limited exchange between regions, NO_3 concentrations fluctuated stronger in the mobile regions than in the immobile regions. Both measured NH_4 and NO_3 concentrations will be used next to improve the model calibration and understanding of complex N fate and transport.

5 References:

Abassi M.K., Adams W.A., 1998. Loss of nitrogen in compacted grassland soil by simultaneous nitrification and denitrification. Plant and Soil 200: 265-277.

De Klein C.A.M., Van Logtestijn R.S.P., De van Meer H.G., Geurink J.H., 1996. Nitrogen loss due to denitrification from cattle slurry injected onto grassland soil with and without a nitrification inhibitor. Plant Soil183: 161-170.

Köhne S., Lennartz B, Köhne J.M., Šimůnek J., 2005. Bromide transport at a tile-drained field site: experiment, and one- and two-dimensional equilibrium and non-equilibrium numerical modeling. J. Hydrol, accepted 8/05.

Nielsen T.H., Nielsen L.P., Revsbech N.P., 1996. Nitrification and coupled nitrification-denitrification associated with a soil-manure interface. Soil Sci. Soc. Am. J. 60: 1829-1840.

Šimůnek, J., Šejna, M., van Genuchten, M.Th., 1999. The HYDRUS-2D software package for simulating two-dimensional movement of water, heat, and multiply solutes in variably saturated media. Version 2.0, IGWMC-TPS-53, International Ground Water Modelling Center, Colorado School of Mines, Golden, Colorado, p.202.

Spatz G., Neuhaus H., Pape A., 1992. Stickstoffdynamik einer Mähweide auf Knickmarsch. J. Agronomy and Crop Science 168: 298-309.

Wilson L.P., Bouwer E.J. 1997. Biodegradation od aromatic compounds under mixed oxygen/denitrifying conditions: A review. J. Ind. Microbiol. Biotech. 18: 116-130.

Zanner C.W, Bloom R.R., 1995. Mineralization, Nitrification and Denitrification in Histosols of Northern Minnesota. Soil Sci Soc. Am. J. 59: 1505-1510.

Recent Applications of HYDRUS in Irrigated Agriculture

T. H. Skaggs[1], T. J. Trout[2], T. J. Kelleners[3], P.J. Shouse[1], J.E. Ayars[2]

[1]George E. Brown, Jr. Salinity Laboratory, USDA-ARS, Riverside, CA, USA
[2]Water Management Research Laboratory, USDA-ARS, Parlier, CA, USA
[3]Dept. of Plants, Soils, and Biometeorology, Utah State University, Logan, UT, USA

Introduction

With its wide ranging capabilities for simulating variably saturated water flow and solute transport, HYDRUS (Šimůnek et al., 1998; 1999) has proven to be a valuable tool for analyzing and designing irrigated agricultural systems. We briefly review three recent projects that illustrate the versatility of the model and software.

Drip Irrigation

Drip irrigation technology gives growers greater control over the application of water, fertilizers, and pesticides; increased precision in water and chemical applications can lead to water savings, improved environmental quality, and increased profits. Realizing the full potential of drip technology requires optimizing the operational parameters that are available to irrigators, such as the frequency and duration of irrigation, the emitter discharge rate and spacing, and the placement of drip tubing. Numerical simulation is an efficient approach to investigating optimal drip management practices. Unfortunately, little work has been done to demonstrate the accuracy of numerical simulations, leading some to question the usefulness of simulation as a research and design tool.

Skaggs et al. (2004) compared HYDRUS-2D simulations of drip irrigation with experimental data. A Hanford sandy loam soil was irrigated using thin-walled drip tubing installed at a depth of 6 cm. Three trials (20, 40, and 60 L m^{-1} applied water) were carried out. At the end of each irrigation and approximately 24 h later, the water content distribution in the soil was determined by gravimetric sampling. Soil hydraulic properties were estimated using the Rosetta pedotransfer function model (Schaap et al., 2001). The HYDRUS-2D predictions of the water content distribution were found to be in very good agreement with the data. Figure 1 shows the simulated and measured wetted soil profile for the 40 L m^{-1} trial.

The results of Skaggs et al. (2004) provide support for the use of HYDRUS-2D as a tool for investigating and designing drip irrigation management practices. The results are especially noteworthy given that the simulations were pure predictions, made without any fitting to the experimental data.

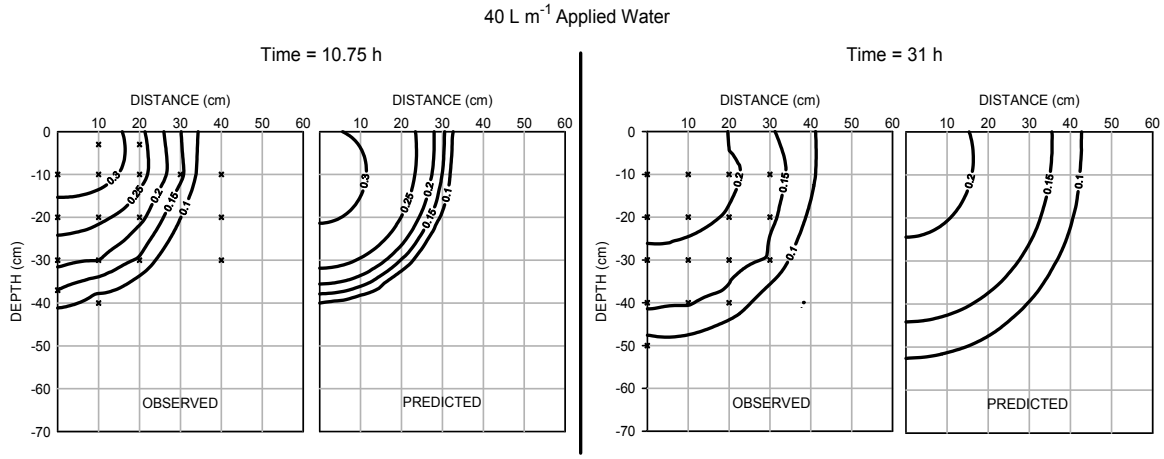

Figure 1 Comparison of measured and predicted volumetric water content following a 10 h irrigation (40 L m^{-1} applied water) from a drip line buried 6 cm below the surface (from Skaggs et al., 2004).

Effects of Salinity and Drought Stress on Transpiration and Drainage

The disposal of agricultural drainage waters into surface waters or onto lands leads to salinization and degradation of soil and water quality. In some instances the impacts of agricultural drainage disposal may be reduced if drainage waters are isolated and reused for irrigation. Over the last 25 years, the recycling of drainage water for irrigation has been examined in numerous experiments and demonstration projects. Scientific and economic questions remain about the suitability of different waters, soils, and crops for reuse operations; optimal management practices are still largely unknown.

While modeling offers a cost-effective means of developing optimal management practices, questions exist about the accuracy of simulations for the dynamic, highly saline environments the may exist in reuse operations. A recent study by Skaggs et al. (2005a,b) compared HYDRUS-1D simulations with extensive drainage and root water uptake data collected on forage crops grown using synthetic drainage waters. Experiments were conducted in a facility consisting of 24 volumetric lysimeters, each measuring 81.5 cm wide × 202.5 cm long × 85 cm deep. Twelve lysimeters were planted in 'Salado' alfalfa (Medicago sativa) and 12 in 'Jose' tall wheatgrass (Agropyron elongatum). Experimental treatments consisted of different combinations of irrigation water salinities (ranging from EC_{iw} = 2.5 dS m^{-1} to 28 dS m^{-1}) and irrigation rates (ranging from deficit to excessive).

To model reductions in root water uptake due to salinity and water stress, Skaggs et al. (2005b) used a multiplicative model for the uptake reduction factor in HYDRUS (Šimůnek et al., 1998):

$$\alpha(h,h_\phi) = \left[1 - A(h_\phi - B)\right] \cdot \frac{1}{1 + (h/h_{50})^p} \qquad (1)$$

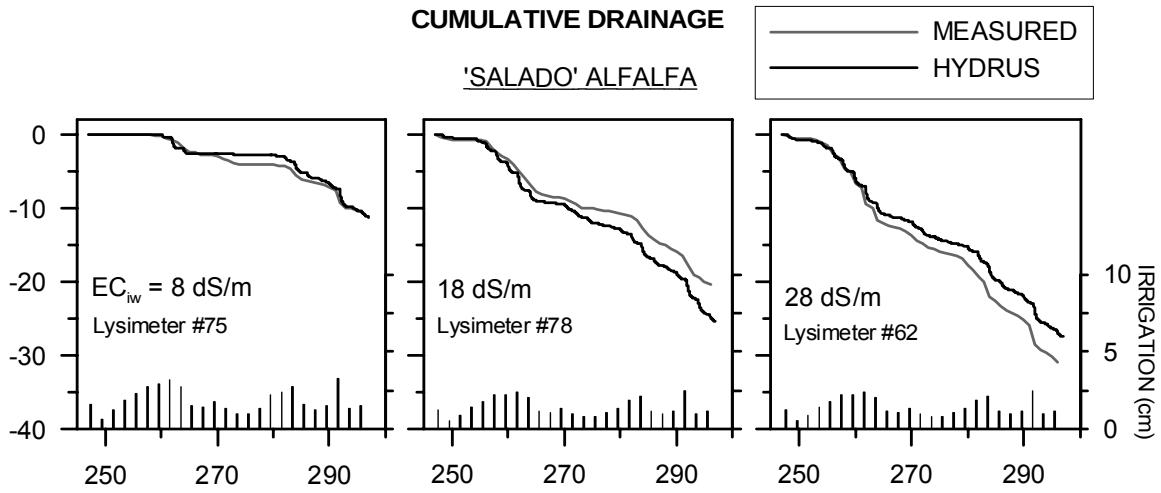

Figure 2. **Measured and simulated cumulative drainage for selected alfalfa lysimeters. Irrigation for each lysimeter is shown along the bottom of each plot (the scale is indicated on the right axes). Although the lysimeters received roughly the same amount of water, drainage increases as EC_{iw} increases because uptake is reduced (from Skaggs et al., 2005b).**

where h is the matric pressure head and h_ϕ is the osmotic pressure head. Values for the parameters A, B, h_{50}, and p for both crops where identified through a global fit to cumulative drainage data. The simulated and measured drainage curves for selected lysimeters are shown in Figure 2. The agreement between the model and the data for the remaining 21 lysimeters was similar to that depicted in Figure 2. Although the model was fitted, it is noteworthy that a single set of parameters was able to reproduce the experimental results over a very broad range of experimental conditions: irrigation waters with EC's ranging from 2.5 to 28 dS/m; and irrigation rates ranging from deficit to luxurious.

Inverse Analysis of Upward Water Flow from Shallow Groundwater

It has long been known that in arid and semi-arid regions upward water flow from shallow groundwater can salinize surface soils. In the San Joaquin Valley, California, this mechanism of salinization has been receiving renewed attention. The west side of the San Joaquin Valley is underlain by shallow groundwater, a result of widespread irrigation. In many areas, the groundwater must be drained from the root zone using subsurface drainage systems. The drainage is saline and contains appreciable amounts of several toxic trace elements, including selenium. Environmental problems associated with the disposal of this drainage have led to efforts to reduce the amount of drainage being generated. At least two drainage reduction strategies raise questions about the salinizing potential of shallow groundwater: land retirement, in which formerly irrigated land is left fallow; and shallow ground water management, in which drain flow is restricted in an effort to maintain the water table near the bottom of the root zone and induce consumption of groundwater by certain crops.

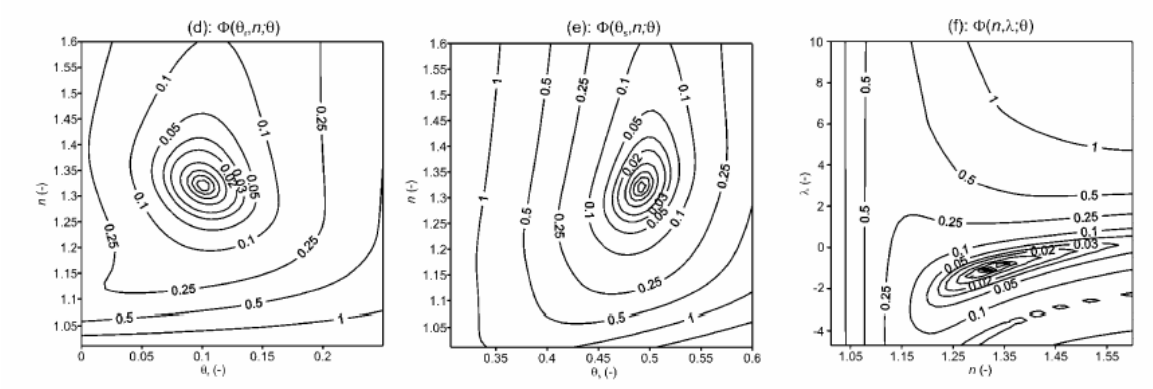

Figure 3. Contour plot of the objective function Φ for the parameter combinations n-θ_r, n-θ_s, and λ-n using $\theta(z,t)$ data in the objective function (from Kelleners et al., 2005).

Calculating rates of upward water flow and root zone salinization with HYDRUS requires identifying appropriate parameter values for the soil hydraulic properties. In Kelleners et al. (2005), the hydraulic properties of a silty clay soil in a large weighing lysimeter were estimated by inverse modeling of a summer fallow period during which capillary rise from the groundwater table replenished the depleted root zone. The analysis was performed with the HYDRUS-1D parameter optimization routines using the objective function:

$$\Phi(\mathbf{b};q) = \sum_{k=1}^{p} w_k \sum_{i=1}^{m_{qk}} \sum_{j=1}^{n_{qik}} \left[q_k^*(z_i,t_j) - q_k(z_i,t_j;\mathbf{b}) \right] \qquad (2)$$

where **b** is the vector of parameters to be optimized, q_k^* is the kth measured datum of type q (which may be water content, matric pressure head, cumulative outflow, etc.), and q_k is the corresponding model calculation. In addition to estimating parameter values, Kelleners et al. (2005) investigated data requirements and problems of parameter uniqueness. Figure 3 shows plots of Φ and the location of minima for different combinations of parameters using water content data in the objective function.

References

Kelleners, T.J., R.W.O Soppe, J.E. Ayars, T.H. Skaggs, and J. Simunek. 2004. Inverse analysis of upward water flow in a groundwater table lysimeter, Vadose Zone J., 4:558–572.

Schaap, M.G., F.J. Leij, and M.Th. van Genuchten. (2001). ROSETTA: A computer program for estimating soil hydraulic properties with hierarchical pedotransfer functions. *J. of Hydrology*, 251, 163–176.

Skaggs, T.H., J.A. Poss, and P.J. Shouse. 2005a. Irrigation of forage crops with saline-sodic drainage waters, 1. Volumetric lysimeter studies. In Review.

Skaggs, T.H., P.J. Shouse, and J.A. Poss. 2005b. Irrigation of forage crops with saline-sodic drainage waters, 2. Modeling drainage and root water uptake. In Review.

Skaggs, T.H., T.J. Trout, J. Simunek, and P.J. Shouse. 2004. Comparison of HYDRUS-2D simulations of drip irrigation with experimental observations, J. Irrig. Drain. Eng., 130:304-310.

Šimůnek, J., M. Šejna, and M. Th. van Genuchten. 1998. *The HYDRUS-1D software package for simulating the one-dimensional movement of water, heat, and multiple solutes in variably saturated media.* Version 2.0. IGWMC. Golden, Colorado.

Šimůnek, J., M. Šejna, and M.Th. van Genuchten. 1999. *The HYDRUS-2D Software package for simulating the two-dimensional movement of water, heat and multiple solutes in variably-saturated media*. IGWMC-TPS 53, Version 2.0. Int. Ground Water Modeling Center, Colorado School of Mines, Golden,

CO.

Seasonal Furrow Irrigation Modelling with HYDRUS2

Thomas Wöhling[1]

Abstract

A seasonal furrow irrigation model (FIM) was developed by iteratively coupling a 1D surface flow model with a series of HYDRUS2 model parameterisations along a single furrow. HYDRUS2 is further linked to a crop model, which calculates daily leaf-area index and final crop yield. FIM simulations of soil water content and yield are in good agreement with field experimental data from a corn plot in Montpellier, France.

Model Formulation

The seasonal furrow irrigation model (FIM) comprises process-based simultaneous modelling of the 1D surface flow, the quasi-3D soil water transport, and the crop growth. The surface flow sub-model FAPS utilizes an analytical solution of the Zero-Inertia open-channel flow equations for modelling the non-uniform flow during both the advance and the early storage phase of an irrigation event (Schmitz et al., 1992). Process adequate simplifications are applied for the late storage phase, the depletion and the recession phase (Wöhling, 2005).

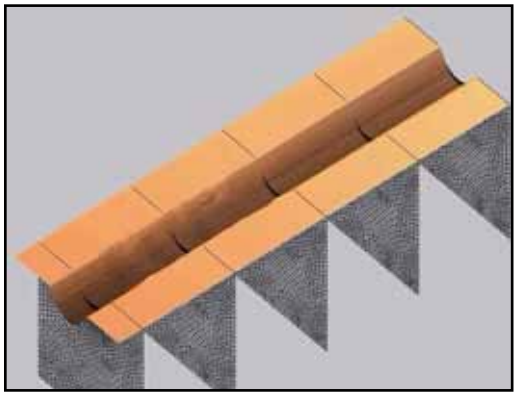

Figure 1: FIM flow domain

The numerical code HYDRUS2 (Simúnek et al., 1996) portrays both the two-dimensional infiltration from arbitrary shaped furrows and the soil water transport in a series of vertical planes along the furrow (Fig. 1). FAPS and HYDRUS2 are iteratively coupled by the infiltration rate and the flow depth (Wöhling et. al, 2004). Due to the increasing /decreasing flow depth during the simulation of an irrigation event, the boundary type of furrow nodes of the HYDRUS2 calculation mesh changes from atmospheric boundary type to prescribed head type and vice versa. Both boundary type and value are assigned to the upper boundary nodes accordingly to the transient conditions, which are determined by the surface flow model and an evapotranspiration module (Wöhling, 2005).

The set of non-linear partial differential equations of the coupled furrow irrigation advance model is solved by a space discretisation in combination with the Newton iteration method. This new solution brought a fundamental improvement as regards convergence, numerical stability and computational time in comparison to the common solution of the considered problem, namely a time-discretisation in combination with the Fixpoint iteration. The new coupled sub-model compares perfectly to data from various laboratory and field irrigation events (Wöhling, 2005; Wöhling et al., 2005).

[1] Research Associate, Dresden University of Technology, Institute of Hydrology and Meteorology, Würzburger Str. 46, D-01187 Dresden, Germany. Email: Thomas.Woehling@mailbox.tu-dresden.de

For modelling the soil water transport during the whole growing period, HYDRUS2 and the crop growth submodel LAI-SIM are coupled by a water-stress index. LAI-SIM includes modules for predicting daily leaf-area index, potential transpiration / evaporation, and root growth (Wöhling, 2005). The HYDRUS2 boundary conditions (during times of redistribution) are:

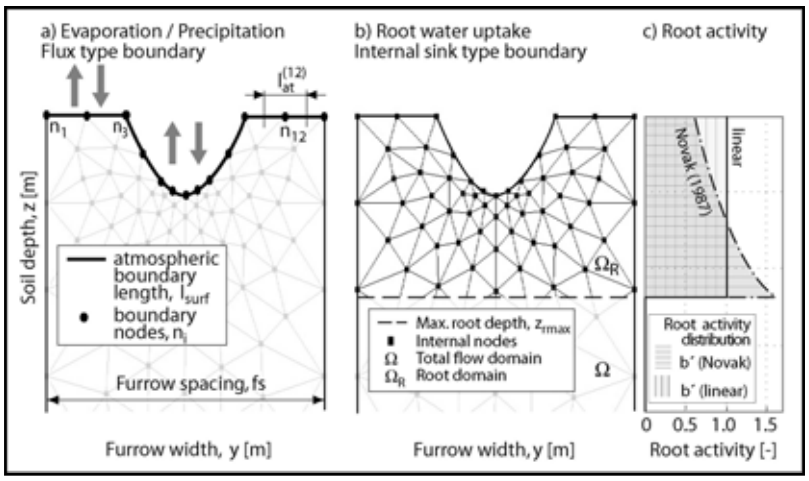

Figure 2: Common boundaries between HYDRUS2 and the crop module LAI-SIM

- atmospheric boundary type at the soil surface: soil evaporation and precipitation (Fig. 2a)
- lateral no-flux boundaries
- seepage face type at the lower boundary
- internal sink type within the rooting zone: root water uptake by the crop (Fig. 2b)

The root depth during the growing season is described by an linear root growth model (Wöhling, 2005) and the root activity is assumed to increase with depth as proposed by Novak (1987) (Fig. 2c).

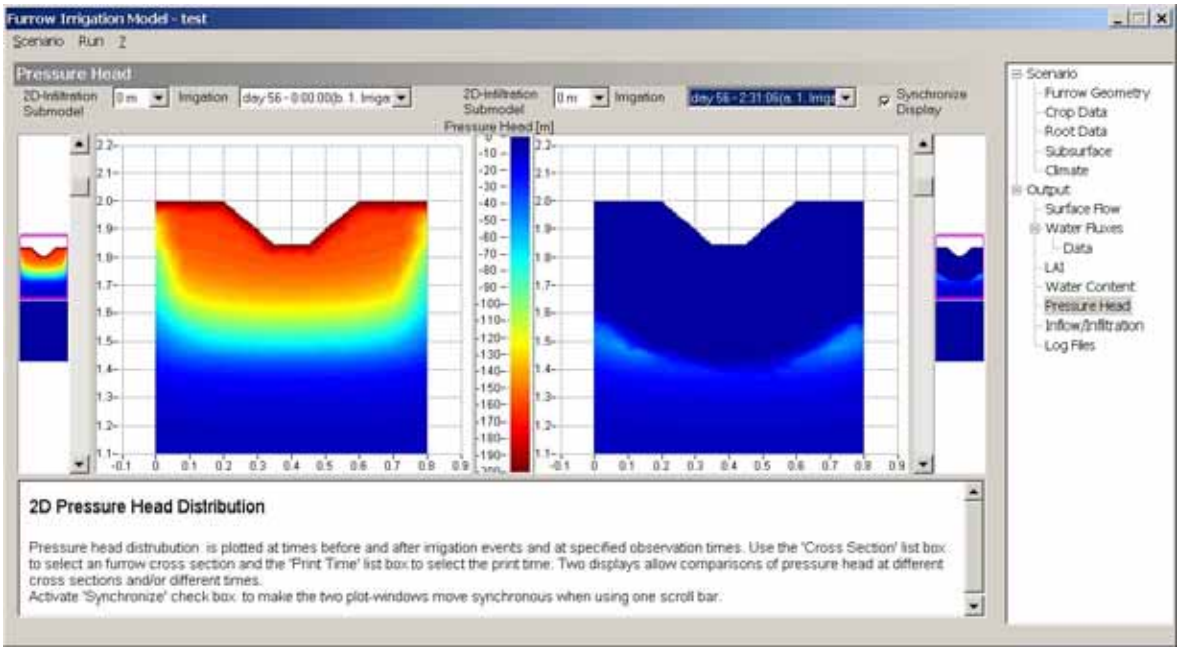

Figure 3: FIM-GUI visualisation of simulated pressure head distribution at the furrow inlet before (left) and after (right) an irrigation event

User Interface

The framework of the seasonal furrow irrigation system, FIM, is set up by a comprehensive event control and time management unit. A user-friendly graphical user

interface (FIM-GUI) supports the parameterisation of the FIM sub-models. The Software package HYDRUS-2**D** and MESHGEN-2D are necessary to generate the HYDRUS2 input files *selector.in, boundary.in, dimensio.in, domain.dat, and meshtria.txt*. These files are subsequently imported with the help of the FIM-GUI. The user can also load and modify previous FIM simulation scenarios and has the option to save both the new parameterisation and the simulation results.
A comprehensive analysis and visualization of the simulation results is also provided by the FIM-GUI. Fig. 3 shows the simulated pressure head distribution of an example run at the furrow inlet at times before (left) and after (right) an irrigation event.

Results

FIM is validated on data from furrow irrigation experiments of growing corn on loamy soil at the 130m long experimental plot at CEMAGREF Montpellier, France (Nemeth, 2001, Mailhol, 2001, Mailhol et al. 2001). Fig. 4 shows the simulated soil moisture distribution at an upstream location at various times of the growing season. The soil water storage, S_{soil}, is determined by integration of the soil moisture in the root zone. Simulated and observed soil water storage are in good agreement (Fig. 5). The simulated corn yield of 12.8 t/ha matches perfectly with the harvest of 12.7 t/ha corn.

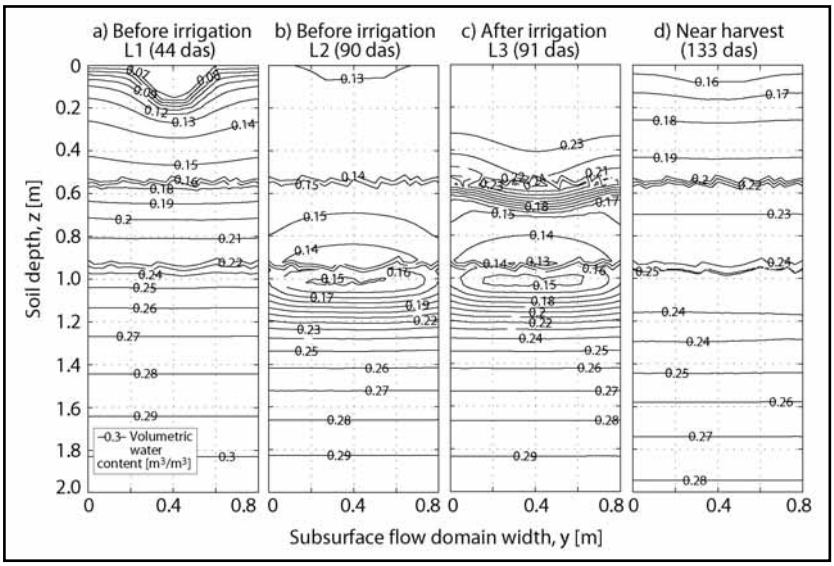

Figure 4: Simulated soil moisture distribution at an upstream location of the Montpellier-experiment at 44, 90, 91 and 133 days after sowing (das)

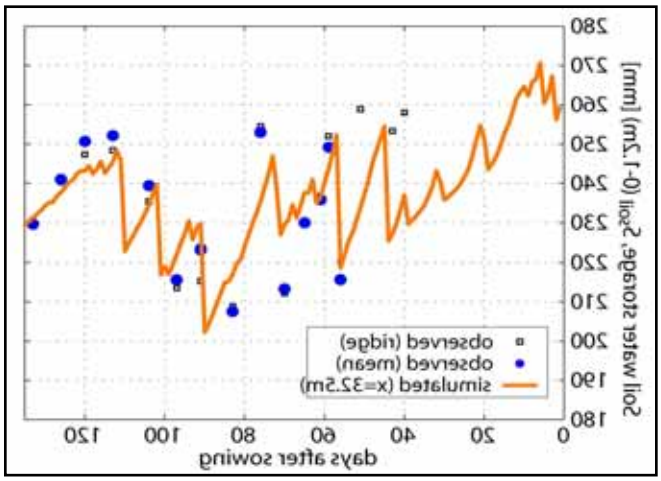

Figure 5: Observed and simulated water storage in the root zone during the growing season of the Montpellier experiment

Conclusions

FIM shows a clear superiority over water balance models (VBM). HYDRUS2 simulates correctly the soil water transport during a growing season of corn at Montpellier (France) and provides detailed information about the quasi 3D water distribution in the soil. FIM estimates irrigation performance criteria, such as irrigation efficiency and distribution uniformity, more precisely than VBM. It can be applied for improving furrow irrigation design and management, for irrigation planning, for cost-benefit analysis, and for estimation of sustainability of furrow irrigation systems.

References

Mailhol, J. C. (2001). Contribution a l´amelioration des pratiques d´irrigation a la raie par une modelisation simplidiee a l´echelle de la parcelle et de la saison (in French. PhD Thesis.

Mailhol, J. C., Ruelle, P., and Nemeth, I. (2001). Impact of fertilisation practices on nitrogen leaching under irrigation. Irr. Sci., 20:139–147.

Nemeth, I. (2001). Devenir de l´azote sous irrigation gravitaire. Application au cas d´un perimetre irrigue au mexique. (in French). PhD thesis, University of Montpellier II.

Novak, V. (1987). Estimation of soil water extraction patterns by roots. Agric. Water Mgt.

Schmitz, G. H. and Seus, G. J. (1992). Mathematical zero-inertia modeling of surface irrigation: advance in furrows. Journal of Irrigation and Drainage Engineering, 118(1):1–18.

Simúnek, J., Sejna, M., and van Genuchten, M. T. (1996). Hydrus-2d. simulating water flow and solute transport in two-dimensional variably saturated media. Version 1.0. User manual, IGWMC-TPS 53 International Ground Water Modeling Center, Colorado School of Mines. IGWMC-TPS 53.

Wöhling, Th. (2005). Physically based modeling of furrow irrigation systems during a growing season. PhD Thesis, Faculty of Forest, Geo und Hydro Science, Dresden University of Technology. ISBN 3-86005-481-3.

Wöhling, Th., Fröhner, A., Schmitz, G.H. and Liedl, R. (2005). Efficient solution of interacting 1D surface - 2D subsurface flow during furrow irrigation advance. Submitted to the Journal of Irrigation and Drainage Engineering.

Wöhling, Th., Singh, R., & Schmitz, G.H. (2004). Physically based modeling of interacting surface-subsurface flow during furrow irrigation. Journal of Irrigation and Drainage, 130(5), 296-303.

Modelling the effects of soil tillage on water and solute transport: the HYDRUS-2D/SISOL coupling

Coquet Y.[1], Šimůnek J.[2], Roger-Estrade J.[3]

[1]UMR INRA/INAPG Environment and Arable Crops, Institut National de la Recherche Agronomique/Institut National Agronomique Paris-Grignon, B.P. 01, 78850 Thiverval-Grignon, France

[2]Department of Environmental Sciences, University of California, Riverside, CA, 92521, USA

[3]UMR INRA/INAPG Agronomy, Institut National de la Recherche Agronomique/Institut National Agronomique Paris-Grignon, B.P. 01, 78850 Thiverval-Grignon, France

Introduction

The topsoil properties play a central role in the dynamics and fate of pollutants in agricultural soils. It is in the surface soil layer that biological activity is most intense and that soil variables controlling degradation, retention and transport of solutes are the most prone to variation. The topsoil is time- and space-variable due to the effects of agricultural practices, mainly tillage, but also fertilizer or manure application, crop harvesting, climate, and biological activity. This variability must be accounted for if one aims at understanding and predicting the impact of agricultural practices on the environment, esp. groundwater quality. The model SISOL (Roger-Estrade et al., 2000) has been developed for predicting the variation through time and space of the structural status of agricultural soils. SISOL has been designed specifically for frequently mouldboard-ploughed soils. It has been tested in a variety of agricultural situations representative of European intensive agricultural systems in loamy soils. SISOL is a 2-D model, describing time changes and spatial variability of soil structure in the ploughed layer, taking into account fragmentation by tillage and climate, soil displacement by ploughing and compaction due to traffic. Description of soil structure is based on the morphological method proposed by Manichon (1987). This paper describes the coupling of HYDRUS-2D with SISOL and presents some illustrations of the effect of soil structure on water transfer and solute leaching.

Materials and Methods

The SISOL Model

The SISOL model predicts the structural status of cultivated soils by assessing the distribution of compacted zones or clods, called Δ zones, within the ploughed layer. These Δ zones are defined by Manichon (1987) as soil zones having no eye-visible macroporosity. They result from severe soil compaction under the wheel tracks of farming machinery. The extent of compacted Δ soil below the wheels is dependent on the soil water content and on the characteristics of the farming machine (tyre width, pressure and characteristics, axle load). Basically, any agricultural operation involving machinery may produce Δ zones within the soil. Empirical relationships are used by SISOL to predict the extent of compacted Δ zones created by each agricultural operation (e.g. sowing, fertilizing, harvesting, etc). These Δ zones may be destroyed within the upper part of the ploughed topsoil when it is superficial tilled (for seed bed preparation or stubble breaking) or by weathering (freezing/thawing and

drying/wetting cycles). Finally, Δ zones may be split up and displaced by ploughing that cuts and rotates soil furrow slices (Figure 1). Additional details about the SISOL model may be found in Roger-Estrade et al. (2000).

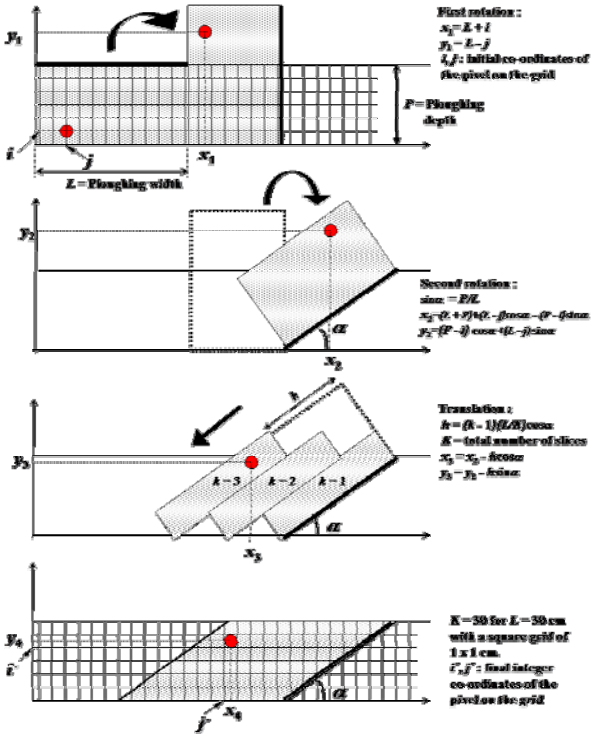

Figure 1.
Modelling of the soil displacement during ploughing (Roger-Estrade et al., 2000).

All these effects are modelled by SISOL that describes the time-evolution of the distribution of the Δ zones within the ploughed soil according to the sequence of farming operations, which is a characteristic of the considered cropping system. A high time-averaged proportion of Δ soil within the tilled layer is considered to have a detrimental effect on crop performance because Δ soil zones impede crop rooting and have a low hydraulic conductivity (Coutadeur et al., 2002) thereby limiting plant access to water and nutrients. The role of these Δ compacted zones on soil water and solute dynamics was further explored by using HYDRUS-2D and coupling it with the SISOL model (Coquet et al., 2005a, 2005b).

Coupling HYDRUS-2D with SISOL

The consequences of the presence of compacted Δ zones on water and solute transport in tilled soils were first evaluated through a field experiment, involving the application of a tracer step input at the surface of a loamy soil that had been prepared for maize sowing (ie after an autumn ploughing and a spring harrowing), and a monitoring of water content, water potential and tracer concentration within the tilled soil (Coquet et al., 2005a). The field experiment was then modelled using HYDRUS-2D (Šimůnek et al., 1999) by accounting explicitly for the locations, sizes and forms of the Δ zones within the ploughed layer. The Δ material had different hydraulic parameters from the non-Δ material. Hydraulic properties of all types of materials have been estimated from independent measurements. The observed water and tracer behaviours were correctly described, including preferential flow in the vicinity of the compacted Δ zones (Coquet et al., 2005b).
To account for the time-variations of the structural status of tilled soils while modelling its water and solute dynamics, we linked HYDRUS-2D to the SISOL model in the following way. After each agricultural operation, HYDRUS-2D reads the output file generated by SISOL, which describes the structure of the ploughed layer using a binary status (Δ or non-Δ)

for each 1 by 1 cm soil pixel, and translates it into a new HYDRUS-2D material distribution. HYDRUS-2D then proceeds with the current simulation until the next agricultural operation. All the information for the SISOL/HYDRUS-2D interaction (ie coordinates and size of SISOL pixels, number and timing of agricultural operations and names of the SISOL output files) is given in a specific HYDRUS-2D input file called SeSoil.in to be placed in the corresponding HYDRUS-2D project.

We chose 3 experimental plots from a long term field trial where 3 cropping systems are compared. This trial is located at Mons-en-chaussée in the northern part of the French Parisian Basin. Cropping system 1 (S1) is characterised by a high compaction risk (mainly due to frequent harvesting in late autumn and seed bed preparation in early spring, when the soil water content is high). In this treatment, the crop sequence is maize/winter wheat/sugar beet/winter wheat. Cropping system 2 (S2) is characterised by the same crop sequence, but the scheduling of cultivation operations is different, in order to minimise compaction (early sugar beet and maize harvesting in autumn and late sowing of these crops in spring, when the soil is dry enough). Crop sequence in cropping system 3 (S3) is rape/winter wheat/pea/winter wheat. In this region of France, harvesting of these crops is usually performed in summer, when the soil is dry, and seed bed preparation is done in the middle of autumn (except for pea sowing, which takes place in February) when the soil is still rather dry. Compaction risk in this system is low. All the plots are mouldboard ploughed once every year, in September before wheat, rape or pea, or in November before sugar beet and maize.

Simulation of the time changes in soil structure of the ploughed layer of these three plots where performed using SISOL over a seven-year period (Roger-Estrade et al., 2000). The simulation was stopped just after winter wheat sowing in the three plots, leading to three SISOL output files. The corresponding material distributions are presented on the left part of figure 2.

Results and Discussion

The HYDRUS-2D/SISOL tool allows the exploration of the effects of agricultural systems on the dynamics of water and solutes in soils. It clearly demonstrated that the abundance and distribution of the compacted Δ zones have a strong effect on pore water velocity (Figure 2).

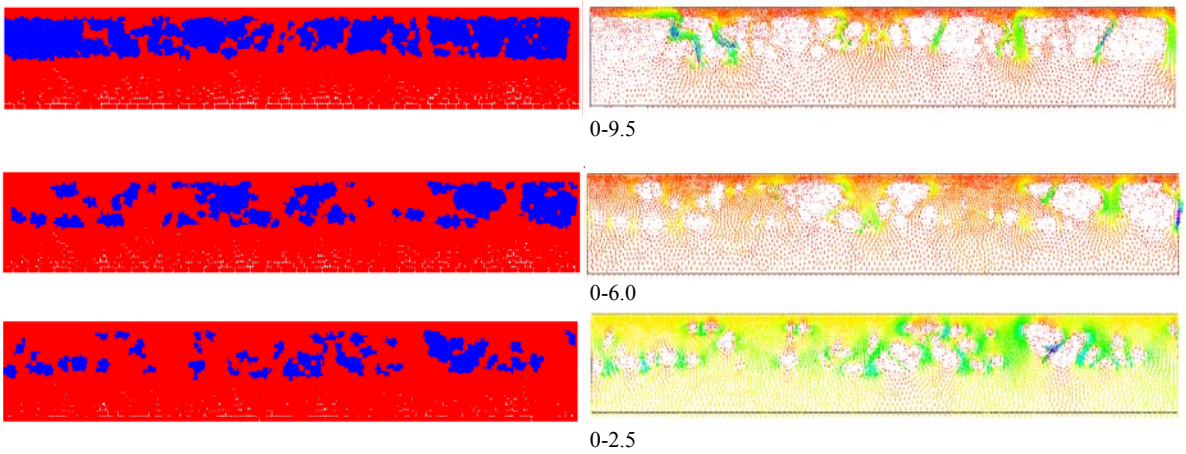

Figure 2. HYDRUS-2D material distribution (Δ soil zones in blue) and nodal fluxes for the 3 cropping systems S1 (top), S2 (middle) and S3 (bottom). Numbers below nodal flux maps show flux range in cm/h. Size of the simulation domain is 0.5 by 3 m.

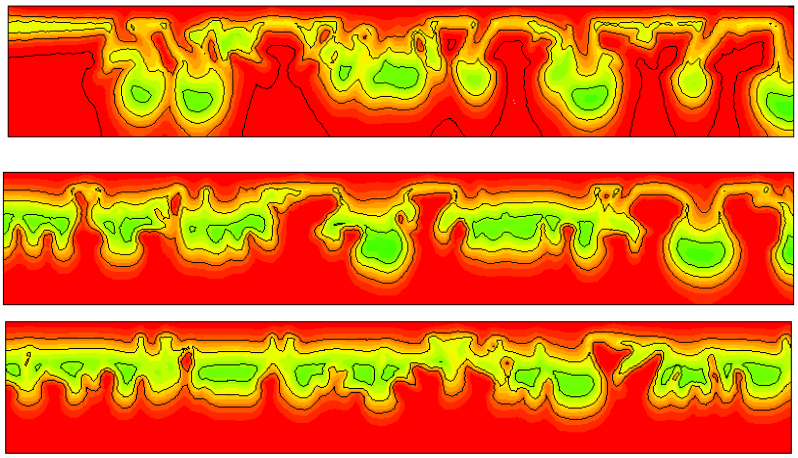

Figure 3. Solute concentration maps for the 3 cropping systems S1 (top), S2 (middle) and S3 (bottom) and the same solute transport scenario: 1 h step-input of solute at a steady-state water flow input rate of 5 mm/h followed by a 11 h elution at the same water flow rate with solute-free rainfall. Size of the simulation domain is 0.5 by 3 m.

The larger the abundance and sizes of the Δ zones, the more heterogeneous is the flow field. Such a flow dynamics has a strong impact on solute transport in soil (figure 3). Solute tends to move faster in some soil regions, essentially in the vicinity of large Δ zones, and reaches the bottom of the soil much earlier in the S1 cropping system than in the S2 and S3 cropping systems. That means that the S1 cropping system is likely to have a greater impact on groundwater than the other two cropping systems, because a larger part of solute may move quickly out of the ploughed layer where the essential of degradation takes place. In that condition, the attenuation of pollutant concentrations through soil may be less effective.
The coupling between HYDRUS-2D and SISOL is quite loose at present. It could indeed be improved by a bi-directional communication between the two softwares. The SISOL model could use the water contents modelled by HYDRUS-2D to evaluate the extent of compaction due to wheeling. However, we believe that the HYDRUS-2D/SISOL tool may already be useful for the environmental risk assessment of cropping systems.

References

Coquet, Y., Coutadeur, C., Labat, C., Vachier, P., van Genuchten, M. Th., Roger-Estrade, J., Šimůnek, J., 2005a. Water and solute transport in a cultivated silt loam soil; 1. Field observations, Vadose Zone J. 4:558-572.

Coquet, Y., Šimůnek, J., Coutadeur, C., van Genuchten, M. Th, Pot, V., Roger-Estrade, J., 2005b. Water and solute transport in a cultivated silt loam soil; 2. Numerical analysis, Vadose Zone J. 4:573-586.

Coutadeur, C., Coquet, Y., Roger-Estrade, J., 2002. Variation of hydraulic conductivity in a tilled soil. Europ. J. Soil Sci. 53:619-628.

Manichon, H., 1997. Observation morphologique de l'état structural et mise en évidence d'effets de compactage des horizons travaillés. *In*: Soil Compaction and Regeneration (eds G. Monnier, M.J. Goss), pp. 39-52. A.A. Balkema, Rotterdam.

Roger-Estrade, J., Richard, G., Boizard, H., Boiffin, J., Caneill, J., Manichon, H., 2000. Modelling structural changes in tilled topsoil over time as a function of cropping systems. Europ. J. Soil Sci. 51:455-474.

Šimůnek, J., M. Šejna, and M.Th. van Genuchten. 1999. The HYDRUS-2D software package for simulating two-dimensional movement of water, heat, and multiple solutes in variably saturated media. Version 2.0, IGWMC - TPS - 53, International Ground Water Modeling Center, Colorado School of Mines, Golden, CO.

Inverse model simulation of Br and herbicide transport using multi-process transport models with HYDRUS-1D

V. Pot[a], J. Šimůnek[b], P. Benoit[a], Y. Coquet[a]

[a]*UMR INRA – INA P-G, Unité Environnement et Grandes Cultures, BP01, 78850 Thiverval-Grignon, France*
[b]*Department of Environmental Sciences, University of California, Riverside, California, USA.*

Abstract

The modified one-dimensional transport model HYDRUS-1D (Šimůnek et al., 1998, 2003) was used to identify and quantify different physical and chemical non-equilibrium transport processes acting in a grassed soil. The convective-dispersive model (CDE), the dual-porosity model (MIM), the dual-permeability model (DP) and the triple-porosity, dual permeability model (DP-MIM) were used to analyze experimental bromide and the herbicide isoproturon breakthrough curves measured from two series of displacement experiments performed on two undisturbed grassed filter strip soil cores, under unsaturated steady-state flow conditions. The CDE, MIM and DP models were combined with both chemical instantaneous and kinetic sorption, while DP-MIM model was combined with chemical instantaneous sorption. Several rainfall intensities (0.070, 0.147, 0.161, 0.308 and 0.326 cm h^{-1}) were used. Two contrasting physical non-equilibrium transport processes occurred. Multiple (three) porosity domains contributed to flow at the highest rainfall intensities, including preferential flow through macropore pathways. Macropores were not active any longer at intermediate and lowest velocities, and the observed preferential transport was described using dual-porosity-type models with a zero or low flow in the matrix domain. Chemical non-equilibrium transport of isoproturon was found at all rainfall intensities and the degree of non-equilibrium sorption increased with increasing rainfall intensities. Significantly higher estimated values of degradation rate parameters as compared to batch data were correlated with the degree of non-equilibrium sorption.

Material and methods

Two undisturbed soil cores (14-cm i.d., 30-cm height) were sampled from the soil surface layer of grassed strip (La Jaillière, Loire-Atlantique, France), planted with perennial rye-grass (*Lolium perenne*). The soil is a hydromorphic silt loam (24% clay, 40% silt, 36% sand). The displacement experiments were conducted at steady-state flow under unsaturated conditions and consisted of injecting a pulse of the $CaCl_2$ solution containing actual concentrations of 66.1 ± 2.1 mg l^{-1} Br, 7.6 ± 1.5 mg l^{-1} isoproturon (IPU) and 8.5 ± 0.2 mg l^{-1} metribuzin (Met). Three and two successive displacement experiments were performed at different rainfall intensities for column I and II, respectively. The solute pulse duration was fixed so that an approximately equal mass of Br, IPU and Met was injected at each velocity. Met results are not shown in this paper (for full data set, see Pot et al., 2005).

The following transport processes were used to analyze the experimental breakthrough curves (BTCs): a) physical and chemical equilibrium transport described using the classical convection-dispersion transport model (Lapidus and Amundson, 1952); b) chemical non-equilibrium transport using the two-site chemical model (Cameron and Klute, 1977); c) physical non-equilibrium transport using the two region model (mobile and immobile water) (van Genuchten and Wierenga, 1976) and the dual-permeability model (Gerke and van Genuchten, 1993); and finally, e) simultaneous physical and chemical non-equilibrium transport using the dual-permeability model (Gerke and van Genuchten, 1993) combined with the two-site chemical model. For all simulations, the linear sorption isotherm was used, and degradation was considered in the liquid phase only.

Physical transport parameters were first estimated by inverting the Br BTCs for both columns using the CDE, MIM, DP and/or DP-MIM transport models. Then, chemical parameters for IPU were estimated by inverting the herbicide BTCs using the physical transport model that best

described Br transport combined with equilibrium or non-equilibrium chemical transport models. Note that non-equilibrium chemical transport is currently not yet available in the HYDRUS-1D model for the physical non-equilibrium DP-MIM transport model.

Results

Br transport

At the highest rainfall intensities, two arrival fronts and a marked shift to the left of peak positions were observed by contrast to the other rainfall intensities suggesting contrasting physical transport processes as a function of rainfall intensity (Figure 1). Similar features of the shape of the curves were observed with simultaneous leaching of IPU and Br (same arrival time of the peaks) at the highest rainfall intensities and delayed leaching of IPU was observed for the lower velocities (Figure 1). A preferential flow of a macropore type was thus suggested at the highest rainfall intensities.

The CDE model did not describe satisfactorily the Br data for either column. For both columns, the DP model, similarly to the MIM model, was not able to describe two arrival fronts that occurred during the Br transport at the highest rainfall intensities, but predicted well the Br transport at the lower velocities. Results found with MIM and DP models were quite similar since instead of an immobile zone considered in the MIM model, the DP model predicted very slow water flow in the matrix zone. However, in the case of the lowest rainfall intensity, the DP model showed that the contribution of the matrix to the total flux can be significant.

The DP-MIM model succeeded in describing the transport of Br at the highest velocity. Differences in pore velocities and water content in the fracture domain together with opposite results found for the two mass transfer rate coefficients (between fracture and matrix domains on the one hand, and between mobile and immobile regions of the matrix domain on the other hand) between both columns explained rather well the observed differences between the two experimental BTCs. The BTC for column I shows two solute fronts of very different concentrations. The pore velocity in the fracture domain is very high and the mass transfer between fracture and matrix domains is small. The long concentration tail is then explained by large exchange between mobile and immobile regions of the matrix domain. The BTC for column II, on the other side, shows two solute peaks of similar magnitude and relatively smooth increases and decreases in concentrations, which requires smaller pore velocity in the fracture domain and faster exchange between the fracture and matrix domains.

IPU transport

Results showed that for all rainfall intensities and regardless of the used physical transport model the chemical equilibrium transport model was not well suited to describe the transport of herbicides in the grassed soil columns while the non-equilibrium chemical model described well the elution tails of the BTCs.

The fitted distribution coefficient (K_d) values were lower than those derived from batch sorption experiments with the same soil data (Madrigal et al., 2002) while the fitted degradation rates were up to 31 times larger than the literature values (Agritox, 2001).
The K_d values increased when rainfall intensities decreased, with comparable values between the two columns while a significant decrease in the sorption kinetic rate was observed as velocity decreased. Maraqa (2001), in a review of column displacement experiments, reported similar trends. A possible explanation is that for lower velocities more sites seem to be at relative equilibrium with the solution, and given the lower sorption kinetic rate the overall rate of reaction is then more or less the same. Since the flow in the matrix region is slower, there is more time to reach equilibrium in the matrix domain and thus the fraction of exchange sites assumed to be in equilibrium with the solution phase of the matrix domain is not a relevant parameter. Equilibrium

sorption in the matrix domain is thus a suitable model. By contrast, for the fracture domain where there is not enough time to reach equilibrium, due to faster flow, non-equilibrium sorption is an appropriate model to explain the observed long elution tails.
The first-order degradation rate was found to increase when velocity increased. Our modeling analysis suggested that the degree of non-equilibrium sorption increased as velocity increased. Thus, our results suggest that the estimated degradation rates are positively related to the degree of non-equilibrium sorption. It supports the hypothesis that chemical irreversible sorption, defined as fast attachment and much slower detachment, occurred most probably on the sorption sites where kinetic sorption occurs. The irreversible sorption acts as a disappearance process at the time scale of our experiments and is therefore accounted for by apparently higher degradation rates by the models.

Conclusions

For the highest rainfall intensities, multiple porosity domains and multiple permeabilities preferential flow were probably active: a) rapid flow through macropore pathways, b) slower flow through a mesoporosity, and c) no-flow in the remaining micropores. For the lower rainfall intensities, macropore flow was not active anymore, the preferential transport observed is of a dual porosity type with a zero or low flow in the matrix domain.
The main conclusion drawn from the modeling analyses is that non-equilibrium chemical transport processes occurred for all velocities and that the degree of non-equilibrium sorption increased with velocity. Significantly higher values of degradation rate parameters as compared to batch data were positively related with the degree of non-equilibrium sorption. This work suggests that the sorption and/or degradation rates obtained from batch experiments can not be used in non-equilibrium transport models to describe the transport experiments unless the actual underlying mechanisms measured by the two techniques are fully identified**.**

References

Agritox: toxixological data base on pesticides, INRA, France, 2001.

Cameron D.R., Klute A., 1977. Convective-dispersive solute transport with a combined equilibrium and kinetic adsorption model. Water Resour. Res., 13, 183-188.

Gerke H.H., van Genuchten M. Th., 1993. A dual-porosity model for simulating the preferential movement of water and solutes in structured porous media. Water Resour. Res., 29, 305-319.

Lapidus L., Amundson N.R., 1952. Mathematics of adsorption in beds. VI. The effect of longitudinal diffusion in ion exchange and chromatographic columns. J. Phys. Chem., 56:, 84-988.

Madrigal I., Benoit P., Barriuso E., Etiévant V., Souiller C., Réal B., Dutertre A., 2002. Capacités de stockage et d'épuration des sols de dispositifs enherbés via-à-vis des produits phytosanitaires. Deuxième partie : Propriétés de rétention de deux herbicides, l'isoproturon et le diflufénicanil dans différents sols de bandes enherbées. Etude et Gestion des Sol*s*, 9, 287-302.

Maraqa, M.A., 2001. Prediction of mass-transfer coefficient for solute transport in porous media. J. Contaminant Hydrol., 50, 1-19.

Pot V., Šimůnek, J., Benoit P. Coquet Y., 2005. Impact of rainfall intensity on the transport of two herbicides in undisturbed grassed filter strip soil cores. J. Contaminant Hydrol., in press.

Šimůnek, J., Šejna M., van Genuchten M. Th., 1998. The HYDRUS-1D software package for simulating the one-dimensional movement of water, heat, and multiple solutes in variably-saturated media. Version 2.0, *IGWMC - TPS - 70,* International Ground Water Modeling Center, Colorado School of Mines, Golden, Colorado, 202 pp.

Šimůnek J., Jarvis N.J., van Genuchten M.Th., Gärdenäs A., 2003. Review and comparison of models for describing non-equilibrium and preferential flow and transport in the vadose zone. J. Hydrol., 272, 14-35.

van Genuchten M.Th., Wierenga P.J., 1976. Mass transfer studies in sorbing porous media I. Analytical solutions. Soil Sci. Soc. Am. J., 40, 473-480.

Figure 1: Br and IPU BTCs measured and calculated for columns I and II at the highest rainfall intensity. Relative concentrations of the effluents are presented against the number of pore volumes.

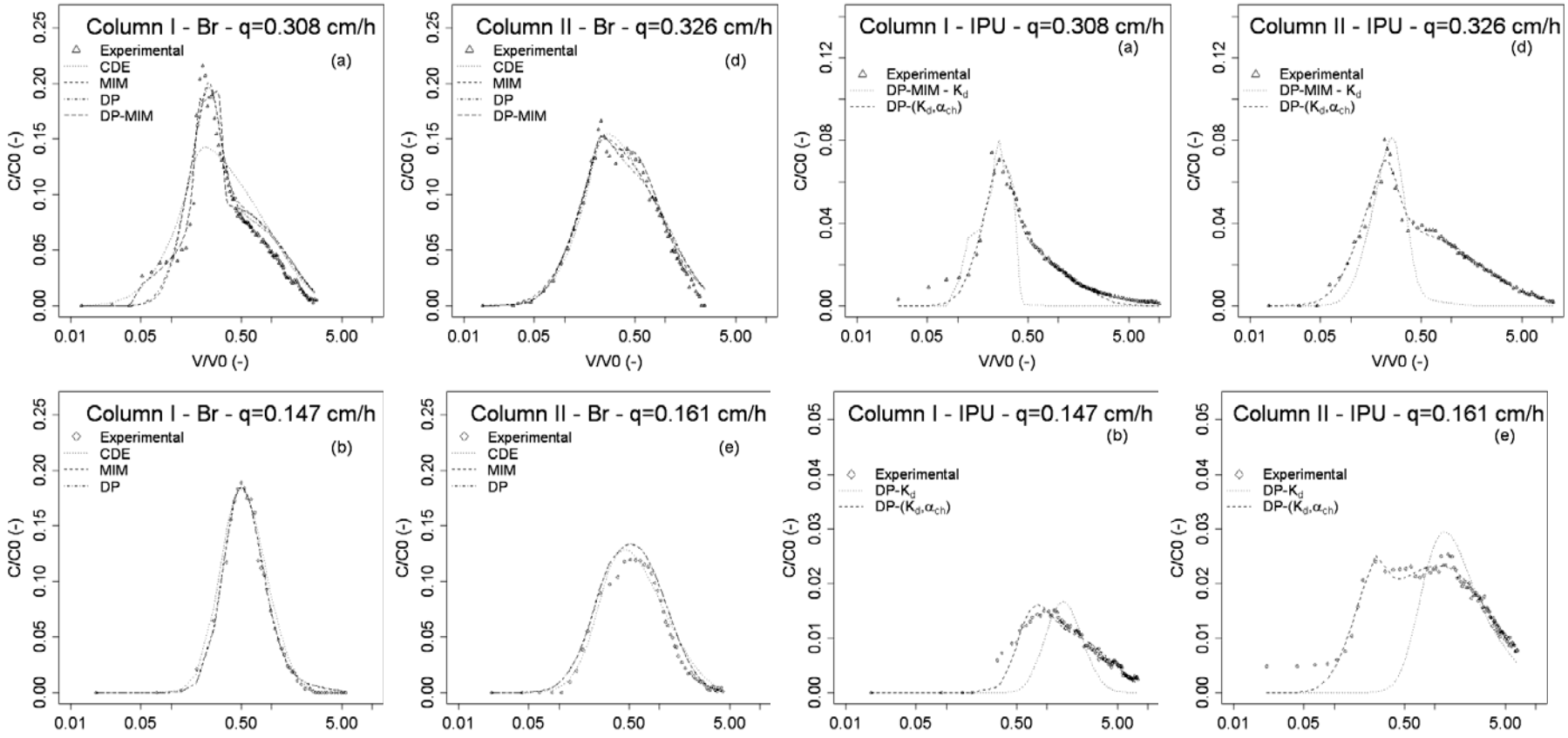

New Features of HYDRUS-1D, Version 3.0

Jiří Šimůnek[1], Rien van Genuchten[2], S. A. Bradford[2], and R. J. Lenhard[3]
[1]University of California Riverside, Department of Environmental Sciences, Riverside, CA 92521, USA, jiri.simunek@ucr.edu
[2]George E. Brown, Jr. Salinity Laboratory, USDA-ARS, Riverside, CA 92507, USA
[3]Idaho National Laboratory, P.O. Box 1625, Idaho Falls, ID 83415, USA

Introduction

Version 3.0 of HYDRUS-1D (Šimůnek et al., 2005), released in May 2005, implements the following new features as compared to version 2.1 (Šimůnek et al., 1998): a) new approaches to simulate preferential and nonequilibrium water flow and solute transport (Šimůnek et al., 2003), b) a new hysteresis module (Lenhard et al., 1991) that avoids the effects of pumping, c) compensated root water uptake (Jarvis, 1994), d) options to simulate the transport of viruses, bacteria, and colloids (Bradford et al., 2003), e) carbon dioxide production and transport (Šimůnek and Suarez, 1993), and f) geochemical transport of major ions (Šimůnek and Suarez, 1994; Šimůnek et al., 1996, 1997). This paper briefly summarizes the new features.

Preferential and Nonequilibrium Water Flow

The variably-saturated flow equation may consider dual-porosity type flow with a fraction of the water being mobile, and a fraction immobile. The approach assumes that the soil matrix can exchange, retain, and store water, but does not permit advective flow. This conceptualization leads to two-region, dual-porosity type flow and transport models that partition the liquid phase into mobile (flowing, inter-aggregate), θ_m, and immobile (stagnant, intra-aggregate), θ_{im}, regions with possible exchange of water and/or solutes between the two regions, usually calculated by means of a first-order rate equation.

The dual-porosity formulation for water flow as used in HYDRUS-1D is based on a mixed formulation, which uses the Richards equation to describe water flow in the fractures (macropores), and a simple mass balance equation to describe moisture dynamics in the matrix as follows (Šimůnek et al., 2003):

$$\begin{aligned} \frac{\partial \theta_m}{\partial t} &= \frac{\partial}{\partial z}\left[K(h)\left(\frac{\partial h}{\partial x} + \cos\alpha \right) \right] - S_m - \Gamma_w \\ \frac{\partial \theta_{im}}{\partial t} &= - S_{im} + \Gamma_w \end{aligned} \qquad (1)$$

where S_m and S_{im} are sink terms for the two regions, and Γ_w is the transfer rate for water from the inter- to the intra-aggregate pores.

The mass transfer rate, Γ_w, in (1) for water between the fracture and matrix regions in dual-porosity studies (e.g., Šimůnek et al., 2003) is often assumed to be proportional to the difference in effective saturations of the two regions using the first-order rate equation:

$$\Gamma_w = \frac{\partial \theta_{im}}{\partial t} = \omega \left[S_e^m - S_e^{im} \right] \qquad (2)$$

where θ_{im} is the matrix water content, ω is a first-order rate coefficient (T^{-1}), and S_e^m and S_e^{im} are effective fluid saturations of the mobile (fracture) and immobile (matrix) regions, respectively. Equation (2) assumes that the mass transfer rate is proportional to the difference in effective saturation, rather than in the pressure head, which should provide a more realistic description of the exchange rate between the fracture and matrix regions.

When the rate of exchange of water between the fracture and matrix regions is assumed to be proportional to the difference in pressure heads between the two pore regions (Gerke and van Genuchten, 1993), the coupling term, Γ_w, becomes:

$$\Gamma_w = \alpha_w (h_f - h_m) \tag{3}$$

in which α_w is a first-order mass transfer coefficient [$L^{-1}T^{-1}$].

Hysteretic Model Without Pumping Effects

While relatively simple to implement, the hysteretic model that was previously used in HYDRUS-1D has been found to sometimes suffer from a so-called pumping effect that can cause the hysteresis loop to move to physically unrealistic parts of the retention function. As an alternative, we incorporated in HYDRUS the hysteresis model of Lenhard et al. (1991) that eliminates pumping by keeping track of historical reversal points.

Compensated Root Water Uptake

The ratio of the actual, T_a [LT^{-1}], to potential, T_p [LT^{-1}], transpiration rates for root uptake without compensation is defined as follows:

$$\frac{T_a}{T_p} = \frac{1}{T_p}\int_{L_R} S dz = \int_{L_R} \alpha(h, h_\phi, z)\, b(z) dz = \omega \tag{4}$$

where $\alpha(h)$ is the water stress response function [-], $b(x)$ is the normalized water uptake distribution [L^{-1}], L_R is the rooting depth [L], S is the root water uptake rate [T^{-1}], and ω is a dimensionless water stress index (Jarvis, 1994). Following Jarvis (1994), we introduce a critical value of the water stress index ω_c, referred to as the root adaptability factor, which represents a threshold value above which reductions in root water uptake in stressed parts of the root zone are fully compensated by increased uptake from other parts:

$$\begin{aligned} \frac{T_{ac}(t)}{T_p(t)} &= \frac{\int_{L_R} \alpha(h, h_\phi, z, t) b(z, t) dz}{\max\left[\omega(t), \omega_c\right]} = \frac{\omega(t)}{\max\left[\omega(t), \omega_c\right]} \le 1 \\ S(h, h_\phi, z, t) &= \alpha(h, h_\phi, z, t) b(x, z, t) L_t \frac{T_p(t)}{\max\left[\omega(t), \omega_c\right]} \end{aligned} \tag{5}$$

where T_{ac} is the actual transpiration rate for compensated root uptake [LT^{-1}]. When the parameter ω_c is equal to one we hence have noncompensated root water uptake, and when ω_c is equal to zero fully compensated uptake results.

Attachment/Detachment Transport Model

Virus, colloid, and bacteria transport and fate models commonly employ a modified form of the advection-dispersion equation:

$$\frac{\partial \theta c}{\partial t} + \rho \frac{\partial s_1}{\partial t} + \rho \frac{\partial s_2}{\partial t} = \frac{\partial}{\partial x}\left(\theta D \frac{\partial c}{\partial x} \right) - \frac{\partial qc}{\partial x} - \mu_w \theta c - \mu_s \rho (s_1 + s_2) \tag{6}$$

where c is the (colloid, virus, bacteria) concentration in the aqueous phase [$N_c L^{-3}$], s is the solid phase (colloid, virus, bacteria) concentration [$N_c M^{-1}$], subscripts 1 and 2 represent two kinetic sorption sites, N_c is the number of colloids (particles), and μ_w and μ_s represent inactivation and degradation processes in the liquid and solid phases, respectively.

Mass transfer between the aqueous and two solid kinetic phases can be described with equations of the form (note that we dropped the subscripts 1 and 2):

$$\rho \frac{\partial s}{\partial t} = \theta k_a \psi c - k_d \rho s \tag{7}$$

where k_a is the first-order deposition (attachment) coefficient [T^{-1}], k_d is the first-order entrainment (detachment) coefficient [T^{-1}], and ψ is a dimensionless colloid retention function [-]. Various functions were implemented for ψ to describe blocking, ripening, or straining phenomena. The attachment coefficient can be calculated using filtration theory.

Carbon Dioxide Production and Transport

The HYDRUS-1D software package now also includes modules for simulating carbon dioxide production and transport. CO_2 transport is assumed to occur by diffusion in both the liquid and gaseous phases, and by advection in the liquid phase. CO_2 production is considered to be the sum of production by soil microorganisms and by plant roots. Various environmental factors, such as temperature and the water content are used to modify the optimum CO_2 production rate.

Geochemical Transport of Major Ions

We also incoporated a new geochemical transport module in HYDRUS-1D based on the UNSATCHEM model of Šimůnek et al. (1996, 1997). The major variables of the chemical system are Ca, Mg, Na, K, SO_4, Cl, NO_3, H_4SiO_4, alkalinity, and CO_2. The model accounts for equilibrium chemical reactions between these components such as complexation, cation exchange and precipitation-dissolution. For the precipitation-dissolution of calcite and dissolution of dolomite, either equilibrium or multicomponent kinetic expressions can be used which include both forward and back reactions. Other dissolution-precipitation reactions considered include gypsum, hydromagnesite, nesquehonite, and sepiolite. Since the ionic strength of soil solutions can vary considerably in time and space and often reach high values, both modified the Debye-Hückel and the Pitzer expressions were incorporated into the model as options to calculate single ion activities.

The new UNSATCHEM module enables quantitative predictions of processes involving major ions, such as simulations of the effects of salinity on plant growth and estimating the amount of water and amendment required to reclaim soil profiles to desired levels of salinity and ESP (exchangeable sodium percentage).

Table 1. Chemical species included in the UNSATCHEM major ion module of HYDRUS-1D.

Aqueous components	7	Ca^{2+}, Mg^{2+}, Na^{+}, K^{+}, SO_4^{2-}, Cl^{-}, NO_3^{-}
Complexed species	10	$CaCO_3^{o}$, $CaHCO_3^{+}$, $CaSO_4^{o}$, $MgCO_3^{o}$, $MgHCO_3^{+}$, $MgSO_4^{o}$, $NaCO_3^{-}$, $NaHCO_3^{o}$, $NaSO_4^{-}$, KSO_4^{-}
Precipitated species	6	$CaCO_3$, $CaSO_4 \cdot 2H_2O$, $MgCO_3 \cdot 3H_2O$, $Mg_5(CO_3)_4(OH)_2 \cdot 4H_2O$, $Mg_2Si_3O_{7.5}(OH) \cdot 3H_2O$, $CaMg(CO_3)_2$
Sorbed (exchangeable) species	4	Ca, Mg, Na, K
CO_2-H_2O species	7	P_{CO2}, $H_2CO_3^{*}$, CO_3^{2-}, HCO_3^{-}, H^{+}, OH^{-}, H_2O
Silica species	3	H_4SiO_4, $H_3SiO_4^{-}$, $H_2SiO_4^{2-}$

References

Bradford, S. A., J. Šimůnek, M. Bettehar, M. Th. van Genuchten, and S. R. Yates, Modeling colloid attachment, straining, and exclusion in saturated porous media, *Environ. Sci. & Technology*, *37*(10), 2242-2250, 2003.

Gerke, H. H., and M. Th. van Genuchten, A dual-porosity model for simulating the preferential movement of water and solutes in structured porous media, *Water Resour. Res.*, *29*, 305-319, 1993.

Jarvis, N.J., The MACRO model (Version 3.1), Technical description and sample simulations. *Reports and Dissertations 19*. Dept. Soil Sci., Swedish Univ. Agric. Sci., Uppsala, Sweden, 51 pp., 1994.

Lenhard, R. J., J. C. Parker, and J. J. Kaluarachchi, Comparing simulated and experimental hysteretic two-phase transient fluid flow phenomena, *Water Resour. Res., 27*(8), 2113-2124, 1991.

Šimůnek, J., and D. L. Suarez, Modeling of carbon dioxide transport and production in soil: 1. Model development, *Water Resour. Res., 29*(2), 487-497, 1993.

Šimůnek, J., and D. L. Suarez, Two-dimensional transport model for variably saturated porous media with major ion chemistry, *Water Resour. Res.*, *30*(4), 1115-1133, 1994.

Šimůnek, J., D. L. Suarez, and M. Šejna, The UNSATCHEM software package for simulating one-dimensional variably saturated water flow, heat transport, carbon dioxide production and transport, and multicomponent solute transport with major ion equilibrium and kinetic chemistry, Version 2.0, *Research Report No. 141*, U.S. Salinity Laboratory, USDA, ARS, Riverside, California, 186pp., 1996.

Šimůnek, J., and D. L. Suarez, Sodic soil reclamation using multicomponent transport modeling, *ASCE J. Irrig. and Drain. Engineering, 123*(5), 367-376, 1997.

Šimůnek, J., K. Huang, M. Šejna, and M. Th. van Genuchten, The HYDRUS-1D software package for simulating the one-dimensional movement of water, heat, and multiple solutes in variably-saturated media. Version 1.0, *IGWMC - TPS - 70,* International Ground Water Modeling Center, Colorado School of Mines, Golden, Colorado, 186pp., 1998.

Šimůnek J., N. J., Jarvis, M. Th. van Genuchten, and A. Gärdenäs, Review and comparison of models for describing non-equilibrium and preferential flow and transport in the vadose zone, Journal of Hydrology, 272, 14-35, 2003.

Šimůnek, J., M. Th. van Genuchten, and M. Šejna, The HYDRUS-1D software package for simulating the one-dimensional movement of water, heat, and multiple solutes in variably-saturated media. Version 3.0, *HYDRUS Software Series 1*, Department of Environmental Sciences, University of California Riverside, Riverside, CA, 270pp., 2005.